J. Fluid Mech. (2024), *vol*. 985, A13, doi:10.1017/jfm.2024.278

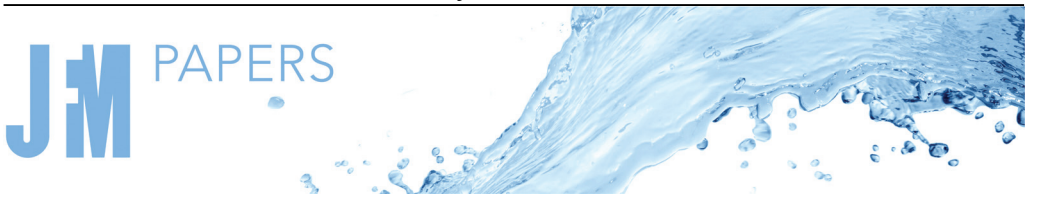

Excitation and evolution of radiating modes in supersonic boundary layers. Part 1. Fundamental resonance with impinging sound waves

Fufeng Qin[1] **and Xuesong Wu**[1],†

[1]Department of Mathematics, Imperial College London, 180 Queen's Gate, London SW7 2AZ, UK

(Received 20 July 2023; revised 1 February 2024; accepted 9 March 2024)

This paper investigates the linear and nonlinear evolution of radiating modes in supersonic boundary layers under the influence of impinging sound waves. It is found that the ensuing boundary-layer response is extraordinarily large for a subset of the sound frequency and incident angle, and the resonant over-reflection, corresponding to the reflection coefficient becoming infinite, occurs at a particular pairing of frequency and incident angle. At this point, the reflected wave coincides with a locally neutral radiating mode, which emits spontaneously sound in the form of Mach waves. A fundamental resonance takes place between the incident wave and the radiating mode. Viewed in a developing boundary layer, the response is rendered finite by introducing non-parallelism and nonlinear effects near the neutral location of the radiating mode, where the sound wave directly excites the radiating mode and/or acts on the pre-existing radiating mode. Inhomogeneous amplitude equations are derived to describe the excitation as well as the nonlinear development of the radiating mode in the two regimes where non-equilibrium and non-parallelism play a leading-order role, respectively. A composite amplitude equation is then constructed to take into account both non-parallelism and non-equilibrium effects. This amplitude equation is, with an appropriate initial condition, solved to quantify the impact of the impinging sound wave on the linear and nonlinear instability characteristics of the radiating mode. The far-field analysis shows that the Mach wave field of the radiating mode is changed significantly due to the incident sound.

Key words: boundary layer stability, boundary layer receptivity, supersonic flow

† Email address for correspondence: x.wu@ic.ac.uk

1. Introduction

There has been considerable interest in laminar–turbulent transition of super- and hypersonic boundary-layer flows due to their key role in the development of high-speed vehicles (Kimmel 2003). An adequate understanding of this physical process is crucial to their design as aerodynamic drag and thermal loading differ drastically depending on whether the flow is laminar or turbulent (Fedorov 2011; Zhong & Wang 2012).

Transition is characterised by a high degree of spatial and temporal complexity (Kachanov 1994). It often starts with amplification of small-amplitude instability waves, which are triggered, via the so-called receptivity (Morkovin 1969; Goldstein & Hultgren 1989), by external perturbations, including acoustic, vortical or entropy waves in the free stream and local imperfections on the surface. The instability modes excited first grow exponentially, which is well predicted by linear stability theory. Once the disturbances become sufficiently strong, nonlinear inter-modal interactions take place, leading to final breakdown to turbulence. In many situations, ambient disturbances may further influence the linear and nonlinear development of the instability waves and thereby affect transition location. This scenario has only received limited attention and it will be studied in this paper. Specifically, we will focus on the evolution of such instability waves in a supersonic boundary layer under the influence of impinging acoustic waves.

1.1. *Intrinsic instabilities in compressible boundary layers*

Theoretical studies of compressible boundary-layer instability as well as extensive computations, performed at different conditions (e.g. Mach number, Reynolds number and wall temperature) have identified a multitude of instability modes, which are now termed the first and second Mack modes, etc. (Mack 1975, 1984) . Lower-branch first modes that are sufficiently oblique are the continuation of the viscous Tollmien–Schlichting (T-S) instability into the supersonic regime, and they are governed by the compressible version of the triple-deck structure (Smith 1989). The remaining first modes and second modes are of inviscid nature, and their existence is associated with a generalised inflection point (Lees & Lin 1946). For insulated walls, the first modes represent dominant instability up to a Mach number of approximately 4, beyond which the second modes prevail. For cooled walls, the second modes can dominate at lower Mach numbers (Mack 1993).

Instability modes can be categorised based on their propagation speeds relative to the free stream. A mode travelling relative to the free stream at a velocity smaller than the sound speed is referred to as a subsonic mode. Its eigenfunction decays exponentially away from the boundary layer. In contrast, a mode propagating supersonically relative to the free stream is referred to as a supersonic or radiating mode because its eigenfunction is oscillatory while attenuating, or remains bounded in the far field when the mode is neutral. Both neutral subsonic and supersonic modes have a critical level (i.e. the position where the base-flow velocity is equal to the phase velocity). The critical level of the former coincides with the generalised inflection point, but that of the latter does not. It is well known that the supersonic modes are present in supersonic jets, and radiate Mach waves; see Tam (1995) and references therein.

The present paper is concerned with the supersonic mode, whose existence in compressible boundary layers is also well known (Mack 1984). Such modes may exist if the wall is cooled sufficiently below the adiabatic temperature (Chuvakhov & Fedorov 2016) or the free-stream enthalpy is high (Salemi & Fasel 2018). They have been reported for flows over flat plates (Mack 1987; Bitter & Shepherd 2015), wedges (Chang, Malik & Hussaini 1990; Chang, Vinh & Malik 1997) and cones (Knisely &

Zhong 2017; Mortensen 2018). Sound radiation by unstable supersonic modes in a hypersonic blunt-cone boundary layer was studied numerically by Knisely & Zhong (2019*a*,*b*).

While proven to be rather successful in describing the dispersion relationship and growth rates of small-amplitude instability waves, linear stability theory fails to predict the course of evolution when the magnitude of the instability mode is no longer small enough. A typical evolution path is that the instability wave goes through almost the entire linear amplification regime, acquiring a sufficiently large amplitude near its neutral position. At high Reynolds numbers, a critical layer emerges, where nonlinear interaction first takes place, and usually other physical factors such as viscous and non-equilibrium effects (associated with the slow modulation of the modal amplitude), although remaining negligible in the main bulk, also come into play (Goldstein & Hultgren 1988; Goldstein & Leib 1988). The continued development of the disturbance under the combined influence of these factors is described by the well-developed nonlinear non-equilibrium critical-layer theory, a review of which is given by Wu (2019). In this theory, the nonlinear dynamics is determined by the composition of modes and the singular nature of the inviscid solution in the outer layer. Once a singularity is removed by introducing viscous and/or non-equilibrium effects in the critical layer, the regularised solution represents a locally large disturbance, which contributes dominant nonlinear effects. The dynamics may take a weakly or strongly nonlinear form.

Nonlinear and non-equilibrium critical layers were considered for externally forced waves in shear flows in the late 1970s, but for free instability modes the study of such critical-layer dynamics started with Hickernell (1984), who considered temporal evolution of a non-inflectional planar Rossby mode on a rotating free shear layer. The interactions in the critical layer turned out to be of weakly nonlinear nature, the analysis of which led to a novel amplitude equation containing a non-local nonlinear term. Goldstein & Leib (1988) and Goldstein & Hultgren (1988) considered a regular Rayleigh instability mode in a free shear layer. They showed that the critical-layer dynamics is strongly nonlinear, and the evolution is governed by an amplitude equation coupled with the vorticity equation, in which the unknown amplitude appears as a coefficient. Goldstein & Leib (1989) studied the nonlinear evolution of a subsonic mode in a supersonic shear layer, for which the inviscid solution of the temperature fluctuation exhibits a simple-pole singularity, which dictates that the interactions are of weakly nonlinear type. An evolution equation was derived, to which the singularity contributes a signature non-local nonlinear term. Leib (1991) extended the analysis to a supersonic mode, which is non-inflectional. The additional logarithmic singularity in the streamwise velocity gives rise to an extra history-dependent nonlinear term. The above studies were the first to solve the non-local nonlinear equations numerically, showing that the amplitude exhibits rather complex behaviours, including finite-distance blow-up and oscillatory saturation. Their analyses are closely related to the present study. Gajjar (1995, 1996) considered the nonlinear development of stationary and travelling vortices in three-dimensional boundary layers. An amplitude equation was derived in each case, with the non-local nonlinearity associated with the three-dimensional nature of the perturbation, and for travelling vortices in the compressible regime with the simple-pole and logarithmic singularities in the temperature and streamwise velocity as well.

There has been a large number of studies of inter-modal interactions within non-equilibrium critical layers (Goldstein 1995; Wu 2019). Important forms of modal composition include pairs of oblique modes with equal frequency but opposite spanwise wavenumbers (Goldstein & Choi 1989; Wu, Lee & Cowley 1993; Leib & Lee 1995), resonant triads of inviscid Rayleigh waves (Wu 1992, 1995) and more generally

phase-locked modes (i.e. modes having nearly the same phase speed) (Wu & Stewart 1996; Wu, Stewart & Cowley 2007).

1.2. *Effects of external disturbances on transition*

External disturbances, including surface roughness elements and free-stream disturbances, may affect the transition route and location through different mechanisms, depending on their position as well as length and time scales. One of the important mechanisms is receptivity, which refers to the process by which external disturbances excite instability modes, and thus determine the initial amplitudes of the latter (Morkovin 1969). It is now well recognised that excitation in general requires a mechanism of length scale conversion or tuning, which is, in the incompressible or subsonic regime, provided by the adjustment in the leading-edge region (Goldstein 1983) and/or scattering of free-stream acoustic waves (Ruban 1984; Goldstein 1985) or vortical disturbances (Duck, Ruban & Zhikharev 1996; Wu 2001*a*,*b*) by surface roughness.

The receptivity mechanisms identified for incompressible, or compressible subsonic, boundary layers remain operational in super- and hyper-sonic regimes, but may take on significantly different characteristics. On the other hand, new mechanisms may arise due to the nature of the instabilities. The excitation of first and second modes by impinging sound waves through the leading-edge mechanism was considered by Fedorov & Khokhlov (1991, 2001) and Fedorov (2003*a*). Their analysis showed that there exist the so-called fast and slow modes, whose phase velocities in the leading-edge region approach those of the oncoming fast and slow acoustic waves, respectively. Both modes are thus excited. As they undergo no or only marginal decay, the leading-edge adjustment mechanism is much more efficient than its counterpart in the subsonic regime, and has been the subject of a series of direct numerical simulations (DNS) (Ma & Zhong 2003, 2005; Balakumar 2005, 2009). Vortical disturbances may generate highly oblique modes (Ricco & Wu 2007), which may be particularly effective for a small specific range of obliqueness angle (Goldstein & Ricco 2018). The mechanism of the acoustic–roughness interaction carries over to the supersonic regime, generating first and second modes in much the same manner as exciting the T-S mode in the subsonic regime when the theory was formulated in a finite-Reynolds-number framework (Fedorov 2003*b*). The (improved) large-Reynolds-number asymptotic analyses showed that, among all possible acoustic waves, those on the triple-deck scales and with incident angles close to $\cos^{-1}(1/M)$ (M being the free-stream Mach number) are particularly effective in generating the viscous first mode (Liu, Dong & Wu 2020), while generation of the second mode was due to a pure surface geometry effect at leading order (Dong, Liu & Wu 2020).

New receptivity mechanisms operate for supersonic boundary layers and have been described theoretically. One of these is the sound–gust interaction (Wu 1999), in which sound and vortical disturbances with suitable wavenumbers and frequencies interact to generate a forcing that is in resonance with and thereby excites the viscous first mode. Sound–sound interaction also generates the viscous first mode, and this mechanism becomes particularly efficient for sound waves on the triple-deck scales (Hernández & Wu 2019). Another distinct mechanism operates in the hypersonic flow past a wedge, where, due to the presence of an oblique shock, there exist viscous instability modes confined in the region below the shock (Cowley & Hall 1990). Qin & Wu (2016) showed that any of the oncoming acoustic, vortical and entropy disturbances interacts with the shock to generate a slow acoustic wave downstream, and with suitable frequency the latter may resonate with and thereby excite the instability. The above three mechanisms do not resort to any surface

roughness, and hence operate in supersonic boundary layers over nominally smooth walls, providing possible explanations for the unstable modes observed.

When external disturbances of sufficient magnitude are present in the main unstable region, they may influence instability characteristics. Surface roughness has received most attention, and is found to play a destabilising role, in most cases causing earlier transition (Klebanoff & Tidstrom 1972; Corke, Barsever & Morkovin 1986). When roughness elements have a length scale much longer than that of the instability, their impact can be accounted for by local linear stability analysis of the altered base flow. Analyses of this kind have been performed for two-dimensional (Nayfeh, Ragab & Al-Maaitah 1988; Masad & Iyer 1994) and three-dimensional roughness (Piot, Casalis & Rist 2008; Choudhari *et al.* 2010; De Tullio *et al.* 2013; Groskopf & Kloker 2016). However, when the length scale of the roughness is comparable to, or shorter than, that of the instability, local stability analysis is no longer tenable, and DNS have been performed instead (Marxen, Iaccarino & Shaqfeh 2010; Edelmann & Rist 2013). The physical mechanism is local scattering: the roughness-induced local mean-flow distortion scatters an oncoming instability wave, changing its amplitude over a short length. A transmission coefficient, defined as the ratio of the amplitude of the transmitted wave downstream to that of the oncoming wave, is a natural measure of the overall effect of the roughness (Wu & Dong 2016; Xu *et al.* 2016). Another mechanism is modal interaction, where the roughness-induced signature interacts resonantly with instability modes so that the growth rate of the latter is changed substantially (Goldstein & Wundrow 1995; He, Butler & Wu 2019; Xu & Wu 2022).

Acoustic waves are dominant external disturbances affecting supersonic boundary-layer transition, especially in conventional wind tunnel experiments (Pate & Schueler 1969; Schneider 2001), as intense noise is emitted from the turbulent boundary layers on the tunnel walls and/or radiated due to turbulence being scattered by wall inhomogeneities such as roughness (Laufer 1961, 1964). Wind tunnel experiments were carried out to establish the relationship between the noise level and transition location. Acoustic waves with particular frequencies lead to considerably earlier transition (Spangler & Wells 1968). By relaminarising the boundary layers on the tunnel walls to reduce the facility-produced acoustic waves, transition was delayed significantly (Kendall 1971).

Because of intense acoustic disturbances to which the test model is exposed, transition in conventional wind tunnels is notably different from that in quiet ones (Beckwith & Miller 1990; King 1992; Schneider 2008). Modern hypersonic quiet wind tunnel technology strives to reproduce flight conditions (Schneider 2015). However, even in the latter acoustic waves are radiated from either the engine or the turbulent boundary layers over neighbouring surfaces of the aircraft, and they are likely to have a significant effect on transition. In view of this, conventional tunnels share some similarities with the flight condition, and experimental data obtained in them on instability and transition may still be useful (Duan, Choudhari & Wu 2014).

1.3. *The aim of the present work*

For either purpose of describing transition scenarios in the presence of impinging acoustic waves and extrapolating wind tunnel data to flight conditions, it is necessary to investigate how they influence the inherent boundary-layer instability and the ensuing transition. Despite its potential importance, there have been few investigations of this aspect, in contrast to extensive studies devoted to receptivity. In this paper, we identify and describe mathematically a mechanism, through which impinging sound waves affect the linear and nonlinear development of instability waves. Specifically, we consider radiating modes,

and demonstrate that, while emitting a sound wave to the far field, a radiating mode is also extremely sensitive to an incident acoustic wave with the same frequency and wavenumber due to a fundamental resonance between them with the incident sound acting as the forcing. This mechanism involves both receptivity and nonlinear modal interaction. While receptivity normally refers to excitation of instability modes near the lower branch, the present resonance takes place near the upper branch, in the vicinity of which an incident wave of small intensity excites a radiating mode of much larger amplitude. When the intensity is of a distinguished order of magnitude but still very low, nonlinearity affects the excitation, and moreover the incident sound influences significantly the linear and nonlinear evolution of the locally excited mode as well as of the oncoming pre-existing mode.

The rest of the paper is organised as follows. In § 2, we formulate the problem pertinent to a free-stream acoustic wave impinging upon the boundary layer. The distinguished asymptotic scalings are deduced under which the incident sound wave affects the excitation and evolution of the radiating mode. Two distinct, the non-equilibrium and the equilibrium non-parallel, regimes are considered. In § 3, we investigate the reflection of an impinging sound wave by the boundary layer. The boundary-layer response and reflection coefficient are determined. A systematic numerical study is performed to show, *inter alia*, that the reflection coefficient becomes infinite for a particular pair of frequency and wavenumber, coinciding with those of the neutral radiating mode. This signals a fundamental resonance between the incident wave and the radiating mode. In § 4, we focus on this particular acoustic wave. Dominant interactions affecting the excitation and evolution take place in the critical layer, and are analysed to derive the amplitude equations in the two regimes mentioned above. These equations are solved numerically to demonstrate the role of the incident sound and nonlinearity in the excitation and evolution of the radiating mode. In order to take into account effects of both non-equilibrium and non-parallelism, we construct a composite amplitude equation in § 5. In § 6, the spontaneously radiated sound wave under the influence of the incident sound is computed. Finally, a summary and conclusions are given in § 7.

2. Formulation

We consider a supersonic boundary-layer flow that forms over a semi-infinite flat plate underneath a uniform free stream, where the density, velocity, shear viscosity and sound speed are denoted by ρ_∞, U_∞, μ_∞ and a_∞, respectively. Based upon these quantities, the Reynolds number R and the Mach number M are defined as

$$R = \rho_\infty U_\infty \delta^*/\mu_\infty, \quad M = U_\infty/a_\infty, \tag{2.1a,b}$$

where the reference length δ^* is the boundary-layer thickness at the location of interest (which is the neutral position of the radiating mode to be considered). To adopt an asymptotic approach and focus on the supersonic regime, we take $R \gg 1$ and $1 < M = O(1)$.

The flow will be described in a Cartesian coordinate system (x, y, z), where x and y are along and normal to the wall, respectively, and z is in the spanwise direction, all non-dimensionalised by δ^*. The time variable t is normalised by δ^*/U_∞. The density ρ, velocity $\boldsymbol{u} = (u, v, w)$, pressure p, temperature T and shear and bulk viscosities μ and μ' are non-dimensionalised by ρ_∞, U_∞, $\rho_\infty U_\infty^2$, T_∞ and μ_∞, respectively. The flow is

governed by the compressible Navier–Stokes (N-S) equations (e.g. Stewartson 1964),

$$\frac{\partial \rho}{\partial t} + \boldsymbol{\nabla} \cdot (\rho \boldsymbol{u}) = 0, \tag{2.2a}$$

$$\rho \frac{\mathrm{D}\boldsymbol{u}}{\mathrm{D}t} = -\boldsymbol{\nabla} p + \frac{1}{R}\left[\boldsymbol{\nabla} \cdot (2\mu \boldsymbol{e}) + \boldsymbol{\nabla}\left(\left(\mu' - \frac{2}{3}\mu\right)\boldsymbol{\nabla} \cdot \boldsymbol{u}\right)\right], \tag{2.2b}$$

$$\rho \frac{\mathrm{D}T}{\mathrm{D}t} = (\gamma - 1)M^2 \frac{\mathrm{D}p}{\mathrm{D}t} + \frac{1}{PrR}\boldsymbol{\nabla} \cdot (\mu \boldsymbol{\nabla} T) + \frac{(\gamma - 1)M^2}{R}\Phi, \tag{2.2c}$$

$$\gamma M^2 p = \rho T, \tag{2.2d}$$

where $\boldsymbol{e}$ and Φ denote the strain-rate tensor and dissipation function, respectively,

$$e_{ij} = \frac{1}{2}\left(\frac{\partial u_i}{\partial x_j} + \frac{\partial u_j}{\partial x_i}\right), \quad \Phi = 2\mu \boldsymbol{e}\!:\!\boldsymbol{e} + \left(\mu' - \frac{2}{3}\mu\right)(\boldsymbol{\nabla} \cdot \boldsymbol{u})^2, \tag{2.3a,b}$$

Pr is the Prandtl number and γ the ratio of specific heats. Furthermore, the conventional assumption of vanishing bulk viscosity, $\mu' = 0$, is invoked.

2.1. *The base flow*

The boundary layer develops on a long length scale, and can be described by introducing the slow variable

$$x_3 = x/R. \tag{2.4}$$

The base-flow density R_B, velocity field (U_B, V_B), pressure P_B and temperature T_B can be expressed as

$$(R_B, U_B, V_B, P_B, T_B) = (\bar{R}(x_3, y), \bar{U}(x_3, y), R^{-1}\bar{V}(x_3, y), 1/(\gamma M^2), \bar{T}(x_3, y)). \tag{2.5}$$

The steady boundary-layer equations admit the similarity solution (Stewartson 1964)

$$\bar{U} = F'(\eta), \quad \bar{T} = \bar{T}(\eta), \tag{2.6a,b}$$

where η is the similarity variable defined, via the Dorodnitsyn–Howarth coordinate transformation, by

$$\eta = \frac{1}{\sqrt{x_3}}\int_0^y \bar{R}\,\mathrm{d}y. \tag{2.7}$$

In terms of η, F and $\bar{T}$, the steady boundary-layer equations reduce to

$$\left.\begin{aligned} \frac{1}{2}FF'' + (\bar{K}F'')' = 0, \\ \bar{T}'' + \frac{PrF + 2\bar{K}'}{2\bar{K}}\bar{T}' + Pr(\gamma - 1)M^2(F'')^2 = 0, \end{aligned}\right\} \tag{2.8}$$

where we have put $\bar{K}(\bar{T}) = \bar{\mu}(\bar{T})/\bar{T}$. For Sutherland's law, $\bar{K}$ is given by

$$\bar{K} = \frac{1 + C_0}{\bar{T} + C_0}\bar{T}^{1/2}, \tag{2.9}$$

where $C_0 = 110.4\,\mathrm{K}/T_\infty$ with T_∞ being the free-stream temperature in Kelvin. The corresponding boundary conditions are

$$F(0) = F'(0) = 0; \quad F' \to 1 \quad \text{as } \eta \to \infty, \tag{2.10}$$

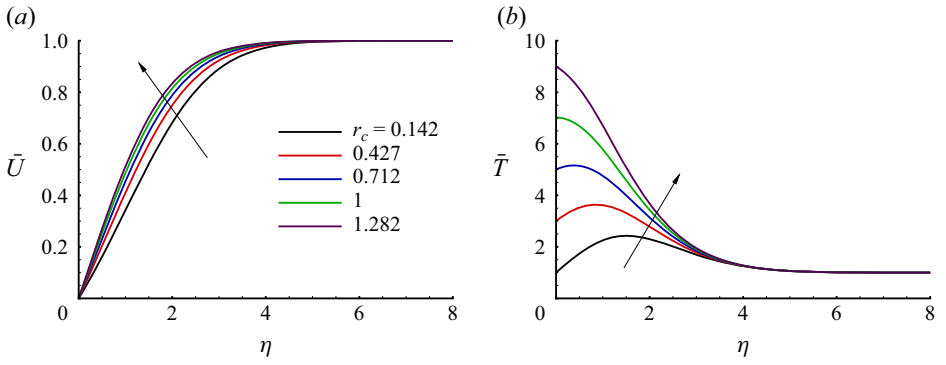

Figure 1. The profiles of the base-flow streamwise velocity (*a*) and temperature (*b*) for different r_c.

and

$$\bar{T}(0) = \bar{T}_w; \quad \bar{T} \to 1 \quad \text{as } \eta \to \infty, \tag{2.11}$$

if the wall is isothermal with a prescribed temperature $\bar{T}_w$.

We consider a perfect gas with ratio of specific heats $\gamma = 1.4$ and Prandtl number $Pr = 0.72$. The free-stream temperature is taken to be $T_\infty = 300\,\text{K}$, and the Mach number $M = 6$. The above chosen parameters are representative of flight conditions (Chuvakhov & Fedorov 2016). The base-flow equations (2.8) are solved by using a shooting method based on a fourth-order Runge–Kutta integrator. The streamwise velocity and temperature for various cooling ratios, defined by the wall temperature over the adiabatic wall temperature, are shown in figure 1. In particular, the base-flow quantities with the cooling ratio $r_c = 0.427$ ($\bar{T}_w = 3$) will be used in the ensuing analysis. As will be shown later, a radiating mode exists only for r_c below a certain value less than unity.

2.2. *Free-stream acoustic waves*

Acoustic waves are one type of elementary disturbances in the free stream, where the base flow is uniform. The density, velocity and pressure components of a two-dimensional acoustic wave, $\epsilon_s(\tilde{r}_s, \tilde{u}_s, \tilde{v}_s, \tilde{p}_s)$, where $\epsilon_s \ll 1$ is the magnitude, are governed by the linearised Euler equations about the uniform background field. Eliminating $\tilde{r}_s$, $\tilde{u}_s$ and $\tilde{v}_s$ from these equations leads to the equation for pressure $\tilde{p}_s$

$$M^2 \left(\frac{\partial}{\partial t} + \frac{\partial}{\partial x} \right)^2 \tilde{p}_s - \nabla^2 \tilde{p}_s = 0. \tag{2.12}$$

The solution takes the form

$$\tilde{p}_s = p_I \exp(\mathrm{i}(\alpha_s x + \gamma_s y - \omega_s t)) + \text{c.c.}, \tag{2.13}$$

where α_s and γ_s are the streamwise and normal wavenumbers, respectively, and ω_s is the frequency; here, γ_s is taken to be positive so that the group velocity in the wall-normal direction is negative, i.e. the disturbance represents an incoming wave.

Substitution of (2.13) into (2.12) yields the dispersion relation for slow acoustic waves

$$c_s \equiv \omega_s/\alpha_s = 1 - \frac{1}{M}\sqrt{1 + (\gamma_s/\alpha_s)^2}, \tag{2.14}$$

where c_s is the phase velocity. We define an incident angle θ_s by $\cos\theta_s = \alpha_s/\sqrt{\alpha_s^2 + \gamma_s^2}$. Use of the dispersion relation (2.14) shows that

$$\theta_s = \arccos\{1/[(1 - c_s)M]\}. \tag{2.15}$$

A sound wave in the free stream is characterised by its frequency and incident angle.

2.3. *Asymptotic scaling*

We are interested in slow acoustic waves and instability modes whose wavelengths are comparable to the boundary-layer thickness (i.e. $\alpha_s = O(1)$). Only slow acoustic waves are considered as they have a critical layer, which is crucial for acoustic waves of moderate amplitude to be able to impact the radiating mode. When such a slow acoustic wave impinges on the boundary layer, the response of the latter is in the form of an absorbed disturbance and a reflected wave. For a sound wave with a particular frequency and a specific incident angle, the reflection coefficient becomes infinite, indicating a fundamental resonance between the impinging sound and the intrinsic radiating mode, through which the latter is excited and its evolution influenced. We will investigate these in the non-equilibrium parallel and equilibrium non-parallel regimes.

2.3.1. *Non-equilibrium parallel regime*

As an inviscid Rayleigh instability mode propagates downstream, its magnitude amplifies exponentially until it reaches a neutral position, $x_{3,n}$ say. Due to the accumulated growth, the mode is likely to enter a nonlinear stage in the vicinity of the neutral position (Goldstein & Leib 1989; Wu 2019). This region is represented as

$$x_3 \approx x_{3,n} + \tilde{\mu}\bar{x}_1, \tag{2.16}$$

where $\tilde{\mu} \ll 1$ and $\bar{x}_1 = O(1)$ is negative. The local base-flow velocity and temperature profiles are expanded as

$$(\bar{U}(x_3, y), \bar{T}(x_3, y)) \approx (\bar{U}(x_{3,n}, y), \bar{T}(x_{3,n}, y)) + \tilde{\mu}(\bar{U}_1(y), \bar{T}_1(y))\bar{x}_1. \tag{2.17}$$

In this region, the growth rate of the mode is $O(\tilde{\mu})$, correspondingly, the amplitude develops over the length scale of $O(\tilde{\mu}^{-1})$, and so we introduce the slow variable

$$\tilde{x} = \tilde{\mu}(x - x_0) \quad \text{with } x_0 = R(x_{3,n} + \tilde{\mu}\bar{x}_1). \tag{2.18}$$

The instability mode is of the travelling-wave form, and in the main layer it can be expressed, to leading order, as

$$(\tilde{\rho}, \tilde{u}, \tilde{v}, \tilde{p}, \tilde{\theta}) = A(\tilde{x})(\hat{\rho}_0(y), \hat{u}_0(y), \hat{v}_0(y), \hat{p}_0(y), \hat{\theta}_0(y))E + \text{c.c.} + \cdots, \tag{2.19}$$

where $E = \exp(\mathrm{i}\alpha\zeta)$, $\zeta = x - ct$ is the coordinate moving at the phase speed, with α and c being the streamwise wavenumber and phase speed, respectively, and $A(\tilde{x})$ is the amplitude

function describing the evolution. The derivative with respect to x then becomes

$$\frac{\partial}{\partial x} \to \frac{\partial}{\partial \zeta} + \tilde{\mu}\frac{\partial}{\partial \tilde{x}}. \tag{2.20}$$

In order to derive the scaling, let us first write down the streamwise momentum equation (of the incompressible N-S equations for convenience) for the perturbation

$$\Big[(\bar{U}-c)\frac{\partial}{\partial \zeta} + \underbrace{\tilde{\mu}\bar{U}\frac{\partial}{\partial \tilde{x}}}_{\textit{non-equilibrium}}\Big]\tilde{u} + \bar{U}'\tilde{v} - \underbrace{R^{-1}\frac{\partial^2 \tilde{u}}{\partial \tilde{y}^2}}_{\textit{viscous}} = -\frac{\partial \tilde{p}}{\partial \zeta} - \tilde{u}\frac{\partial \tilde{u}}{\partial \zeta} - \tilde{v}\frac{\partial \tilde{u}}{\partial y} - \tilde{\mu}\tilde{u}\frac{\partial \tilde{u}}{\partial \tilde{x}} + \cdots. \tag{2.21}$$

The scaling is fixed by considering the main and critical layers. In the main layer, the disturbance is linear and inviscid, and its streamwise velocity exhibits a jump of $O(\tilde{\epsilon}\tilde{\mu})$, which is to be determined by analysis of the critical layer. Suppose that the critical-layer width is $O(\delta_c)$. The advection term in (2.21) is $O(\delta_c)$, whereas the terms associated with the non-equilibrium and viscous effects are $O(\tilde{\mu})$ and $O(R^{-1}/\delta_c^2)$, respectively. The requirement that these terms are all balanced leads to

$$\delta_c = O(\tilde{\mu}), \quad \delta_c = O(R^{-1/3}). \tag{2.22a,b}$$

In the critical layer, the vertical velocity of the perturbation $\tilde{v}$ is $O(\tilde{\epsilon})$, but the logarithmic singularity $\ln(y - y_c)$ of the inviscid solution for the streamwise velocity suggests that the vorticity, or $\tilde{u}_y$, is $O(\tilde{\epsilon}\delta_c^{-1})$. The forcing proportional to the product of these two is thus $O(\tilde{\epsilon}^2\delta_c^{-1})$. It then induces a mean-flow distortion as well as a second harmonic; their streamwise velocity is $O(\tilde{\epsilon}^2\delta_c^{-2})$ as is deduced by balancing the forcing and the non-equilibrium term in (2.21). The fundamental wave interacts with them to produce a forcing of $O(\tilde{\epsilon}^3\delta_c^{-3})$ at cubic level, which regenerates an $O(\tilde{\epsilon}^3\delta_c^{-4})$ streamwise velocity of the fundamental. If the latter is comparable to the $O(\tilde{\epsilon}\tilde{\mu})$ jump in the main layer, i.e. if $\tilde{\mu} = O(\tilde{\epsilon}^{2/5})$, the nonlinear effect enters the amplitude equation (Leib 1991; Wu & Cowley 1995). Under this scaling the temperature fluctuation also contributes a nonlinear effect (Goldstein & Leib 1989). Due to the resonant nature of the forcing, the $O(\tilde{\epsilon})$ radiating mode can be excited by a much weaker incident wave with the magnitude

$$\tilde{\epsilon}_s = \tilde{\epsilon}\tilde{\mu} = O(\tilde{\epsilon}^{7/5}). \tag{2.23}$$

We then write

$$\tilde{\mu} = \tilde{\epsilon}^{2/5} = \delta_c, \quad R^{-1} = \lambda\tilde{\mu}^3, \tag{2.24a,b}$$

where λ is the $O(1)$ Haberman parameter measuring the importance of the viscosity. The above relations form the basis of non-equilibrium critical-layer theory describing the interaction between the incident sound and the radiating mode.

2.3.2. *Equilibrium non-parallel regime*

The equilibrium non-parallel regime is pertinent to the region where the length scale over which the growth rate varies is comparable to the length scale over which the amplitude

evolves (Wu 2005). This region is represented by

$$x_3 = x_{3,n} + R^{-1/2}\bar{x} \quad \text{with } \bar{x} = O(1). \tag{2.25}$$

We take δ^* to be the boundary-layer thickness at the neutral position, and with the latter being chosen to be origin of the coordinate we can set $x_{3,n} = 0$. Inspection of (2.21) shows that in this region the non-equilibrium effect, $\bar{\mu} = O(R^{-1/2})$, is much smaller than the viscous effect. The critical layer is thus of equilibrium type and viscosity dominated, having a width $\delta_c = O(R^{-1/3})$. A similar scaling argument shows that the balance between the outer and inner jumps leads to

$$\bar{\epsilon} = \delta_c^2 \bar{\mu}^{1/2} = O(R^{-11/12}). \tag{2.26}$$

Again noting the resonant nature of the forcing, we can infer that the radiating mode of $O(\bar{\epsilon})$ can be excited by an incident sound wave with a much smaller magnitude

$$\bar{\epsilon}_s = O(\bar{\epsilon}\bar{\mu}) = O(R^{-17/12}). \tag{2.27}$$

The local mean velocity and temperature profiles can be approximated by

$$(\bar{U}(x_3, y), \bar{T}(x_3, y)) \approx (\bar{U}(x_{3,n}, y), \bar{T}(x_{3,n}, y)) + R^{-1/2}(\bar{U}_1(y), \bar{T}_1(y))\bar{x}, \tag{2.28}$$

to the required order. With the key scalings identified, the effects of sound waves on the evolution of the radiating mode will be analysed in a self-consistent manner.

2.4. *Existence of the radiating mode*

For inviscid instability, the linearised Euler equations for instability modes can be reduced to the Rayleigh equation for the pressure

$$\mathscr{L}\hat{p}_0 \equiv \left\{ \frac{\partial^2}{\partial y^2} + \left(\frac{\bar{T}'}{\bar{T}} - \frac{2\bar{U}'}{\bar{U} - c} \right) \frac{\partial}{\partial y} - \alpha^2 \left[1 - \frac{M^2(\bar{U} - c)^2}{\bar{T}} \right] \right\} \hat{p}_0 = 0. \tag{2.29}$$

For a neutral radiating mode, the boundary condition consists of the impermeability condition at the wall and a finite amplitude at the infinity, namely, $\hat{p}_0'(0) = 0$ and $\hat{p}_0$ is bounded as $y \to \infty$.

In order to find eigenvalues of the Rayleigh equation, it is convenient to write equation (2.29) in terms of the similarity valuable η defined by (2.7) (in which $x_3 = x_{3,n} = 1$). The Rayleigh equation (2.29) becomes

$$\hat{p}_0'' - \frac{2\bar{U}'}{\bar{U} - c}\hat{p}_0' - \alpha^2 \bar{T}^2 \left[1 - \frac{M^2(\bar{U} - c)^2}{\bar{T}} \right] \hat{p}_0 = 0, \tag{2.30}$$

where the derivative is with respect to η, and the boundary condition becomes

$$\hat{p}_0'(0) = 0, \quad \hat{p}_0 \text{ is bounded} \quad \text{as } \eta \to \infty. \tag{2.31}$$

More precisely, the wavenumber and phase velocity of the eigenmode must satisfy the condition, $\alpha^2[1 - M^2(1 - c)^2] < 0$, or equivalently, $c < 1 - 1/M$, so that the far-field behaviour of the mode takes the form of an outgoing wave

$$\hat{p}_0 \sim \mathscr{C}_\infty \exp(-\mathrm{i}\alpha q \eta) \quad \text{as } \eta \to \infty, \tag{2.32}$$

where $\mathscr{C}_\infty$ is the normalisation factor, and $q = \sqrt{M^2(1 - c)^2 - 1}$.

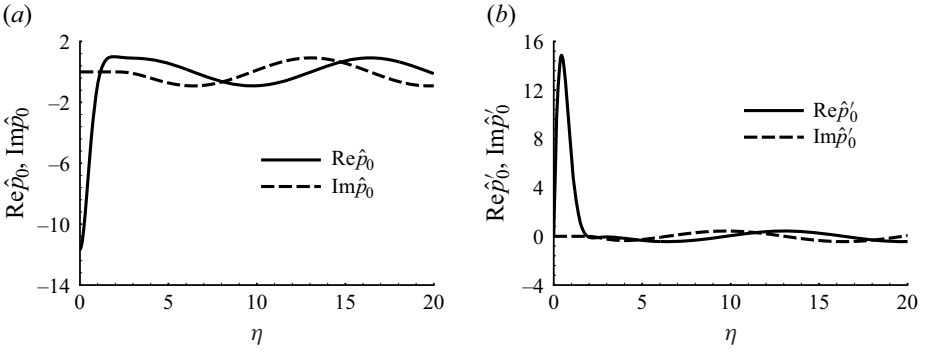

Figure 2. The eigenfunction of a two-dimensional supersonic mode: (*a*) $\hat{p}_0$ and (*b*) $\hat{p}_0'$.

Near the critical level η_c, where $\bar{U}(\eta_c) - c = 0$, we seek solutions of Frobenius type to the Rayleigh equation. It can be shown that, as $\bar{\eta} \equiv \eta - \eta_c \to 0$,

$$\hat{p}_0 = \bar{a}^{\pm}\bar{\phi}_a + \bar{\phi}_b, \tag{2.33}$$

where the constants $\bar{a}^{\pm}$ take different values above and below the critical level, and

$$\bar{\phi}_a = \bar{\eta}^3 + \frac{3}{4}\frac{\bar{U}_c''}{\bar{U}_c'}\bar{\eta}^4 + \frac{1}{10}\left[\frac{2\bar{U}_c'''}{\bar{U}_c'} + \frac{3}{2}\left(\frac{\bar{U}_c''}{\bar{U}_c'}\right)^2 + \alpha^2\bar{T}_c^2\right]\bar{\eta}^5 + \cdots, \tag{2.34}$$

$$\bar{\phi}_b = \frac{\alpha^2\bar{T}_c^2}{3}\left(\frac{2\bar{T}_c'}{\bar{T}_c} - \frac{\bar{U}_c''}{\bar{U}_c'}\right)\ln|\bar{\eta}|\bar{\phi}_a + 1 - \frac{\alpha^2}{2}\bar{T}_c^2\bar{\eta}^2 + \bar{\chi}\,\bar{\eta}^4 + \cdots, \tag{2.35}$$

with

$$\bar{\chi} = \frac{\alpha^2\bar{T}_c^2}{4}\left[\frac{1}{2}\left(\frac{\bar{U}_c''}{\bar{U}_c'}\right)^2 - \frac{2}{3}\frac{\bar{U}_c'''}{\bar{U}_c'} - \frac{\alpha^2}{2}\bar{T}_c^2 + \frac{\bar{T}_c''}{\bar{T}_c} + \left(\frac{\bar{T}_c'}{\bar{T}_c}\right)^2\right] - \frac{M^2\alpha^2}{4}(\bar{U}_c')^2\bar{T}_c - \frac{11}{48}\alpha^2\bar{T}_c^2\frac{\bar{U}_c''}{\bar{U}_c'}\left(\frac{2\bar{T}_c'}{\bar{T}_c} - \frac{\bar{U}_c''}{\bar{U}_c'}\right). \tag{2.36}$$

The analytical formula above supplements the numerical method to solve the eigenvalue problem, the details of which are relegated to Appendix A.1.

For the base-flow condition considered, we find a radiating mode with

$$\alpha = 0.355336, \quad c = 0.723147, \tag{2.37a,b}$$

and plot the corresponding eigenfunction in figure 2. As is shown, the radiating (supersonic) mode exhibits a wavy structure in the far field, in contrast to the subsonic mode which decays exponentially outside the boundary layer. This feature is closely related to the Mach wave radiation (Wu 2005). The dependence of the radiating mode on the base-flow parameters is studied. The variation of the streamwise wavenumber and phase velocity of the neutral radiating mode with the Mach number M for a fixed wall temperature $\bar{T}_w = 3$ is shown in figure 3. A radiating mode exists only in a small range of Mach number. Similarly, for a fixed Mach number ($M = 6$), a radiating mode could only be found in a small range of the cooling ratio, as is shown in figure 4.

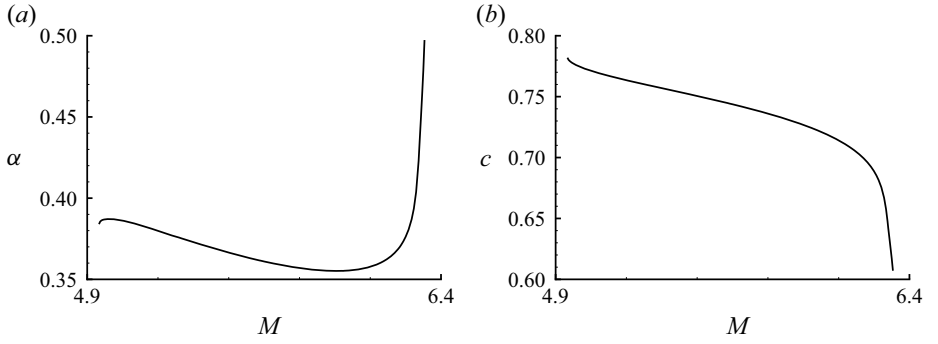

Figure 3. Variation of the wavenumber α (a) and the phase speed c (b) of the neutral radiating mode with the Mach number M for a fixed wall temperature $\bar{T}_w = 3$ ($r_c = 0.427$).

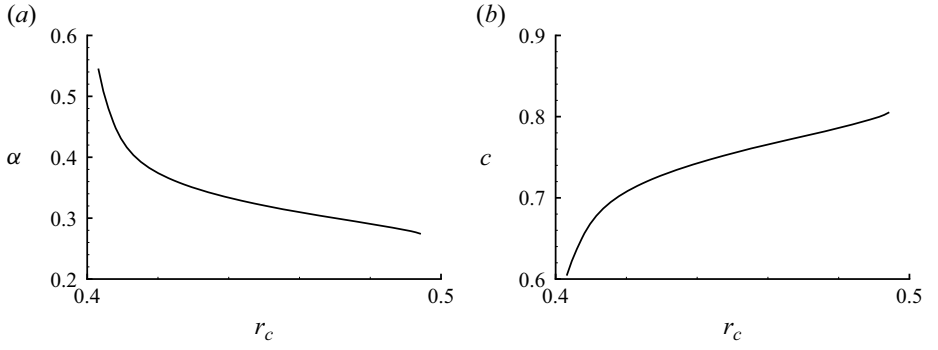

Figure 4. Variation of the wavenumber α (a) and the phase speed c (b) of the neutral radiating mode with the cooling ratio r_c for a fixed Mach number $M = 6$.

3. Reflection of impinging sound waves

In this section, we consider the reflection of an impinging slow acoustic wave by a supersonic boundary layer. The ensuing response is described by a double-layered structure consisting of the main layer and a critical layer, as is shown in figure 5.

3.1. *Main layer*

In the main layer, where $y = O(1)$, the disturbance expands as

$$(\tilde{\rho}, \tilde{u}, \tilde{v}, \tilde{p}, \tilde{\theta}) = \epsilon_s(\check{\rho}_s(x_3, y), \check{u}_s(x_3, y), \check{v}_s(x_3, y), \check{p}_s(x_3, y), \check{\theta}_s(x_3, y))E_s + \text{c.c.} + \cdots, \tag{3.1}$$

where $E_s = \exp(\mathrm{i}\alpha_s(x - c_s t))$, and the dependence on x_3 is parametric. Substitution of (3.1) into (2.2) followed by linearisation yields the equations

$$\mathrm{i}\alpha_s(\bar{U} - c_s)\check{\rho}_s + \bar{R}'\check{v}_s + \bar{R}(\mathrm{i}\alpha_s\check{u}_s + \check{v}_{s,y}) = 0, \tag{3.2a}$$

$$\mathrm{i}\alpha_s(\bar{U} - c_s)\check{u}_s + \bar{U}'\check{v}_s = -\mathrm{i}\alpha_s\bar{T}\check{p}_s, \tag{3.2b}$$

$$\mathrm{i}\alpha_s(\bar{U} - c_s)\check{v}_s = -\bar{T}\check{p}_{s,y}, \tag{3.2c}$$

$$\mathrm{i}\alpha_s(\bar{U} - c_s)\check{\theta}_s + \bar{T}'\check{v}_s = \mathrm{i}\alpha_s(\gamma - 1)M^2(\bar{U} - c_s)\bar{T}\check{p}_s, \tag{3.2d}$$

$$\gamma M^2\check{p}_s = \bar{R}\check{\theta}_s + \bar{T}\check{\rho}_s, \tag{3.2e}$$

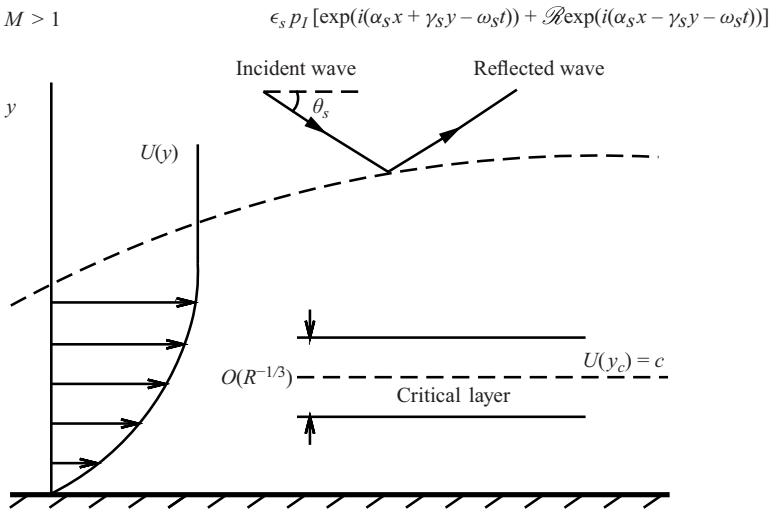

Figure 5. A sketch of the reflection of sound waves by the boundary layer.

where the prime '$\prime$' in the base-flow quantities denotes the partial differentiation with respect to y. Elimination of $\check{\rho}_s$, $\check{u}_s$, $\check{v}_s$ and $\check{\theta}_s$ leads to the compressible Rayleigh equation for pressure $\check{p}_s$

$$\check{p}_{s,yy} + \left(\frac{\bar{T}'}{\bar{T}} - \frac{2\bar{U}'}{\bar{U} - c_s}\right)\check{p}_{s,y} - \alpha_s^2\left[1 - \frac{M^2(\bar{U} - c_s)^2}{\bar{T}}\right]\check{p}_s = 0. \tag{3.3}$$

The above equation must be solved subject to the impermeability condition, $\check{p}_{s,y}(0) = 0$, as implied by (3.2c). In the far field, the pressure takes the form

$$\check{p}_s \sim p_I[\exp(\mathrm{i}\gamma_s y) + \mathscr{R}(x_3)\exp(-\mathrm{i}\gamma_s y)] \quad \text{as } y \to \infty, \tag{3.4}$$

which represents an incident wave and a reflected wave; here, $\gamma_s = \alpha_s\sqrt{M^2(1 - c_s)^2 - 1}$, and $\mathscr{R}$ is the reflection coefficient. The solution exhibits a singularity at the critical level $y_c(x_3)$, at which $\bar{U}(x_3, y_c) = c_s$. As $\tilde{\eta} \equiv y - y_c \to 0$, the local solution to (3.3) is constructed by using the Frobenius method as

$$\check{p}_s = a_s^{\pm}(x_3)\phi_{sa} + b_s^{\pm}(x_3)\left[\phi_{sb} + \frac{\alpha_s^2}{3}\left(\frac{\bar{T}_c'}{\bar{T}_c} - \frac{\bar{U}_c''}{\bar{U}_c'}\right)\ln|\tilde{\eta}|\phi_{sa}\right], \tag{3.5}$$

where

$$\phi_{sa} = \tilde{\eta}^3 + \chi_{sa}\tilde{\eta}^4 + \frac{1}{10}\left[3\left(\frac{\bar{T}_c'}{\bar{T}_c} - \frac{\bar{U}_c''}{\bar{U}_c'}\right)^2 - \frac{3}{2}\left(\frac{\bar{U}_c''}{\bar{U}_c'}\right)^2 + \frac{2\bar{U}_c'''}{\bar{U}_c'} - \frac{3\bar{T}_c''}{\bar{T}_c} + 3\left(\frac{\bar{T}_c'}{\bar{T}_c}\right)^2 + \alpha_s^2\right]\tilde{\eta}^5 + \cdots, \tag{3.6}$$

$$\phi_{sb} = 1 - \frac{\alpha_s^2}{2}\tilde{\eta}^2 + \chi_{sb}\tilde{\eta}^4 + \cdots, \tag{3.7}$$

with

$$\chi_{sa} = -\frac{3}{4}\left(\frac{\bar{T}_c'}{\bar{T}_c} - \frac{\bar{U}_c''}{\bar{U}_c'}\right), \tag{3.8}$$

$$\chi_{sb} = \frac{\alpha_s^2}{4}\left[\frac{\bar{T}_c''}{\bar{T}_c} - \left(\frac{\bar{T}_c'}{\bar{T}_c}\right)^2 + \frac{1}{2}\left(\frac{\bar{U}_c''}{\bar{U}_c'}\right)^2 - \frac{2}{3}\frac{\bar{U}_c'''}{\bar{U}_c'} - \frac{M^2(\bar{U}_c')^2}{\bar{T}_c} - \frac{\alpha_s^2}{2} + \frac{11}{12}\left(\frac{\bar{T}_c'}{\bar{T}_c} - \frac{\bar{U}_c''}{\bar{U}_c'}\right)^2\right]. \tag{3.9}$$

The pressure, velocities and temperature of the disturbance have the expressions

$$\check{p}_s = b_s^{\pm}\left[1 - \frac{\alpha_s^2}{2}\tilde{\eta}^2 + \frac{\alpha_s^2}{3}\left(\frac{\bar{T}_c'}{\bar{T}_c} - \frac{\bar{U}_c''}{\bar{U}_c'}\right)\tilde{\eta}^3\ln|\tilde{\eta}| + (a_s^{\pm}/b_s^{\pm})\tilde{\eta}^3\right] + O(\tilde{\eta}^4\ln|\tilde{\eta}|), \tag{3.10a}$$

$$\check{v}_s = -\mathrm{i}\alpha_s b_s^{\pm}\frac{\bar{T}_c}{\bar{U}_c'}\left[1 - \left(\frac{\bar{T}_c'}{\bar{T}_c} - \frac{\bar{U}_c''}{\bar{U}_c'}\right)\tilde{\eta}\ln|\tilde{\eta}| + \left(\frac{2}{3}\frac{\bar{T}_c'}{\bar{T}_c} - \frac{1}{6}\frac{\bar{U}_c''}{\bar{U}_c'} - \frac{3a_s^{\pm}}{\alpha_s^2 b_s^{\pm}}\right)\tilde{\eta}\right] + O(\tilde{\eta}^2\ln|\tilde{\eta}|), \tag{3.10b}$$

$$\check{u}_s = b_s^{\pm}\frac{\bar{T}_c}{\bar{U}_c'}\left[-\left(\frac{\bar{T}_c'}{\bar{T}_c} - \frac{\bar{U}_c''}{\bar{U}_c'}\right)\ln|\tilde{\eta}| + \frac{5}{6}\frac{\bar{U}_c''}{\bar{U}_c'} - \frac{1}{3}\frac{\bar{T}_c'}{\bar{T}_c} - \frac{3a_s^{\pm}}{\alpha_s^2 b_s^{\pm}}\right] + O(\tilde{\eta}\ln|\tilde{\eta}|), \tag{3.10c}$$

$$\check{\theta}_s = b_s^{\pm}\frac{\bar{T}_c\bar{T}_c'}{(\bar{U}_c')^2}\left[\frac{1}{\tilde{\eta}} - \left(\frac{\bar{T}_c'}{\bar{T}_c} - \frac{\bar{U}_c''}{\bar{U}_c'}\right)\ln|\tilde{\eta}|\right] + O(1). \tag{3.10d}$$

Clearly, the temperature perturbation $\check{\theta}_s$ has a simple-pole singularity, while the streamwise velocity $\check{u}_s$ exhibits a logarithmic singularity, indicating that the main-layer solution breaks down as $\tilde{\eta} \to 0$. Thus we need to analyse the critical layer.

3.2. *Critical layer*

By balancing the advection and viscous terms in the momentum or energy equation, we find the critical-layer thickness $\delta = O(R^{-1/3})$. Then taking $\delta = R^{-1/3}$, we introduce an inner variable

$$Y = (y - y_c)/\delta. \tag{3.11}$$

In view of the inner limit of the outer expansion (3.10*a*)–(3.10*d*), the inner expansion takes the form

$$\tilde{u} = \epsilon_s(\ln\delta U_{sl0} + U_{s1} + \cdots)E_s + \text{c.c.}, \tag{3.12a}$$

$$\tilde{v} = \epsilon_s(V_{s0} + \delta\ln\delta V_{sl0} + \delta V_{s1} + \cdots)E_s + \text{c.c.}, \tag{3.12b}$$

$$\tilde{p} = \epsilon_s(P_{s0} + \delta^2 P_{s1} + \delta^3\ln\delta P_{sl1} + \cdots)E_s + \text{c.c.}, \tag{3.12c}$$

$$\tilde{\theta} = \epsilon_s(\delta^{-1}\Theta_{s0} + \ln\delta\Theta_{sl0} + \Theta_{s1} + \cdots)E_s + \text{c.c.}. \tag{3.12d}$$

At leading order, the y-momentum equation gives $P_{s0,Y} = 0$, which implies $P_{s0} = P_{s0}(x_3)$. Matching with the main-layer solution leads to

$$b_s^+ = P_{s0} = b_s^- \equiv b_s. \tag{3.13}$$

The continuity, x-momentum and energy equations for the leading-order terms read $V_{s0,Y} = 0$, and

$$\bar{U}_c' V_{s0} = -\mathrm{i}\alpha_s \bar{T}_c P_{s0}, \tag{3.14a}$$

$$\mathrm{i}\alpha_s \bar{U}_c' Y \Theta_{s0} + \bar{T}_c' V_{s0} = \bar{T}_c \bar{\mu}_c Pr^{-1} \Theta_{s0,YY}, \tag{3.14b}$$

respectively. The solution is found to be

$$V_{s0} = -\mathrm{i}\alpha_s b_s \bar{T}_c / \bar{U}_c', \tag{3.15a}$$

$$\Theta_{s0} = \mathrm{i}\alpha_s \frac{\bar{T}_c \bar{T}_c'}{\bar{U}_c'} b_s \int_0^\infty \exp(-s_{sp}\xi^3 - \mathrm{i}\alpha_s \bar{U}_c' Y \xi)\,\mathrm{d}\xi \quad \text{with } s_{sp} = \tfrac{1}{3}(\alpha_s \bar{U}_c')^2 \bar{T}_c \bar{\mu}_c Pr^{-1}. \tag{3.15b}$$

It is found that the logarithm terms match their counterparts in the outer solution automatically. At the next order, the continuity and x-momentum equations yield

$$\mathrm{i}\alpha_s \bar{U}_c' Y(-\Theta_{s0}/\bar{T}_c^2) + (\mathrm{i}\alpha_s U_{s1} + V_{s1,Y})/\bar{T}_c - (\bar{T}_c'/\bar{T}_c^2) V_{s0} = 0, \tag{3.16a}$$

$$\mathscr{L}_s U_{s1} + \bar{U}_c' V_{s1} + \bar{U}_c'' Y V_{s0} = -\mathrm{i}\alpha_s \bar{T}_c' Y P_{s0} + \bar{T}_c \bar{U}_c' \bar{\mu}_c' \Theta_{s0,Y}, \tag{3.16b}$$

where $\bar{\mu}_c' = (\mathrm{d}\bar{\mu}/\mathrm{d}\bar{T})|_{y=y_c}$, and the operator $\mathscr{L}_s$ is defined by

$$\mathscr{L}_s = \mathrm{i}\alpha_s \bar{U}_c' Y - \bar{T}_c \bar{\mu}_c \frac{\partial^2}{\partial Y^2}. \tag{3.17}$$

Eliminating V_{s1} in the above two equations, and solving the resulting equation, the solution is found to be

$$\begin{aligned} U_{s1,Y} = {} & \mathrm{i}\alpha_s \frac{\bar{T}_c'(\bar{T}_c \bar{\mu}_c' - \bar{\mu}_c Pr^{-1})}{\bar{\mu}_c(1 - Pr^{-1})} b_s \int_0^\infty [1 - \exp(-(s_{sp} - s_s)\xi^3)] \\ & \times \exp(-s_s\xi^3 - \mathrm{i}\alpha_s \bar{U}_c' Y \xi)\,\mathrm{d}\xi \\ & - \mathrm{i}\alpha_s \bar{T}_c \left(\frac{\bar{T}_c'}{\bar{T}_c} - \frac{\bar{U}_c''}{\bar{U}_c'}\right) b_s \int_0^\infty \exp(-s_s\xi^3 - \mathrm{i}\alpha_s \bar{U}_c' Y \xi)\,\mathrm{d}\xi, \end{aligned} \tag{3.18}$$

where $s_s = \frac{1}{3}(\alpha_s \bar{U}_c')^2 \bar{T}_c \bar{\mu}_c$. Matching U_{s1} with its outer counterpart (3.10c) determines the jump

$$a_s^+ - a_s^- = \frac{\alpha_s^2}{3}\left(\frac{\bar{T}_c'}{\bar{T}_c} - \frac{\bar{U}_c''}{\bar{U}_c'}\right) b_s \pi \mathrm{i}. \tag{3.19}$$

This jump is used together with the numerical method to obtain the reflection coefficient and boundary-layer response; the details are described in Appendix A.2.

3.3. *The reflection coefficient and boundary-layer response*

For each incident wave, we compute $\mathscr{R}$ and $\tilde{b}$, where $\tilde{b}$, introduced in (A16) as the ratio of the pressure amplitude in the critical layer to the amplitude of the incident wave, is a measure of the boundary-layer response. For the particular incident wave satisfying the resonant condition, $(\alpha_s, c_s) = (0.355, 0.723)$, it is found that $\mathscr{R} = 1.299 \times 10^7 + 5.140 \times 10^7\mathrm{i}$ and $\tilde{b} = 5.725 \times 10^7 - 7.032 \times 10^6\mathrm{i}$. They are numerically large, indeed practically infinite, indicating that the resonant over-reflection coincides with the onset of a neutral radiating mode.

Recalling that $\omega_s = \alpha_s c_s$ and (2.15), we can regard $|\mathscr{R}|$ and $|\tilde{b}|$ as functions of θ_s and ω_s. Figure 6(*a*,*b*) shows contours of $|\mathscr{R}|$ and $|\tilde{b}|$ in the θ_s–ω_s plane with increments $\Delta\theta_s = 0.1$ and $\Delta\omega_s = 10^{-3}$. For most frequencies and incident angles, the boundary-layer response $|\tilde{b}|$ is finite and indeed rather small, while the reflection coefficient remains almost unchanged around the value of unity, indicating that these reflected acoustic waves have roughly the same magnitude as that of incident ones, and the boundary layer does not play a role in the reflection process. A prominent feature is that there appear two long strips indicating a very steep gradient, one of which passes through the resonant point (52.987, 0.257), where the response becomes infinite. The reflection coefficient increases rapidly when approaching either of the two strips. To show further details of the strips, we compute contours of two small regions in the lower strip using a smaller increment, and the results are displayed in figure 6(*c*,*e*). The reflection coefficient soars to very large values for a narrow frequency band, resulting in elongated contours enclosing the resonant point. Strong over-reflection occurs for (θ_s, ω_s) in the strips. Similarly, $|\tilde{b}|$ acquires large values in the strips, as is shown by figure 6(*b*) and the enlarged views of the two selected zones (figure 6*d*,*f*). These imply that the incident wave facilitates transfer of a considerable amount of energy from the shear flow while the reflected wave absorbs a significant amount from it.

To show further the dependence of the boundary-layer response on the parameters, we plot the variations of the reflection coefficient $|\mathscr{R}|$ and response $|\tilde{b}|$ with frequency ω_s at different incident angles. Figure 7(*a*,*b*) depicts the variations of $|\mathscr{R}|$ and $|\tilde{b}|$ with ω_s at $\theta_s = 40^\circ$, respectively. Two sharp peaks appear at $\omega_s = 0.233$ and 0.614, which lie in the strips in the contours. In order to determine the nature of these peak values, calculations of the variations near the peaks are performed. The panels in figure 7(*a*,*b*) zoom into the range near $\omega_s = 0.233$ and 0.614. The sharp peaks turn out to be finite in these ranges. The peak values in the upper strip (the zoomed views near $\omega_s = 0.614$) are markedly smaller than those in the lower strip (the zoomed views near $\omega_s = 0.233$). Notably, the frequency range over which the peak varies in the upper strip is of $O(10^{-4})$, which is much smaller than $O(10^{-3})$ in the lower strip. Figure 7(*c*,*d*) plots the variations of $|\mathscr{R}|$ and $|\tilde{b}|$ with ω_s at $\theta_s = 52.987^\circ$, which is the resonant angle. Two sharp peaks at $\omega_s = 0.257$ and 0.702 are observed. As ω_s approaches 0.257 (the resonant frequency), $|\mathscr{R}|$ and $|\tilde{b}|$ become unbounded as is shown by enlarged views near $\omega_s = 0.257$, signalling the onset of resonance, while the zoomed views near $\omega_s = 0.702$ show the abrupt rise of $|\mathscr{R}|$ and $|\tilde{b}|$ to their peak values in the upper strip. Figure 7(*e*,*f*) shows the variations of $|\mathscr{R}|$ and $|\tilde{b}|$ with ω_s at $\theta_s = 61.4^\circ$. The patterns resemble those at $\theta_s = 40^\circ$.

4. Fundamental resonance

It was demonstrated in the previous section that, for the acoustic wave satisfying the resonant condition, resonant over-reflection takes place, with the reflected wave coinciding with a neutral radiating mode. We considered the response of the boundary layer at a fixed location to impinging waves of different frequencies and incident angles. In this setting, the resonance occurs for a specific pairing of ω_s and θ_s. An alternative view is to consider the response of the boundary layer at different x_3 to the same incident wave with a fixed ω_s and θ_s, and then the resonance takes place at a streamwise location $x_{3,s}$. In the vicinity of this position, the reflected wave evolves in the streamwise direction into the radiating mode. The generation and evolution of such a mode will be explored in this section. The excitation process is similar to the receptivity of T-S waves studied in Qin & Wu (2016), but the difference is that the present radiating mode is of inviscid nature and on the upper

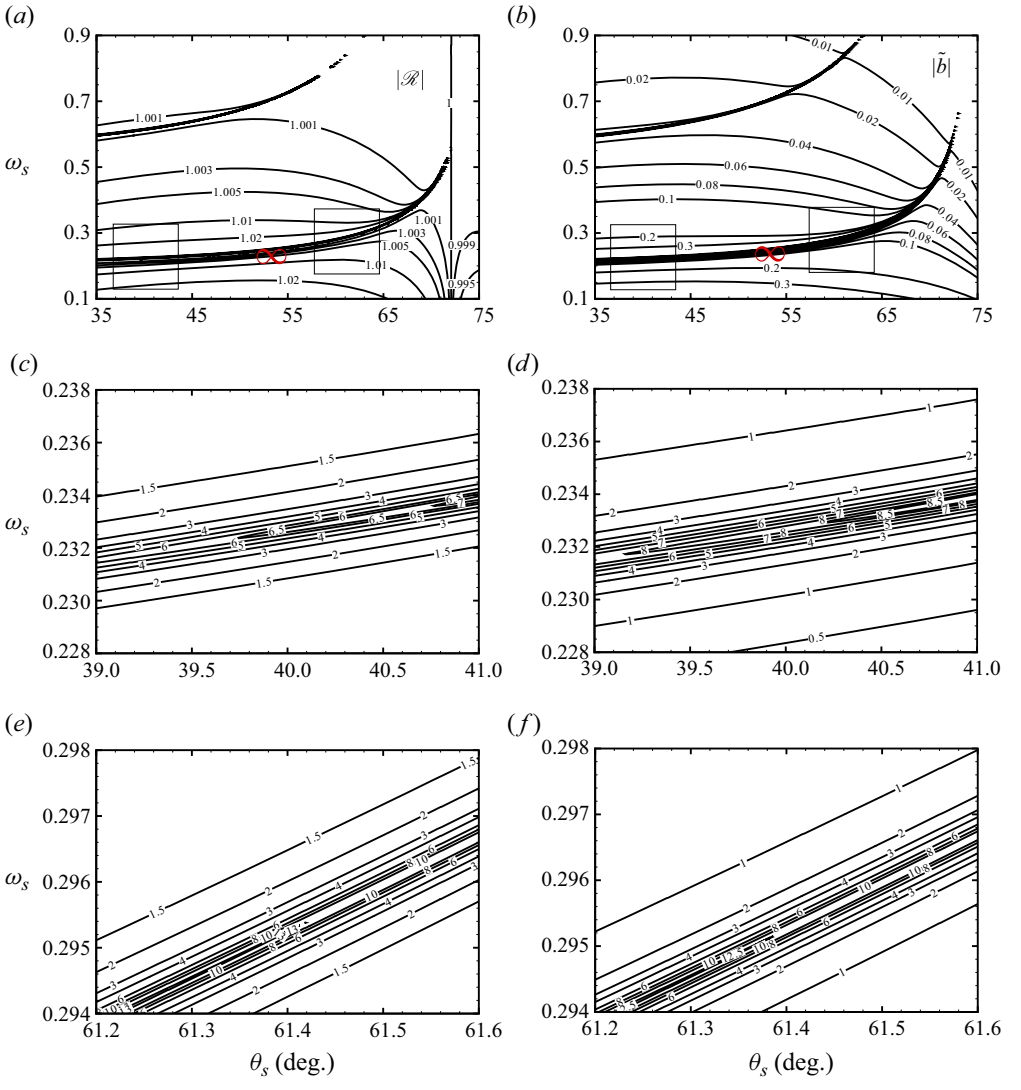

Figure 6. Contours of $|\mathscr{R}|$ (*a*) and $|\tilde{b}|$ (*b*) in the θ_s–ω_s plane. The resonant point is located at (52.987, 0.257). (*c*,*d*) Zoom into the range $39 < \theta_s < 41$. (*e*,*f*) Zoom into the range $61.2 < \theta_s < 61.6$.

(right) branch of the neutral curve, and thus has a critical layer, which is sensitive to nonlinear effects. The radiating mode locally excited is likely to develop nonlinearly on a relatively short length scale. Another fact is that a non-neutral radiating mode is likely to be present upstream of the resonance location, and when approaching the resonant (neutral) position, it is likely to have acquired, through the accumulated growth, a large enough amplitude to become nonlinear (Leib 1991; Wu 2019), while it is also influenced substantially by the incident sound. For locally excited and pre-existing radiating modes, the direct effect of the impinging sound can be accounted for by an appropriate amplitude equation of the mode, which is to be derived. Depending on the intensity of the acoustic wave, the critical-layer dynamics may be different. The excitation and evolution of the radiating mode in both the non-equilibrium parallel and equilibrium non-parallel regimes will be analysed in the following.

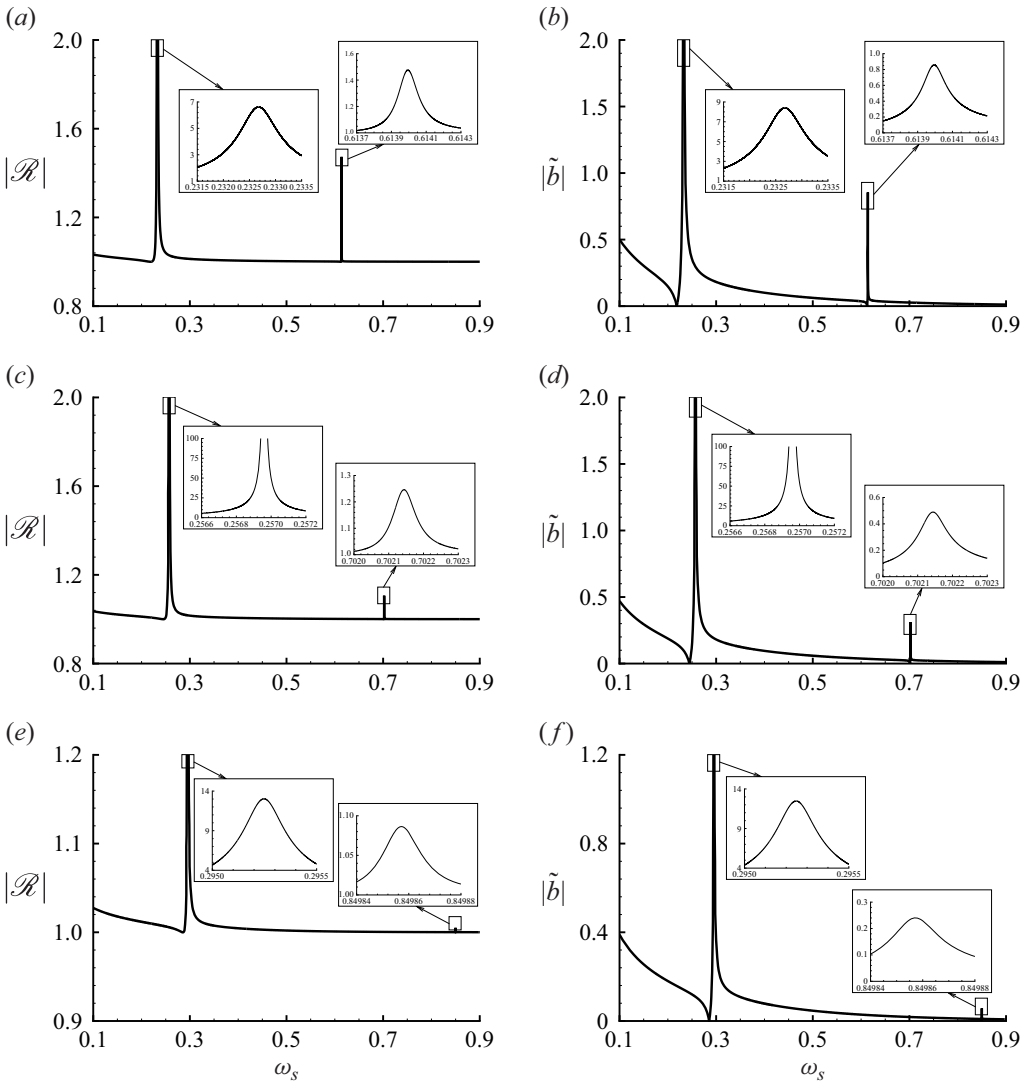

Figure 7. Variations of $|\mathscr{R}|$ and $|\tilde{b}|$ with ω_s at $\theta_s = 40^\circ$ (*a*,*b*), 52.987° (*c*,*d*) and 61.4° (*e*,*f*).

We note that nonlinear evolution and excitation were simultaneously included in the work by Hall & Smith (1982) on the T-S mode in an incompressible boundary layer forced by a moving wavy wall. There the focus was on the vicinity of the lower-branch neutral curve. Since the T-S wave upstream experiences considerable decay, the nonlinearity effect is associated with the locally excited mode, and is expected to be significant only if the external forcing is sufficiently strong.

4.1. *Non-equilibrium parallel regime*

The scaling argument in § 2.3.1 shows that the radiating mode evolves nonlinearly with the rate $\tilde{\mu} = \tilde{\epsilon}^{2/5}$ when its amplitude $\tilde{\epsilon} = O(R^{-5/6})$, and such a mode may be excited and/or affected by the incident sound of a much smaller magnitude $\tilde{\epsilon}_s = \tilde{\epsilon}\tilde{\mu} = O(R^{-7/6})$ due to resonance. Detuning effects may be included by allowing the wavenumber of the sound to

differ from that of the radiating mode by an $O(\tilde{\mu})$ amount, that is,

$$\alpha_s = \alpha + \tilde{\mu}\tilde{\alpha}_d, \quad \omega_s = \omega, \tag{4.1a,b}$$

where $\tilde{\alpha}_d$ is an $O(1)$ detuning parameter.

4.1.1. *Main layer*

In the main layer, the disturbance expands as

$$(\tilde{\rho}, \tilde{u}, \tilde{v}, \tilde{p}, \tilde{\theta}) = \tilde{\epsilon}_s\tilde{\mu}^{-1}[\tilde{A}(\tilde{x})(\hat{\rho}_0, \hat{u}_0, \hat{v}_0, \hat{p}_0, \hat{\theta}_0) + \tilde{\mu}(\hat{\rho}_1, \hat{u}_1, \hat{v}_1, \hat{p}_1, \hat{\theta}_1)]E + \text{c.c.} + \cdots, \tag{4.2}$$

where $E = \exp(\mathrm{i}\alpha(x - ct))$ is the carrier wave, and the first term represents a radiating mode, which may be locally excited and/or propagates from upstream with $\tilde{A}(\tilde{x})$ being its amplitude function. Substitution of (4.2) into (2.2) followed by linearisation yields the leading-order equations for the disturbance

$$\mathrm{i}\alpha(\bar{U} - c)\hat{\rho}_0 + \bar{R}'\hat{v}_0 + \bar{R}(\mathrm{i}\alpha\hat{u}_0 + \hat{v}_0') = 0, \tag{4.3a}$$

$$\mathrm{i}\alpha(\bar{U} - c)\hat{u}_0 + \bar{U}'\hat{v}_0 = -\mathrm{i}\alpha\bar{T}\hat{p}_0, \tag{4.3b}$$

$$\mathrm{i}\alpha(\bar{U} - c)\hat{v}_0 = -\bar{T}\hat{p}_0', \tag{4.3c}$$

$$\mathrm{i}\alpha(\bar{U} - c)\hat{\theta}_0 + \bar{T}'\hat{v}_0 = \mathrm{i}\alpha(\gamma - 1)M^2(\bar{U} - c)\bar{T}\hat{p}_0, \tag{4.3d}$$

$$\gamma M^2\hat{p}_0 = \bar{R}\hat{\theta}_0 + \bar{T}\hat{\rho}_0. \tag{4.3e}$$

Elimination of $\hat{\rho}_0$, $\hat{u}_0$, $\hat{v}_0$ and $\hat{\theta}_0$ leads to the familiar compressible Rayleigh equation (2.29) for the leading-order pressure $\hat{p}_0$. As $y \to \infty$,

$$\hat{p}_0 \sim \mathscr{C}_\infty \exp(-\mathrm{i}\alpha q y) \quad \text{with } q = \sqrt{M^2(1 - c)^2 - 1}, \tag{4.4}$$

which represents an outgoing wave that persists away from the main layer. Here, $\mathscr{C}_\infty$ is a constant that is determined by normalisation of the eigenfunction.

Let $\hat{\eta} \equiv y - y_c \to 0$, the solution near the critical level y_c is obtained using the Frobenius method as

$$\hat{p}_0 \sim \frac{\bar{U}_c'}{\bar{T}_c}\left\{\frac{\alpha^2}{3}a^{\pm}\phi_a + \phi_b + \frac{\alpha^2}{3}\left(\frac{\bar{T}_c'}{\bar{T}_c} - \frac{\bar{U}_c''}{\bar{U}_c'}\right)\ln|\hat{\eta}|\phi_a\right\}, \tag{4.5}$$

where ϕ_a and ϕ_b have the same expressions as ϕ_{sa} and ϕ_{sb} given by (3.6) and (3.7), respectively, with α replacing α_s. It follows from (4.3*b*)–(4.3*d*) that, as $\hat{\eta} \to 0$,

$$\hat{u}_0 \sim -\left(\frac{\bar{T}_c'}{\bar{T}_c} - \frac{\bar{U}_c''}{\bar{U}_c'}\right)\ln|\hat{\eta}| + \frac{5}{6}\frac{\bar{U}_c''}{\bar{U}_c'} - \frac{1}{3}\frac{\bar{T}_c'}{\bar{T}_c} - a^{\pm} + \cdots, \tag{4.6}$$

$$\hat{v}_0 \sim -\mathrm{i}\alpha\left\{1 - \left(\frac{\bar{T}_c'}{\bar{T}_c} - \frac{\bar{U}_c''}{\bar{U}_c'}\right)\hat{\eta}\ln|\hat{\eta}| + \left(\frac{2}{3}\frac{\bar{T}_c'}{\bar{T}_c} - \frac{1}{6}\frac{\bar{U}_c''}{\bar{U}_c'} - a^{\pm}\right)\hat{\eta} + \cdots\right\}, \tag{4.7}$$

$$\hat{\theta}_0 \sim \frac{\bar{T}_c'}{\bar{U}_c'\hat{\eta}}. \tag{4.8}$$

The temperature perturbation exhibits the same simple-pole singularity as that of an inflectional mode (Goldstein & Leib 1989), while the logarithmic singularity is present

only for a supersonic mode, whose critical level does not correspond to the generalised inflection point (Leib 1991). Equation (4.6) indicates a jump of $\hat{u}_0$

$$\hat{u}_0^+ - \hat{u}_0^- = -(a^+ - a^-) + \cdots . \tag{4.9}$$

At the next order, the second terms in the expansion (4.2), $(\hat{\rho}_1, \hat{u}_1, \hat{v}_1, \hat{p}_1, \hat{\theta}_1)$, are found to satisfy the inhomogeneous version of (4.3*a*)–(4.3*e*) (Qin 2024). By eliminating $\hat{\rho}_1$, $\hat{u}_1$, $\hat{v}_1$ and $\hat{\theta}_1$ from those equations, we can show that $\hat{p}_1$ satisfies an inhomogeneous Rayleigh equation (Wu 2005; Qin 2024)

$$\mathscr{L}\hat{p}_1 = \tilde{A}'\frac{2\mathrm{i}c}{\alpha}\left\{\frac{\bar{U}'\hat{p}_0'}{(\bar{U}-c)^2} + \frac{\alpha^2}{c}\left[\frac{M^2\bar{U}(\bar{U}-c)}{\bar{T}} - 1\right]\hat{p}_0\right\} - \bar{x}_1\tilde{A}\Delta_1, \tag{4.10}$$

where we have put

$$\begin{aligned}\Delta_1 = &\left\{\frac{2\bar{U}'}{\bar{U}-c}\left(\frac{\bar{U}_1}{\bar{U}-c} - \frac{\bar{U}_1'}{\bar{U}'}\right) + \frac{\bar{T}'}{\bar{T}}\left(\frac{\bar{T}_1'}{\bar{T}'} - \frac{\bar{T}_1}{\bar{T}}\right)\right\}\hat{p}_0' \\ &+ \alpha^2 M^2\frac{(\bar{U}-c)^2}{\bar{T}}\left(\frac{2\bar{U}_1}{\bar{U}-c} - \frac{\bar{T}_1}{\bar{T}}\right)\hat{p}_0.\end{aligned} \tag{4.11}$$

As $y \to \infty$, the incident acoustic wave must be included in the far-field boundary condition, which reads

$$\begin{aligned}\hat{p}_1 \sim\ & p_I \exp(\mathrm{i}\tilde{\alpha}_d\tilde{x})[\exp(\mathrm{i}\alpha q y) + \hat{\mathscr{R}}(\tilde{x})\exp(-\mathrm{i}\alpha q y)] \\ &+ q^{-1}[1 - M^2(1-c)]\mathscr{C}_\infty\tilde{A}' y\exp(-\mathrm{i}\alpha q y).\end{aligned} \tag{4.12}$$

On the other hand, by the method of dominant balance we deduce that, as $y \to y_c$,

$$\begin{aligned}\hat{p}_1 \sim\ & \frac{\alpha^2}{\bar{T}_c}\left(\frac{\mathrm{i}c}{\alpha}\tilde{A}' - \bar{U}_{1c}\bar{x}_1\tilde{A}\right)\left\{\hat{\eta} - \left(\frac{\bar{T}_c'}{\bar{T}_c} - \frac{\bar{U}_c''}{\bar{U}_c'}\right)\hat{\eta}^2\ln|\hat{\eta}|\right. \\ &\left. - \left[a^\pm + \frac{1}{3}\left(\frac{\bar{T}_c'}{\bar{T}_c} - \frac{\bar{U}_c''}{\bar{U}_c'}\right)\right]\hat{\eta}^2 + \frac{1}{3}j\hat{\eta}^3\ln|\hat{\eta}|\right\} + \frac{\bar{U}_c'}{\bar{T}_c}(\mathrm{i}\alpha\tilde{A}')\hat{\eta}^2 \\ &+ \left(\frac{\alpha^2\bar{U}_c'}{3\bar{T}_c}\bar{x}_1\tilde{A}\right)j_1\hat{\eta}^3\ln|\hat{\eta}| + c^\pm\phi_a + d\left[\phi_b + \frac{\alpha^2}{3}\left(\frac{\bar{T}_c'}{\bar{T}_c} - \frac{\bar{U}_c''}{\bar{U}_c'}\right)\ln|\hat{\eta}|\phi_a\right],\end{aligned} \tag{4.13}$$

where $c^\pm$ and d are arbitrary functions of $\tilde{x}$, and the constants, j and j_1, have the expressions

$$j = \frac{\bar{T}_c''}{\bar{T}_c} - \frac{\bar{U}_c'''}{\bar{U}_c'} - \left(\frac{\bar{T}_c'}{\bar{T}_c}\right)^2 + \left(\frac{\bar{U}_c''}{\bar{U}_c'}\right)^2 + 3\left(\frac{\bar{T}_c'}{\bar{T}_c} - \frac{\bar{U}_c''}{\bar{U}_c'}\right)^2 - 2\left(\frac{\bar{T}_c'}{\bar{T}_c} - \frac{\bar{U}_c''}{\bar{U}_c'}\right)\frac{\bar{U}_c'}{\bar{U}_c}, \tag{4.14}$$

$$j_1 = \frac{\bar{T}_c'}{\bar{T}_c}\left(\frac{\bar{T}_{1c}'}{\bar{T}_c'} - \frac{\bar{T}_{1c}}{\bar{T}_c}\right) + \frac{\bar{U}_c''}{\bar{U}_c'}\left(\frac{\bar{U}_{1c}'}{\bar{U}_c'} - \frac{\bar{U}_{1c}''}{\bar{U}_c''}\right) - 2\left(\frac{\bar{T}_c'}{\bar{T}_c} - \frac{\bar{U}_c''}{\bar{U}_c'}\right)\frac{\bar{U}_{1c}}{\bar{U}_c}. \tag{4.15}$$

It follows from the x- and y-momentum equations that

$$\hat{u}_1 = -\frac{\bar{T}}{\bar{U}-c}\hat{p}_1 - \frac{\bar{T}\bar{U}'}{\alpha^2(\bar{U}-c)^2}\hat{p}_{1,y} + \cdots . \tag{4.16}$$

Thus, the jump of $\hat{u}_1$ is found to relate to $(c^+ - c^-)$ by the equation

$$\hat{u}_1^+ - \hat{u}_1^- = -\frac{3\bar{T}_c}{\alpha^2 \bar{U}_c'}(c^+ - c^-) + \cdots . \tag{4.17}$$

In order for the inhomogeneous equation (4.10) to have an acceptable solution, it has to satisfy a solvability condition. This can be derived by multiplying both sides of (4.10) by $\hat{p}_0 \bar{T}/(\bar{U}-c)^2$ and integrating from 0 to ∞, leading to

$$-\frac{\bar{T}}{(\bar{U}-c)^2}[(\hat{p}_0\hat{p}_{1,y} - \hat{p}_0'\hat{p}_1)|_{y\to y_c^-}^{y\to y_c^+} - (\hat{p}_0\hat{p}_{1,y} - \hat{p}_0'\hat{p}_1)|_{y=\infty}] = \frac{2\mathrm{i}c}{\alpha} I_2 \tilde{A}' - I_1 \bar{x}_1 \tilde{A}, \tag{4.18}$$

where use has been made of the impermeability condition $\hat{p}_0'(0) = \hat{p}_{1,y}|_{y=0} = 0$, and

$$I_1 = \int_0^\infty \left\{ \left[\frac{2\bar{U}'}{\bar{U}-c}\left(\frac{\bar{U}_1}{\bar{U}-c} - \frac{\bar{U}_1'}{\bar{U}'}\right) + \frac{\bar{T}'}{\bar{T}}\left(\frac{\bar{T}_1'}{\bar{T}'} - \frac{\bar{T}_1}{\bar{T}}\right)\right] \frac{\bar{T}\hat{p}_0\hat{p}_0'}{(\bar{U}-c)^2} + \alpha^2 M^2 \left(\frac{2\bar{U}_1}{\bar{U}-c} - \frac{\bar{T}_1}{\bar{T}}\right)\hat{p}_0^2 \right\} \mathrm{d}y, \tag{4.19}$$

$$I_2 = \int_0^\infty \left\{ \frac{\bar{T}\bar{U}'\hat{p}_0\hat{p}_0'}{(\bar{U}-c)^4} + \frac{\alpha^2}{c}\left[\frac{M^2\bar{U}}{\bar{U}-c} - \frac{\bar{T}}{(\bar{U}-c)^2}\right]\hat{p}_0^2 \right\} \mathrm{d}y. \tag{4.20}$$

It should be noted that both sides of (4.18) contain singular terms, which turn out to be of the same form, and hence are cancelled out in such a manner that the integrals I_1 and I_2 are interpreted as Hadamard finite parts. By applying the far-field condition (4.4) and (4.12), we obtain

$$\frac{1}{\bar{U}_c'}\left\{3(c^+ - c^-) - \frac{2\alpha^2}{\bar{T}_c}\left(\frac{\mathrm{i}c}{\alpha}\tilde{A}' - \bar{U}_{1c}\bar{x}_1\tilde{A}\right)\left(\frac{\bar{T}_c'}{\bar{T}_c} - \frac{\bar{U}_c''}{\bar{U}_c'}\right)(a^+ - a^-) - \alpha^2 d(a^+ - a^-)\right\} - \frac{2\mathrm{i}\alpha q \mathscr{C}_\infty}{(1-c)^2} p_I \exp(\mathrm{i}\tilde{\alpha}_d \tilde{x}) = -\left(\frac{2\mathrm{i}c}{\alpha} I_2 \tilde{A}' - I_1 \bar{x}_1 \tilde{A}\right). \tag{4.21}$$

The jumps $(a^+ - a^-)$ and $(c^+ - c^-)$ will be determined by analysing the critical-layer dynamics.

4.1.2. *Critical layer*

The singularity of the main-layer solution is to be removed by introducing the non-equilibrium and viscous effects within the critical layer, which determine the critical-layer width to be $O(\tilde{\epsilon}^{2/5})$, and so the appropriate local transverse coordinate is

$$Y = (y - y_c)/\tilde{\epsilon}^{2/5}. \tag{4.22}$$

The asymptote of the inviscid solution, (4.5) and (4.6)–(4.8), suggests that the perturbation in the critical layer expands as

$$\tilde{u} = \tilde{\epsilon}_s \tilde{\mu}^{-1}(U_1 E + \tilde{\epsilon}^{1/5} U_M + \tilde{\epsilon}^{2/5} U_2 E) + \text{c.c.} + \cdots , \tag{4.23a}$$

$$\tilde{v} = \tilde{\epsilon}_s \tilde{\mu}^{-1}(V_0 E + \tilde{\epsilon}^{2/5} V_1 E + \tilde{\epsilon}^{3/5} V_M + \tilde{\epsilon}^{4/5} V_2 E) + \text{c.c.} + \cdots , \tag{4.23b}$$

$$\tilde{p} = \tilde{\epsilon}_s \tilde{\mu}^{-1}(P_0 E + \tilde{\epsilon}^{2/5} P_1 E + \tilde{\epsilon}^{4/5} P_2 E) + \text{c.c.} + \cdots , \tag{4.23c}$$

$$\tilde{\theta} = \tilde{\epsilon}_s \tilde{\mu}^{-1} \tilde{\epsilon}^{-2/5}(\Theta_1 E + \tilde{\epsilon}^{1/5} \Theta_M + \tilde{\epsilon}^{2/5} \Theta_2 E) + \text{c.c.} + \cdots . \tag{4.23d}$$

Strictly speaking, the expansions actually contain logarithm terms, but they are not needed in the calculation of the jumps and hence are not written out for brevity. Substituting (4.23) into (2.2), we then obtain the equations governing the terms at different orders in the expansion.

At leading order, inspection of the x- and y-momentum equations gives

$$P_0 = (\bar{U}_c'/\bar{T}_c)\tilde{A}, \quad V_0 = -\mathrm{i}\alpha\tilde{A}. \tag{4.24a,b}$$

Expansion of the energy equation shows that

$$\mathscr{L}_p\Theta_1 + \bar{T}_c'V_0 = 0, \tag{4.25}$$

with the operator $\mathscr{L}_p$ being defined by

$$\mathscr{L}_p = c\frac{\partial}{\partial\tilde{x}} + \mathrm{i}\alpha(\bar{U}_c'Y + \bar{U}_{1c}\bar{x}_1) - \lambda\bar{T}_c\bar{\mu}_c Pr^{-1}\frac{\partial^2}{\partial Y^2}. \tag{4.26}$$

Equation (4.25) is solved by use of Fourier transform to give

$$\Theta_1 = \mathrm{i}\alpha\bar{T}_c'\int_0^\infty \exp(-s_p\xi^3 - \mathrm{i}\alpha\bar{U}_c'\bar{Y}\xi)\tilde{A}(\tilde{x} - c\xi)\,\mathrm{d}\xi, \tag{4.27}$$

where we have put $\bar{Y} \equiv Y + (\bar{U}_{1c}/\bar{U}_c')\bar{x}_1$ and $s_p = \frac{1}{3}\lambda(\alpha\bar{U}_c')^2\bar{T}_c\bar{\mu}_c Pr^{-1}$.

At the next order, expansion of the continuity and x-momentum equations yields

$$-c\Theta_{1,\tilde{x}}/\bar{T}_c^2 + \mathrm{i}\alpha(\bar{U}_c'Y + \bar{U}_{1c}\bar{x}_1)(-\Theta_1/\bar{T}_c^2) + \frac{1}{\bar{T}_c}(\mathrm{i}\alpha U_1 + V_{1,Y}) - \frac{\bar{T}_c'}{\bar{T}_c^2}V_0 = 0, \tag{4.28a}$$

$$\begin{aligned}\mathscr{L}_\mu U_1 + \bar{U}_c'V_1 + (\bar{U}_c''Y + \bar{U}_{1c}'\bar{x}_1)V_0 = {}& -\mathrm{i}\alpha\bar{T}_cP_1 - \bar{T}_cP_{0,\tilde{x}} - \mathrm{i}\alpha(\bar{T}_c'Y + \bar{T}_{1c}\bar{x}_1)P_0 \\ & + \lambda\bar{T}_c\bar{\mu}_c'\bar{U}_c'\Theta_{1,Y},\end{aligned} \tag{4.28b}$$

where $\mathscr{L}_\mu$ is the same as $\mathscr{L}_p$ provided that Pr is set to unity. The above two equations can be combined to obtain an equation for $U_{1,Y}$, which is solved to give

$$\begin{aligned}U_{1,Y} = {}& \mathrm{i}\alpha\bar{U}_c'\frac{\bar{T}_c'(\bar{T}_c\bar{\mu}_c' - \bar{\mu}_cPr^{-1})}{\bar{T}_c\bar{\mu}_c(1 - Pr^{-1})}\int_0^\infty [1 - \exp(-(s_p - s)\xi^3)] \\ & \times \exp(-s\xi^3 - \mathrm{i}\alpha\bar{U}_c'\bar{Y}\xi)\tilde{A}(\tilde{x} - c\xi)\,\mathrm{d}\xi \\ & - \mathrm{i}\alpha\bar{U}_c'\left(\frac{\bar{T}_c'}{\bar{T}_c} - \frac{\bar{U}_c''}{\bar{U}_c'}\right)\int_0^\infty \exp(-s\xi^3 - \mathrm{i}\alpha\bar{U}_c'\bar{Y}\xi)\tilde{A}(\tilde{x} - c\xi)\,\mathrm{d}\xi,\end{aligned} \tag{4.29}$$

where $s = \frac{1}{3}\lambda(\alpha\bar{U}_c')^2\bar{T}_c\bar{\mu}_c$. Matching U_1 with its outer counterpart determines the jump

$$a^+ - a^- = \left(\frac{\bar{T}_c'}{\bar{T}_c} - \frac{\bar{U}_c''}{\bar{U}_c'}\right)\pi\mathrm{i}. \tag{4.30}$$

The self-interaction of the fundamental mode at quadratic level generates a mean-flow distortion, which interacts in turn with the fundamental at cubic level. The analysis is presented in Appendix B. The key outcome is the nonlinear jump (B8). Inserting the jumps

(4.30) and (B8) into (4.21), we obtain the evolution equation for the amplitude function $\tilde{A}$ (cf. Leib 1991)

$$\tilde{A}'(\tilde{x}) = \sigma\bar{x}_1\tilde{A} + \Upsilon\int_0^\infty\int_0^\infty K(\xi,\eta)\tilde{A}(\tilde{x}-c\xi)\tilde{A}(\tilde{x}-c\xi-c\eta)\tilde{A}^*(\tilde{x}-2c\xi-c\eta)\,\mathrm{d}\eta\mathrm{d}\xi + \tilde{F}\exp(\mathrm{i}\tilde{\alpha}_d\tilde{x}), \tag{4.31}$$

where

$$\sigma = (-\mathrm{i}\alpha/c)\left\{I_1 + \frac{\alpha^2}{\bar{T}_c}\left[\frac{\bar{U}_{1c}}{\bar{U}_c'}\left(j - 2\left(\frac{\bar{T}_c'}{\bar{T}_c} - \frac{\bar{U}_c''}{\bar{U}_c'}\right)^2\right) - j_1\right]\pi\mathrm{i}\right\}/G, \tag{4.32}$$

$$\Upsilon = 2\pi\alpha^7(\bar{U}_c')^2\bar{T}_c'/(c\bar{T}_c^2G), \tag{4.33}$$

$$\tilde{F} = 2\alpha^2 q\mathscr{C}_\infty p_I/[c(1-c)^2G], \tag{4.34}$$

with

$$G = 2I_2 + \frac{\alpha^2}{\bar{T}_c\bar{U}_c'}\left[j - 2\left(\frac{\bar{T}_c'}{\bar{T}_c} - \frac{\bar{U}_c''}{\bar{U}_c'}\right)^2\right]\pi\mathrm{i}. \tag{4.35}$$

The amplitude equation (4.31) is inhomogeneous with the forcing representing the impact of the incident sound, and it describes both the excitation and evolution of the radiating mode.

4.1.3. *Nonlinear response*

Consider now the physical processes which are described by (4.31). The noise level in the conventional wind tunnel is of $O(10^{-3})$ (Masutti *et al.* 2012; Cerminara *et al.* 2019), but in flight conditions it can be one to two orders of magnitude lower (Schneider 2008, 2015). It is impossible to infer from the overall noise level the amplitude of a component, but just as a rule of thumb, we take $p_s = O(10^{-4})$. Recall that the pressure of the acoustic wave takes the form $p_s = \tilde{\epsilon}_s p_I\exp(\mathrm{i}(\alpha_s x + \gamma_s y - \omega_s t)) + \text{c.c.}$, and it follows that the rescaled amplitude of the incident sound

$$p_I = p_s/\tilde{\epsilon}_s = p_s/R^{-7/6} \approx 4.64\text{–}68.13, \tag{4.36}$$

for Reynolds numbers in the range of 10^4–10^5. Varying p_I in the above range with a fixed R alternatively corresponds to different p_s.

The inhomogeneous amplitude equation (4.31) admits an equilibrium solution of the form

$$\tilde{A} = A_e \equiv a_e\exp(\mathrm{i}\tilde{\alpha}_d\tilde{x}), \tag{4.37}$$

where a_e is a complex constant to be determined. This solution represents the nonlinear boundary-layer response to the incident sound. Substitution of (4.37) into (4.31) yields

$$(\mathrm{i}\tilde{\alpha}_d - \kappa_0)a_e = \bar{l}a_e|a_e|^2 + \tilde{F}, \tag{4.38}$$

where we have put $\kappa_0 = \sigma\bar{x}_1$, and

$$\bar{l} = \Upsilon\int_0^\infty\int_0^\infty K(\xi,\eta)\,\mathrm{d}\eta\mathrm{d}\xi. \tag{4.39}$$

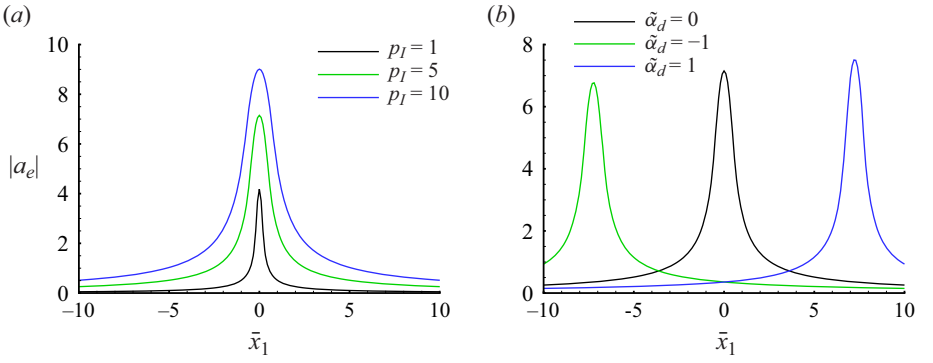

Figure 8. Effects of the forcing and detuning on the nonlinear response with $\lambda = 1$. (*a*) Effects of p_I on a_e with $\tilde{\alpha}_d = 0$. (*b*) Effects of $\tilde{\alpha}_d$ on a_e with $p_I = 5$.

On writing $a_e = |a_e|\,\mathrm{e}^{\mathrm{i}\phi}$ and $\tilde{F} = |\tilde{F}|\,\mathrm{e}^{\mathrm{i}\theta_F}$ $(-\pi < \theta_F \leq \pi)$, (4.38) becomes

$$(\mathrm{i}\tilde{\alpha}_d - \kappa_{0r} - \mathrm{i}\kappa_{0i})|a_e| = (\bar{l}_r + \mathrm{i}\bar{l}_i)|a_e|^3 + |\tilde{F}|\,\mathrm{e}^{\mathrm{i}\theta}, \tag{4.40}$$

where $\theta = \theta_F - \phi$. Separation of the real and imaginary parts gives

$$-\kappa_{0r}|a_e| - \bar{l}_r|a_e|^3 = |\tilde{F}|\cos\theta, \quad (\tilde{\alpha}_d - \kappa_{0i})|a_e| - \bar{l}_i|a_e|^3 = |\tilde{F}|\sin\theta. \tag{4.41a,b}$$

Eliminating θ leads to the response equation

$$(\bar{l}_r^2 + \bar{l}_i^2)b_e^3 + 2[\kappa_{0r}\bar{l}_r - \bar{l}_i(\tilde{\alpha}_d - \kappa_{0i})]b_e^2 + [\kappa_{0r}^2 + (\tilde{\alpha}_d - \kappa_{0i})^2]b_e - |\tilde{F}|^2 = 0, \tag{4.42}$$

where we have put $b_e = |a_e|^2 > 0$. From (4.41*a*,*b*), we obtain $\theta = \theta_0$ or $\theta = \theta_0 + \pi$, where

$$\theta_0 = \arctan\left[\frac{\bar{l}_i|a_e|^2 + \kappa_{0i} - \tilde{\alpha}_d}{\bar{l}_r|a_e|^2 + \kappa_{0r}}\right]. \tag{4.43}$$

The phase of the nonlinear response can be obtained as $\phi = \theta_F - \theta$.

The dependence of the nonlinear response on $\bar{x}_1$ for various values of p_I and $\tilde{\alpha}_d$ is shown in figure 8. The nonlinear response attains its maximum at some point, beyond which it decreases rapidly. The maximum value of $|a_e|$ increases with the sound magnitude p_I, indicating that sound waves of higher intensity induce larger boundary-layer response. Note that the response would have been infinite at a particular value of $\bar{x}_1 = \tilde{\alpha}_d/\sigma$ if nonlinearity were ignored, but remains finite in the presence of the latter, which plays a regularising role. For large p_I, a_e scales as $p_I^{1/3}$. Changing the detuning parameter $\tilde{\alpha}_d$ simply shifts the nonlinear response curve, but the overall behaviour remains almost the same. It should be noted that the equilibrium solution is only physically meaningful for $\bar{x}_1 < 0$ because when $\bar{x}_1 = O(R^{-1/3})$ and negative, the equilibrium solution evolves into the radiating mode as will be described in § 4.2.

4.1.4. *Effects on the linear growth rate*

In general, the solution to (4.31) can be written as

$$\tilde{A} = (a_e + A_0(\tilde{x}))\exp(\mathrm{i}\tilde{\alpha}_d\tilde{x}). \tag{4.44}$$

By substituting (4.44) into (4.31), we obtain

$$\begin{aligned} A_0'(\tilde{x}) = {} & (\kappa_0 - \mathrm{i}\tilde{\alpha}_d)A_0 + \Upsilon|a_e|^2 \int_0^\infty\!\!\int_0^\infty K(\xi,\eta)[A_0(\tilde{x}-c\xi) + A_0(\tilde{x}-c\xi-c\eta)]\,\mathrm{d}\eta\mathrm{d}\xi \\ & + \Upsilon a_e^2 \int_0^\infty\!\!\int_0^\infty K(\xi,\eta)A_0^*(\tilde{x}-2c\xi-c\eta)\,\mathrm{d}\eta\mathrm{d}\xi \\ & + \Upsilon a_e \int_0^\infty\!\!\int_0^\infty K(\xi,\eta)[A_0(\tilde{x}-c\xi) + A_0(\tilde{x}-c\xi-c\eta)]A_0^*(\tilde{x}-2c\xi-c\eta)\,\mathrm{d}\eta\mathrm{d}\xi \\ & + \Upsilon a_e^* \int_0^\infty\!\!\int_0^\infty K(\xi,\eta)A_0(\tilde{x}-c\xi)A_0(\tilde{x}-c\xi-c\eta)\,\mathrm{d}\eta\mathrm{d}\xi \\ & + \Upsilon \int_0^\infty\!\!\int_0^\infty K(\xi,\eta)A_0(\tilde{x}-c\xi)A_0(\tilde{x}-c\xi-c\eta)A_0^*(\tilde{x}-2c\xi-c\eta)\,\mathrm{d}\eta\mathrm{d}\xi. \end{aligned} \tag{4.45}$$

This may be viewed as describing the stability of the nonlinear response, but more appropriately as describing the instability of the boundary layer in the presence of the impinging sound, which now appears multiplicatively despite the fact that it originally enters as an additive term in (4.31).

Linearising the above equation, we have

$$\begin{aligned} A_0'(\tilde{x}) = {} & (\kappa_0 - \mathrm{i}\tilde{\alpha}_d)A_0 + \Upsilon|a_e|^2 \int_0^\infty\!\!\int_0^\infty K(\xi,\eta)[A_0(\tilde{x}-c\xi) + A_0(\tilde{x}-c\xi-c\eta)]\,\mathrm{d}\eta\mathrm{d}\xi \\ & + \Upsilon a_e^2 \int_0^\infty\!\!\int_0^\infty K(\xi,\eta)A_0^*(\tilde{x}-2c\xi-c\eta)\,\mathrm{d}\eta\mathrm{d}\xi. \end{aligned} \tag{4.46}$$

Let us seek a solution of the form

$$A_0 = A_{0r} + \mathrm{i}A_{0i}, \quad (A_{0r}, A_{0i}) = (a_r, a_i)\,\mathrm{e}^{\kappa\tilde{x}} + \text{c.c.}, \tag{4.47a,b}$$

where a_r and a_i are both complex constants. Then A_0 can be written as

$$A_0 = (a_r + \mathrm{i}a_i)\,\mathrm{e}^{\kappa\tilde{x}} + (a_r^* + \mathrm{i}a_i^*)\,\mathrm{e}^{\kappa^*\tilde{x}}. \tag{4.48}$$

Substitution of (4.48) into (4.46) and collection of terms proportional to $\mathrm{e}^{\kappa\tilde{x}}$ and $\mathrm{e}^{\kappa^*\tilde{x}}$ leads to the eigenvalue problem

$$\begin{aligned} & \begin{pmatrix} \kappa_{0r} + \Upsilon_r|a_e|^2\chi_0 + (\Upsilon a_e^2)_r\bar{\chi}_0 & -\kappa_{0i} + \tilde{\alpha}_d - \Upsilon_i|a_e|^2\chi_0 + (\Upsilon a_e^2)_i\bar{\chi}_0 \\ \kappa_{0i} - \tilde{\alpha}_d + \Upsilon_i|a_e|^2\chi_0 + (\Upsilon a_e^2)_i\bar{\chi}_0 & \kappa_{0r} + \Upsilon_r|a_e|^2\chi_0 - (\Upsilon a_e^2)_r\bar{\chi}_0 \end{pmatrix} \begin{pmatrix} a_r \\ a_i \end{pmatrix} \\ & = \kappa \begin{pmatrix} a_r \\ a_i \end{pmatrix}, \end{aligned} \tag{4.49}$$

where we have put

$$\begin{aligned} \chi_0 &= \int_0^\infty\!\!\int_0^\infty K(\xi,\eta)(\exp(-\kappa c\xi) + \exp(-\kappa c\xi - \kappa c\eta))\,\mathrm{d}\eta\mathrm{d}\xi \\ &= \int_0^\infty [K_0(\xi) + K_1(\xi)]\exp(-2s\xi^3 - \kappa c\xi)\,\mathrm{d}\xi, \end{aligned} \tag{4.50}$$

$$\bar{\chi}_0 = \int_0^\infty\int_0^\infty K(\xi,\eta)\exp(-2\kappa c\xi - \kappa c\eta)\,\mathrm{d}\eta\mathrm{d}\xi = \int_0^\infty K_1(\xi)\exp(-2s\xi^3 - 2\kappa c\xi)\,\mathrm{d}\xi; \tag{4.51}$$

here, K_0 and K_1 are given by

$$\left.\begin{aligned} K_0 &= \left(\frac{1}{3s}+\frac{1}{3s_p}\right)\exp(-(s_p-s)\xi^3) + \frac{\bar{T}_c}{\bar{T}_c'}\left(\frac{\bar{T}_c'}{\bar{T}_c}-\frac{\bar{U}_c''}{\bar{U}_c'}\right)\frac{1}{3s} \\ &\quad -\frac{\bar{T}_c\bar{\mu}_c' - \bar{\mu}_c Pr^{-1}}{\bar{\mu}_c(1-Pr^{-1})}\left[\frac{1}{3s}-\frac{1}{3s_p}\exp(-2(s_p-s)\xi^3)\right], \\ K_1 &= \left(\frac{\xi^2}{3s\xi^2+\kappa c}+\frac{\xi^2}{3s_p\xi^2+\kappa c}\right)\exp(-(s_p-s)\xi^3) + \frac{\bar{T}_c}{\bar{T}_c'}\left(\frac{\bar{T}_c'}{\bar{T}_c}-\frac{\bar{U}_c''}{\bar{U}_c'}\right)\frac{\xi^2}{3s\xi^2+\kappa c} \\ &\quad -\frac{\bar{T}_c\bar{\mu}_c' - \bar{\mu}_c Pr^{-1}}{\bar{\mu}_c(1-Pr^{-1})}\left[\frac{\xi^2}{3s\xi^2+\kappa c}-\frac{\xi^2}{3s_p\xi^2+\kappa c}\exp(-2(s_p-s)\xi^3)\right]. \end{aligned}\right\} \tag{4.52}$$

The requirement that a_r and a_i are non-vanishing gives the characteristic equation for the modified growth rate

$$\mathcal{F} \equiv (\kappa - \Upsilon_r|a_e|^2\chi_0 - \kappa_{0r})^2 + (\Upsilon_i|a_e|^2\chi_0 + \kappa_{0i} - \tilde{\alpha}_d)^2 - |\Upsilon a_e^2|^2\bar{\chi}_0^2 = 0. \tag{4.53}$$

The function $\mathcal{F}$ is real if κ is, and thus, if the equation $\mathcal{F}=0$ admits a complex root κ, so does its complex conjugate. The equation is solved numerically using Newton iteration. The corresponding eigenvector (a_r, a_i) is obtained from (4.49) and written as

$$a_r = a_0 a_{r0} \equiv |a_0||a_{r0}|\exp(\mathrm{i}(\theta_1+\phi_0)), \quad a_i = a_0 a_{i0} \equiv |a_0||a_{i0}|\exp(\mathrm{i}(\theta_2+\phi_0)), \tag{4.54a,b}$$

where (a_r, a_i) is normalised such that $|a_{r0}|^2 + |a_{i0}|^2 = 1$, and $a_0 = |a_0|\,\mathrm{e}^{\mathrm{i}\phi_0}$ is a complex constant. Thus the perturbation A_0 can be written as

$$A_0 = 2|a_0|\,\mathrm{e}^{\kappa_r\tilde{x}}[|a_{r0}|\cos(\kappa_i\tilde{x}+\theta_1+\phi_0) + \mathrm{i}|a_{i0}|\cos(\kappa_i\tilde{x}+\theta_2+\phi_0)]. \tag{4.55}$$

Figure 9 shows the effects of p_I on the modified growth rate κ_r. In general, κ_r is enhanced by the impinging sound, especially in the region where the nonlinear response is significant (cf. figure 8). As $\bar{x}_1 \to -\infty$, κ_r approaches the unperturbed growth rate κ_{0r}. The modified growth rate increases with p_I. Since the function $\mathcal{F}$ is real for real values of κ, it may admit real roots for certain parameters. Indeed, the solution changes from a complex conjugate pair to two real roots at certain positions with one being significantly larger than the other. These real roots are associated with the 'phase-locking' phenomenon, that is, we can write $A_0 = |\check{a}_0|\exp(\mathrm{i}\check{\phi}_0 + \kappa\tilde{x})$, where $\check{a}_0 = 2|a_0|[|a_{r0}|\cos(\theta_1+\phi_0) + \mathrm{i}|a_{i0}|\cos(\theta_2+\phi_0)] \equiv |\check{a}_0|\exp(\mathrm{i}\check{\phi}_0)$. Now the total amplitude $\tilde{A}$ can be expressed as $\tilde{A} = (|a_e|\,\mathrm{e}^{\mathrm{i}\phi} + |\check{a}_0|\exp(\mathrm{i}\check{\phi}_0 + \kappa\tilde{x}))\exp(\mathrm{i}\tilde{\alpha}_d\tilde{x})$, indicating that the phases of the nonlinear response and the perturbation are 'locked' in the sense that their difference is independent of $\tilde{x}$.

Figure 10 shows the variation of the modified growth rate with $\bar{x}_1$ for three values of $\tilde{\alpha}_d$. Altering $\tilde{\alpha}_d$ shifts the distribution of both κ_r and κ_i. Again, the complex roots κ develop into two branches of real roots in the region where the nonlinear response is large. All these results indicate that, for the parameters examined, the impinging sound enhances the linear growth rate substantially.

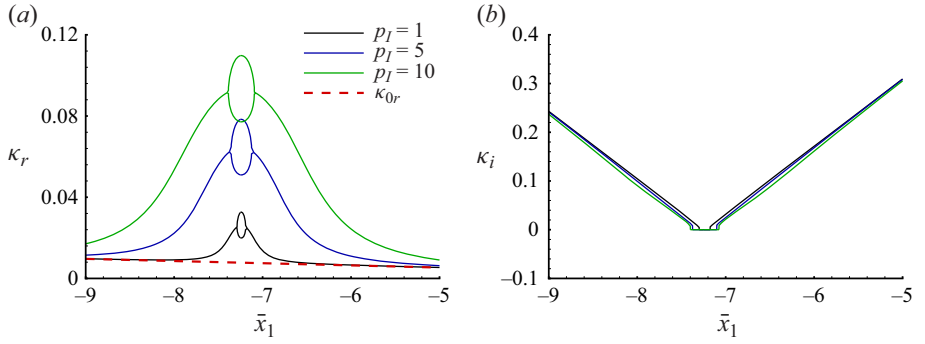

Figure 9. Effects of the forcing on the modified growth rate κ with $\tilde{\alpha}_d = -1$ and $\lambda = 1$: (*a*) κ_r and (*b*) κ_i. The dashed line represents the linear growth rate in the absence of the incident sound.

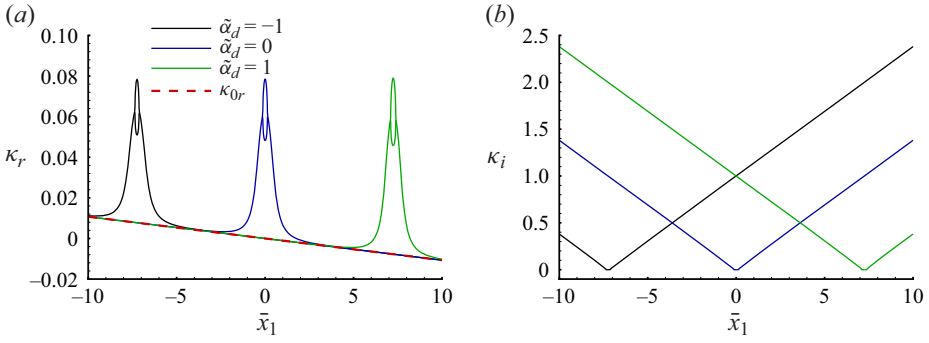

Figure 10. Effects of detuning on the modified growth rate κ with $p_I = 5$ and $\lambda = 1$: (*a*) κ_r and (*b*) κ_i. The dashed line represents the linear growth rate in the absence of the incident sound.

4.1.5. *Nonlinear evolution*

We proceed to consider the effect of the impinging sound on the nonlinear development by solving numerically the nonlinear amplitude equation (4.45), subject to the appropriate initial condition (4.55) as $\tilde{x} \to -\infty$. The sixth-order Adams–Moulton method is used, and the integral term is approximated by Simpson's rule. Results of the effects are shown in figure 11. The amplitude always develops into a singularity at some point. Increasing the intensity of the sound wave advances the blow-up behaviour (figure 11*a*). We also examine the effects of viscosity on the nonlinear development, which generally delays the occurrence of the finite-distance singularity (figure 11*b*), similar to what has been found in previous studies of free-mode evolution (Goldstein & Leib 1989; Wu *et al.* 1993).

4.2. *Equilibrium non-parallel regime*

As is shown in § 2.3.2, a sound influences nonlinearly the excitation and evolution of the radiating mode in the equilibrium regime when its magnitude $\bar{\epsilon}_s = \bar{\epsilon} R^{-1/2} = O(R^{-17/12})$, and its frequency/wavenumber is the same/close to those of the radiating mode, that is,

$$\omega_s = \omega, \quad \alpha_s = \alpha + R^{-1/2}\bar{\alpha}_d, \tag{4.56a,b}$$

where $\bar{\alpha}_d$ is an $O(1)$ detuning parameter. For $R = 10^4$–10^5, $\bar{p}_I = p_s/\bar{\epsilon}_s = p_s/R^{-17/12} \approx$ 46.4–1211.5.

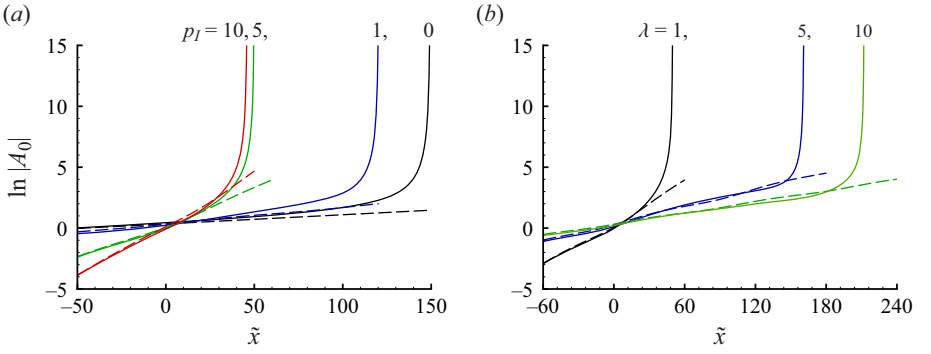

Figure 11. Effects of sound intensity and viscosity on the nonlinear evolution of the radiating mode. (*a*) Nonlinear development for different values of p_I with $\lambda = 1$. (*b*) Nonlinear development for different values of λ with $p_I = 5$. The dashed lines represent the corresponding linear solution (4.55). Here, we have taken $\bar{x}_1 = -7$, $\tilde{\alpha}_d = -1$ and $a_0 = 1$.

4.2.1. *The amplitude equation*

The analysis in the main layer is only slightly modified with expansion (4.2) being replaced by

$$(\tilde{\rho}, \tilde{u}, \tilde{v}, \tilde{p}, \tilde{\theta}) = \bar{\epsilon}_s R^{1/2}[\bar{A}(\bar{x})(\hat{\rho}_0, \hat{u}_0, \hat{v}_0, \hat{p}_0, \hat{\theta}_0) + R^{-1/2}(\hat{\rho}_1, \hat{u}_1, \hat{v}_1, \hat{p}_1, \hat{\theta}_1)]E + \text{c.c.} + \cdots . \tag{4.57}$$

The corresponding solvability condition (4.21) becomes

$$\frac{1}{\bar{U}_c'}\left\{3(c^+ - c^-) - \frac{2\alpha^2}{\bar{T}_c}\left(\frac{\mathrm{i}c}{\alpha}\bar{A}' - \bar{U}_{1c}\bar{x}\bar{A}\right)\left(\frac{\bar{T}_c'}{\bar{T}_c} - \frac{\bar{U}_c''}{\bar{U}_c'}\right)(a^+ - a^-) - \alpha^2 d(a^+ - a^-)\right\}$$
$$- \frac{2\mathrm{i}\alpha q\mathscr{C}_\infty}{(1-c)^2}\bar{p}_I \exp(\mathrm{i}\bar{\alpha}_d\bar{x}) = -\left(\frac{2\mathrm{i}c}{\alpha}I_2\bar{A}' - I_1\bar{x}\bar{A}\right), \tag{4.58}$$

which corresponds to (4.21) but with the parameter $\bar{x}_1$ being replaced by variable $\bar{x}$. The jump $(a^+ - a^-)$ remains as (4.30), while $(c^+ - c^-)$ was given in Wu (2005) (see also Qin 2024), that is,

$$c^+ - c^- = \frac{1}{3}\frac{\alpha^2}{\bar{T}_c}\left(\frac{\mathrm{i}c}{\alpha}\bar{A}' - \bar{U}_{1c}\bar{x}\bar{A}\right)j\pi\mathrm{i} + \left(\frac{\alpha^2\bar{U}_c'}{3\bar{T}_c}\bar{x}\bar{A}\right)j_1\pi\mathrm{i}$$
$$+ d\frac{\alpha^2}{3}\left(\frac{\bar{T}_c'}{\bar{T}_c} - \frac{\bar{U}_c''}{\bar{U}_c'}\right)\pi\mathrm{i} + \frac{\Lambda}{3}\bar{A}|\bar{A}|^2, \tag{4.59}$$

where Λ is given by

$$\Lambda = -\frac{2\pi\mathrm{i}\alpha^4\bar{U}_c'}{3\bar{T}_c^2\bar{\mu}_c}\left\{\frac{\bar{T}_c'(\bar{T}_c\bar{\mu}_c' - \bar{\mu}_c Pr^{-1})}{\bar{T}_c\bar{\mu}_c(1 - Pr^{-1})}(Pr^{4/3} - 1) + \left(\frac{\bar{T}_c'}{\bar{T}_c} - \frac{\bar{U}_c''}{\bar{U}_c'}\right)\right.$$
$$\left. + \frac{\bar{T}_c'}{\bar{T}_c}(1 + Pr)^{2/3}(2Pr)^{1/3}\right\}(2s)^{-1/3}\Gamma\left(\frac{1}{3}\right), \tag{4.60}$$

with Γ denoting the gamma function and s being the same as that in (4.29) provided that λ is set to unity. Inserting (4.30) and (4.59) into (4.58), we obtain the amplitude equation

for $\bar{A}$,

$$\bar{A}'(\bar{x}) = \sigma\bar{x}\bar{A} + l\bar{A}|\bar{A}|^2 + \bar{F}\exp(\mathrm{i}\bar{\alpha}_d\bar{x}), \tag{4.61}$$

where σ is given in (4.32), $\bar{F} = \tilde{F}$ as given by (4.34) and

$$l = \mathrm{i}\alpha\Lambda/(c\bar{U}_c'G). \tag{4.62}$$

4.2.2. *The initial amplitude without oncoming free modes*

On dropping in (4.61) the nonlinear term, which is negligible in the upstream region, and solving the linear equation, the initial condition is specified as

$$\bar{A}(\bar{x}) = \exp(\sigma\bar{x}^2/2)\left[\breve{a}_0 + \bar{F}\int_0^{\bar{x}}\exp(\mathrm{i}\bar{\alpha}_d\tau - \sigma\tau^2/2)\,\mathrm{d}\tau\right] \quad \text{as } \bar{x}\to-\infty, \tag{4.63}$$

where $\breve{a}_0$ is an arbitrary constant. It should be noted that, although the first term is a complementary solution of the linearised version of (4.61), it does not represent a free oncoming mode. This is because the first term is exponentially small in the upstream region, whereas the second term is algebraically small, and when approximated asymptotically, the remainder contains the exponentially small term corresponding to the free mode. Therefore our immediate task is to determine the specific value of $\breve{a}_0$ such that the free mode is absent in the upstream region. This is achieved by using the idea of optimal truncation in asymptotic approximation.

For that purpose, we split the integration interval into $(0, \tau_0)$ and $(\tau_0, \bar{x})$ and perform integration by parts to the integral over the latter to obtain

$$\begin{aligned}\bar{A}(\bar{x}) = \exp(\sigma\bar{x}^2/2)\Bigg[\breve{a}_0 + \bar{F}\Bigg(&I_0 - \exp(\mathrm{i}\bar{\alpha}_d\tau_0 - \sigma\tau_0^2/2)\sum_{n=0}^{N}\frac{\sigma^n(-1)^n1\cdot3\cdot5\cdots(2n-1)}{(\mathrm{i}\bar{\alpha}_d - \sigma\tau_0)^{2n+1}}\\ &+ \exp(\mathrm{i}\bar{\alpha}_d\bar{x} - \sigma\bar{x}^2/2)\sum_{n=0}^{N}\frac{\sigma^n(-1)^n1\cdot3\cdot5\cdots(2n-1)}{(\mathrm{i}\bar{\alpha}_d - \sigma\bar{x})^{2n+1}}\\ &+ (-1)^N\int_{\bar{x}}^{\tau_0}\frac{\exp(\mathrm{i}\bar{\alpha}_d\tau - \sigma\tau^2/2)\sigma^{N+1}1\cdot3\cdot5\cdots(2N+1)}{(\mathrm{i}\bar{\alpha}_d - \sigma\tau)^{2N+2}}\,\mathrm{d}\tau\Bigg)\Bigg],\end{aligned} \tag{4.64}$$

where τ_0 is constant and

$$I_0 = \int_0^{\tau_0}\exp(\mathrm{i}\bar{\alpha}_d\tau - \sigma\tau^2/2)\,\mathrm{d}\tau. \tag{4.65}$$

The optimal truncation of the asymptotic expansion is the one that makes the remainder exponentially small by retaining the right number of terms, $N = N_{op}$, where N_{op} is the maximum number of terms whose size is monotonically decreasing for a fixed large negative $\bar{x}$, and is dependent of $\bar{x}$. The expression for N_{op} is determined as follows.

$\bar{\alpha}_d$	τ_0	$\bar{x}_\infty$	N_{op}	$\bar{a}_{op}/\bar{p}_I$
0	−15	−20	28	−0.18985 − 0.14595i
4	−15	−20	166	−0.01761 + 0.00208i

Table 1. The initial amplitude without oncoming free modes determined by the optimal truncation for $\bar{p}_I = 115.94$.

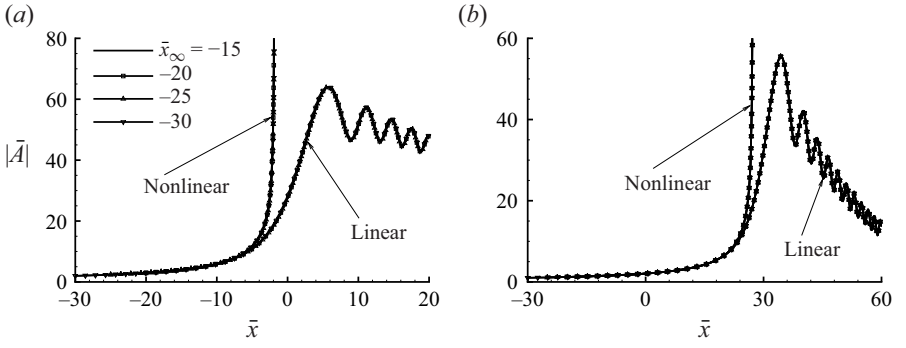

Figure 12. Linear and nonlinear evolution for $\bar{p}_I = 115.94$ starting from different upstream positions $\bar{x}_\infty$; (*a*) $\bar{\alpha}_d = 0$ and $\breve{a}_0 = -22.011 - 16.921\mathrm{i}$, (*b*) $\bar{\alpha}_d = 4$ and $\breve{a}_0 = -2.042 + 0.241\mathrm{i}$.

Let f_n be the nth term in (4.64). Then consider the ratio of the two consecutive terms

$$f_{n+1}/f_n = -\sigma(2n+1)/(\mathrm{i}\bar{\alpha}_d - \sigma\bar{x}_\infty)^2, \tag{4.66}$$

for a large $\bar{x} = \bar{x}_\infty$. If we require $|f_{n+1}/f_n| < 1$, then

$$n < (|(\mathrm{i}\bar{\alpha}_d - \sigma\bar{x}_\infty)^2/\sigma| - 1)/2. \tag{4.67}$$

Thus the terms in the expansion are in decreasing order for $n \le N_{op}$, where

$$N_{op} = [(|(\mathrm{i}\bar{\alpha}_d - \sigma\bar{x}_\infty)^2/\sigma| - 1)/2] + 1, \tag{4.68}$$

with $[I]$ representing the largest integer that is smaller than I; the magnitude of the terms with $n > N_{op}$ increases. With the optimal truncation, the remainder is made sufficiently small. The complementary solution would be absent if we choose $\breve{a}_0$ to be

$$\breve{a}_0 = \bar{a}_{op} \equiv -\bar{F}\left[I_0 - \exp(\mathrm{i}\bar{\alpha}_d\tau_0 - \sigma\tau_0^2/2)\sum_{n=0}^{N_{op}} \frac{\sigma^n(-1)^n 1\cdot 3\cdot 5\cdots(2n-1)}{(\mathrm{i}\bar{\alpha}_d - \sigma\tau_0)^{2n+1}}\right]. \tag{4.69}$$

The values of $\bar{a}_{op}$ calculated using (4.69) are listed in table 1 for $\bar{\alpha}_d = 0$ and 4. We evaluate the linear solution (4.63) and solve the nonlinear equation (4.61) with the initial condition being imposed at different upstream positions $\bar{x}_\infty$ with $\breve{a}_0 = \bar{a}_{op}$. As is shown in figure 12, the solutions starting from different $\bar{x}_\infty$ overlap each other, suggesting that the particular initial amplitude is independent of the upstream position; the initial condition with $\breve{a}_0 = \bar{a}_{op}$ represents solely the locally forced response.

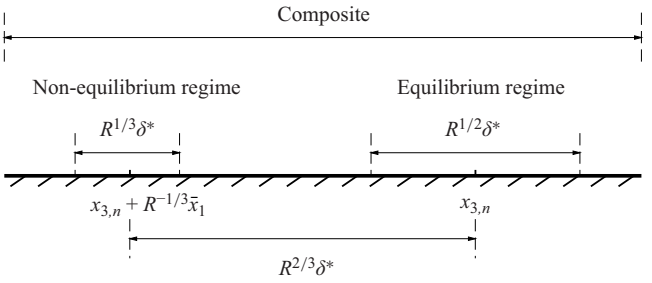

Figure 13. A sketch illustrating different evolution regimes.

5. Non-parallelism and the composite amplitude equation

Having obtained the amplitude equations in the non-equilibrium parallel and equilibrium non-parallel regimes, respectively, it is straightforward to construct a composite amplitude equation that accommodates both regimes. The respective validity regions and the associated length scales are shown in figure 13.

5.1. *Construction of the composite amplitude equation*

Recall that, in the equilibrium regime, the evolution occurs in the vicinity of the neutral position (figure 13)

$$x_3 = x_{3,n} + R^{-1/2}\bar{x} \quad \text{with } \bar{x} = O(1), \tag{5.1}$$

and the amplitude equation is (4.61) with $\bar{\alpha}_d$ being defined by (4.56*a*,*b*). On the other hand, in the non-equilibrium regime, where without loss of generality the Haberman parameter is taken to be $\lambda = 1$, the evolution occurs in the vicinity of the neutral position

$$x_3 \approx x_{3,n} + R^{-1/3}\bar{x}_1 \quad \text{with } \bar{x}_1 = O(1), \tag{5.2}$$

and the amplitude is governed by (4.31) with $\tilde{\alpha}_d$ being specified by (4.1*a*,*b*).

Let us first construct the composite solution starting from the non-equilibrium regime. Noting (2.18), i.e.

$$\tilde{x} = R^{2/3}(x_3 - (x_{3,n} + R^{-1/3}\bar{x}_1)), \tag{5.3}$$

we can approximate the base flow by

$$(\bar{U}(x_3, y), \bar{T}(x_3, y)) \approx (\bar{U}(x_{3,n}, y), \bar{T}(x_{3,n}, y)) + R^{-1/3}(\bar{U}_1(y), \bar{T}_1(y))(\bar{x}_1 + R^{-1/3}\tilde{x}). \tag{5.4}$$

Following Wu & Huerre (2009), we construct a composite amplitude equation by retaining the $O(R^{-2/3})$ term in (5.4) so that the first term on the right-hand side of (4.31) is modified to $\sigma(\bar{x}_1 + R^{-1/3}\tilde{x})$, and the carrier of the forcing becomes $\exp(\mathrm{i}\tilde{\alpha}_d(\tilde{x} + R^{1/3}\bar{x}_1 + R^{2/3}x_{3,n}))$. From (5.1) and (5.3) follows

$$\bar{x} = R^{1/6}\bar{x}_1 + R^{-1/6}\tilde{x}. \tag{5.5}$$

Note that, in the equilibrium regime, we expanded the perturbation as

$$p = \bar{\epsilon}_s R^{1/2}[\bar{A}(\bar{x})\hat{p}_0 + R^{-1/2}\hat{p}_1 + \cdots], \tag{5.6}$$

where

$$\bar{\epsilon}_s = R^{-17/12}, \quad \bar{p}_I = p_s/\bar{\epsilon}_s, \tag{5.7a,b}$$

whilst, in the non-equilibrium regime, we expand the perturbation as

$$p = \tilde{\epsilon}_s R^{1/3}[\tilde{A}(\tilde{x})\hat{p}_0 + R^{-1/3}\hat{p}_1 + \cdots], \tag{5.8}$$

where

$$\tilde{\epsilon}_s = R^{-7/6}, \quad p_I = p_s/\tilde{\epsilon}_s. \tag{5.9a,b}$$

Thus we have the relations $\bar{A}(\bar{x}) = R^{1/12}\tilde{A}(\tilde{x})$ and $\bar{p}_I = R^{1/4}p_I$ ($\bar{F} = R^{1/4}\tilde{F}$). On using these relations as well as (5.5), and noting $\bar{\alpha}_d = R^{1/6}\tilde{\alpha}_d$, the amplitude equation (4.31) is rewritten as

$$\bar{A}'(\bar{x}) = \sigma\bar{x}\bar{A} + \Upsilon R^{2/3}\int_0^\infty\int_0^\infty K(\xi,\eta;\bar{s})\bar{A}(\bar{x}-c\xi)\bar{A}(\bar{x}-c\xi-c\eta) \times \bar{A}^*(\bar{x}-2c\xi-c\eta)\,\mathrm{d}\eta\mathrm{d}\xi + \bar{F}\exp(\mathrm{i}\bar{\alpha}_d\bar{x}), \tag{5.10}$$

where $\bar{s} = sR^{1/2}$, and we have taken $x_{3,n} = 0$ without loss of generality.

The same composite amplitude equation may alternatively be constructed starting from the equilibrium regime by retaining the small non-equilibrium term in the critical-layer operator, which then becomes

$$R^{-1/6}c\frac{\partial}{\partial\bar{x}} + \mathrm{i}\alpha\bar{U}_c'Y - \bar{T}_c\bar{\mu}_c Pr^{-1}\frac{\partial^2}{\partial Y^2}. \tag{5.11}$$

In Appendix C, we show that the evolution problems in the equilibrium and non-equilibrium regimes can be properly recovered from the composite theory.

The initial condition of the composite amplitude equation (5.10) is obtained by neglecting the nonlinear term, leading to

$$\bar{A}(\bar{x}) = \breve{a}_0\exp(\sigma\bar{x}^2/2) + \bar{F}\exp(\sigma\bar{x}^2/2)\int_0^{\bar{x}}\exp(\mathrm{i}\bar{\alpha}_d\tau - \sigma\tau^2/2)\,\mathrm{d}\tau \quad \text{as } \bar{x}\to-\infty. \tag{5.12}$$

We can write $\breve{a}_0 = \bar{a}_{op} + \hat{a}_0$ so that the term $\hat{a}_0\exp(\sigma\bar{x}^2/2)$ represents the free mode.

5.2. *Effects of forcing and free modes*

We first solve the composite amplitude equation (5.10) without forcing (i.e. $\bar{F} = 0$). The results are shown in figure 14. For all the values of $\breve{a}_0$ examined, the numerical solution and the corresponding initial condition overlap as expected in the upstream linear phase. For small values of $\breve{a}_0$, the numerical solution remains linear in the entire course of the development. As the initial amplitude becomes larger, $\bar{A}$ amplifies faster than in the linear limit, suggesting that nonlinear effects enhance the growth of the free radiating mode before it attenuates. When $\breve{a}_0$ exceeds a threshold value, the solution blows up at a finite distance.

Next, we solve the composite amplitude equation (5.10) numerically for a range of forcing amplitude $\bar{p}_I$ with $\breve{a}_0$ taken to be $\breve{a}_0 = \bar{a}_{op}$ ($\hat{a}_0 = 0$), so that there is no oncoming free mode. Each solution represents the locally excited disturbance through resonance and describes its subsequent development into a radiating mode. The solutions are presented in figure 15. The corresponding linear solution (5.12), the solution to (4.61) in the equilibrium regime and the nonlinear response in the non-equilibrium regime (recast in terms of the coordinate of the composite theory, (C3)) are also plotted for comparison. For small values of $\bar{p}_I$, the perturbation remains weak that the solutions to the composite and equilibrium

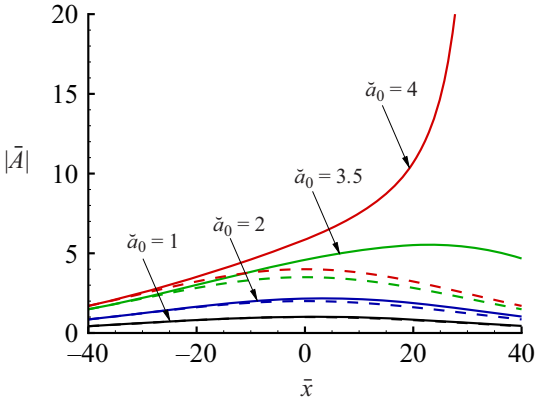

Figure 14. Effects of the initial amplitude on the solution to (5.10) with $\bar{F} = 0$. The dashed lines represent the corresponding linear solution (5.12).

amplitude equations overlap with the linear solution in the whole range (figure 15*a*). After reaching its peak value, the amplitude decays in an oscillatory manner. For a moderate value of $\bar{p}_I$, the nonlinear effect comes into play during the attenuation phase, causing a slow decay of the disturbance in the downstream region, while the non-equilibrium effect is rather small, as indicated by the agreement between the composite and equilibrium solutions (figure 15*b*). However, non-equilibrium effect becomes significant with further increase of $\bar{p}_I$ (figure 15*c*) and suppresses the disturbance. When $\bar{p}_I$ is large enough, instead of attenuation, the disturbance amplifies in the downstream region, and appears to terminate at a finite-distance singularity (figure 15*d*). On entering the nonlinear stage, non-equilibrium becomes important, as indicated by the fact that the solution to the composite amplitude equation saturates/grows at a smaller rate than that in the equilibrium regime.

Figure 16 shows the effects of the forcing (i.e. $\bar{p}_I$) on the evolution in the presence of a pre-existing free mode ($\hat{a}_0 \neq 0$). Two cases are considered, for which the free mode remains bounded (figure 16*a*) and blows up (figure 16*b*). While the amplitude upstream increases monotonically in the case of either solely a free mode (figure 14) or just the locally forced disturbance (figure 15), when both are present their total amplitude becomes oscillatory even in the earlier linear stage. Figure 16(*a*) shows that moderate forcing inhibits the mode, whereas further increase of the forcing enhances the amplification of the disturbance and may lead to blow-up. Similar behaviours are observed in figure 16(*b*), where moderate forcing delays the development of a finite-distance singularity and sufficiently large forcing does the opposite.

We consider further the evolution of the combined free and locally excited modes. The solutions to the composite amplitude equation for a fixed $\bar{p}_I = 10$ but different initial amplitudes of the free mode are displayed in figure 17. A free mode with initial amplitudes $\hat{a}_0 = 1$ and 3 influences the overall behaviour of the evolution appreciably (figure 17*b*,*c*). Interestingly, the free mode suppresses the disturbance downstream (figure 17*c*). However, when its initial amplitude is increased to $\hat{a}_0 = 5$, the free mode promotes the disturbance instead, causing the latter to blow up at a finite distance (figure 17*d*). The phase of the initial amplitude of the free mode also plays an important role in the evolution, as is displayed in figure 18. Figure 18(*a*) shows that changing the phase either suppresses or promotes the disturbance significantly. The free mode with particular phases can cause a finite-distance singularity even though the mode

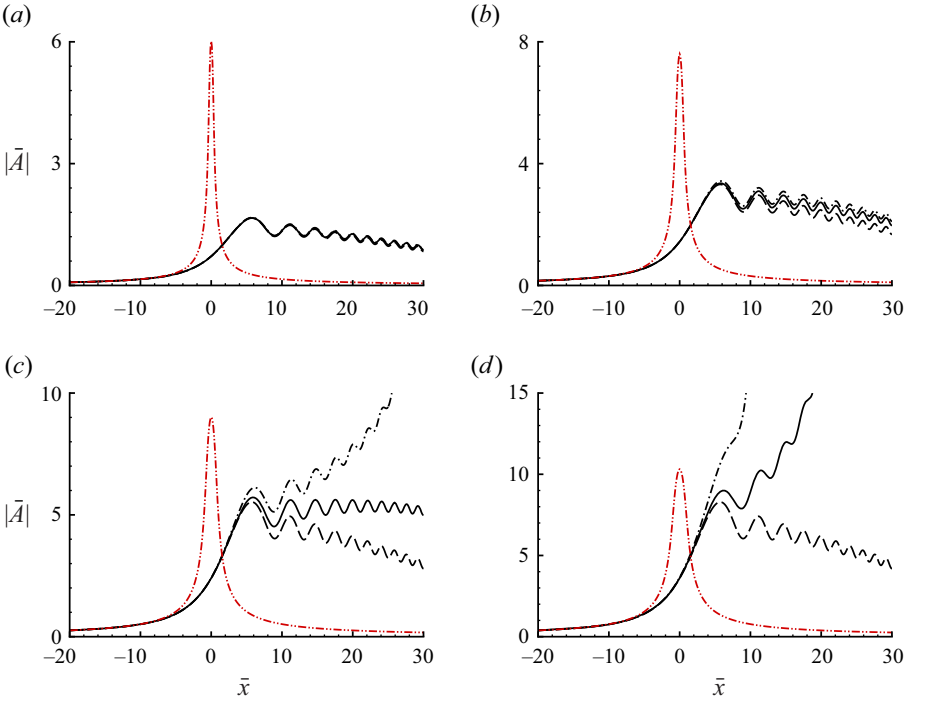

Figure 15. Effects of the forcing on the evolution predicted by the composite amplitude equation (5.10) with $\breve{\alpha}_d = 0$ and $\breve{a}_0 = \bar{a}_{op}$ ($\hat{a}_0 = 0$) for $\bar{p}_I = 3$ (*a*), $\bar{p}_I = 6$ (*b*), $\bar{p}_I = 10$ (*c*) and $\bar{p}_I = 15$ (*d*). Solid lines: solution to (5.10) with $R = 10^4$; dashed lines: linear solution (5.12); dashed-dotted lines: solution to (4.61) in the equilibrium regime; (red) dashed-dotted-dotted lines: nonlinear response given by (C3) in terms of the coordinate of the composite theory.

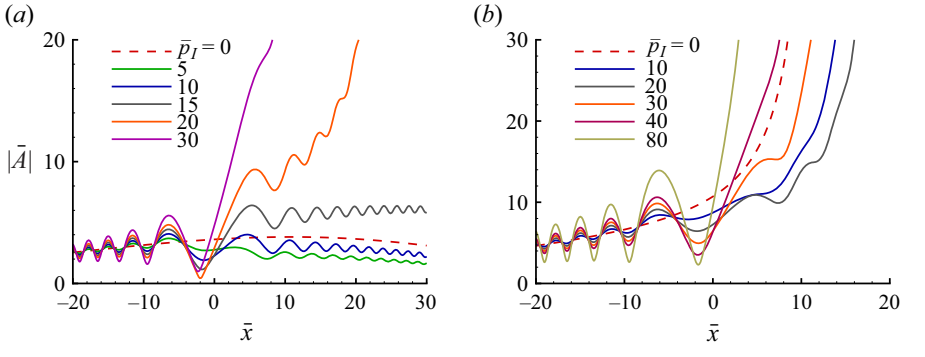

Figure 16. Effects of the forcing on the evolution in the presence of a pre-existing free mode with an initial amplitude $\hat{a}_0$: (*a*) $\hat{a}_0 = 3$ and (*b*) $\hat{a}_0 = 5$.

with the same initial magnitude but different phases saturates. The important role of the phase is also observed for the case where the disturbance blows up, as is shown in figure 18(*b*): the shift of the phase either advances or delays the formation of finite-distance singularity.

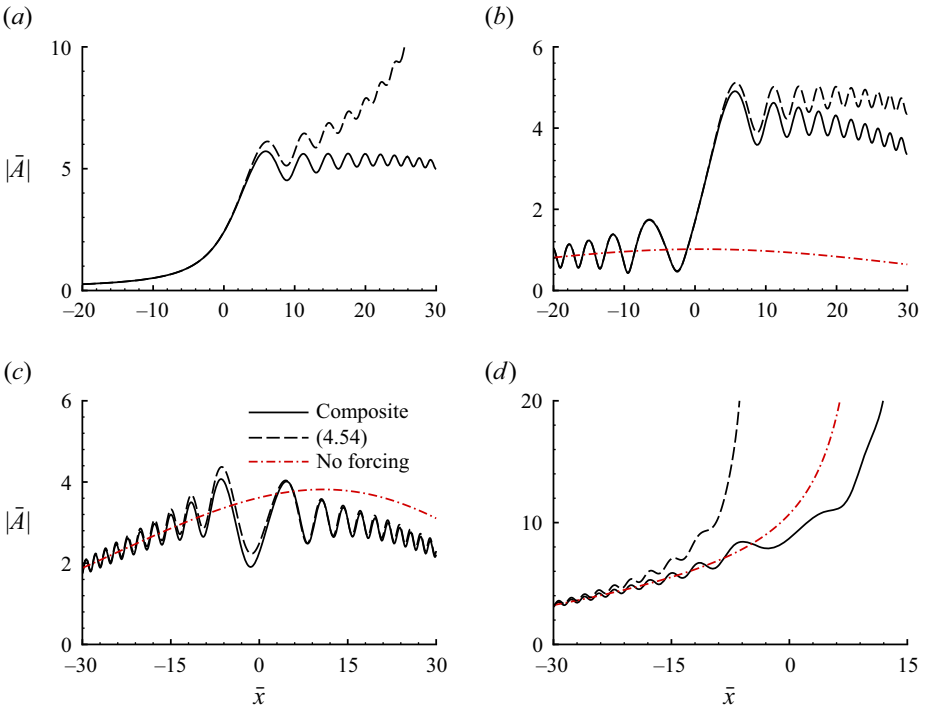

Figure 17. Evolution of the combined free and locally excited modes. The solid lines represent the solution to the composite amplitude equation (5.10) with $R = 10^4$, $\bar{p}_I = 10$, $\bar{\alpha}_d = 0$ and $\breve{a}_0 = \bar{a}_{op} + \hat{a}_0$ for $\hat{a}_0 = 0$ (*a*), $\hat{a}_0 = 1$ (*b*), $\hat{a}_0 = 3$ (*c*) and $\hat{a}_0 = 5$ (*d*). The dashed lines represent the nonlinear solution to (4.61), and the dashed-dotted lines represent the nonlinear evolution of a free mode with the same $\hat{a}_0$ but without forcing.

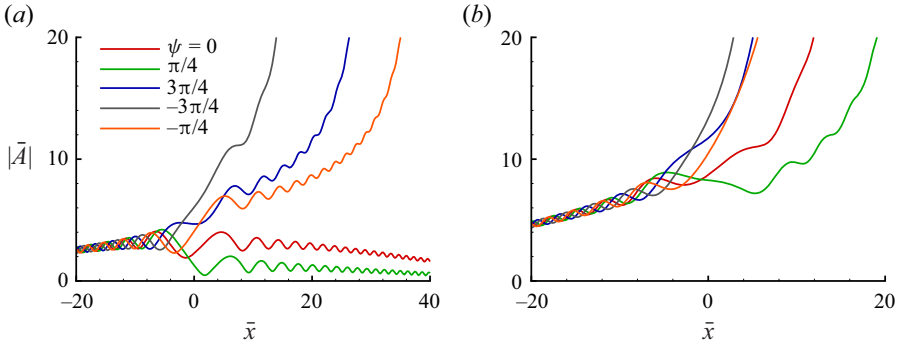

Figure 18. Effects of the phase of the free-mode initial amplitude, $\hat{a}_0 \equiv |\hat{a}_0|\, e^{i\psi}$, on the evolution of the combined free and locally excited modes with $R = 10^4$, $\bar{p}_I = 10$ and $\bar{\alpha}_d = 0$ for $|\hat{a}_0| = 3$ (*a*) and $|\hat{a}_0| = 5$ (*b*).

6. Mach wave radiation

Similar to its counterpart on a free shear layer and a circular jet (Tam & Burton 1984*a*,*b*), a supersonic instability mode on a boundary layer undergoing amplification–attenuation can radiate a highly directional sound wave in the form of a Mach wave beam, as was described by Wu (2005). We shall follow his asymptotic approach to determine the complete structure of the Mach wave beam, formally in the non-parallel equilibrium regime.

The disturbance outside of the boundary layer, $(\tilde{\rho}, \tilde{u}, \tilde{v}, \tilde{p}, \tilde{\theta})$, is governed by the linearised Euler equations. Eliminating $\tilde{\rho}$, $\tilde{u}$, $\tilde{v}$ and $\tilde{\theta}$ from these equations leads to the wave equation for the pressure $\tilde{p}$

$$\mathscr{L}_w\tilde{p} \equiv \left\{M^2\left(\frac{\partial}{\partial t}+\frac{\partial}{\partial x}\right)^2-\left(\frac{\partial^2}{\partial x^2}+\frac{\partial^2}{\partial y^2}\right)\right\}\tilde{p}=0. \tag{6.1}$$

6.1. *Near field of the Mach wave beam*

As in Wu (2005), the main-layer expansion (4.57) becomes disordered when $y = O(R^{1/2})$ in view of the solution (4.12) for the pressure. The appropriate solution can be sought by introducing the variable

$$\bar{y} = R^{-1/2}y. \tag{6.2}$$

Accordingly, by the multiple-scale method, we have

$$\frac{\partial}{\partial x} \to \frac{\partial}{\partial x}+R^{-1/2}\frac{\partial}{\partial \bar{x}}, \quad \frac{\partial}{\partial y} \to \frac{\partial}{\partial y}+R^{-1/2}\frac{\partial}{\partial \bar{y}}. \tag{6.3a,b}$$

The perturbation now expands as

$$\begin{aligned}(\tilde{\rho}, \tilde{u}, \tilde{v}, \tilde{p}, \tilde{\theta}) = \bar{\epsilon}_s R^{1/2}[&(\rho_0, u_0, v_0, p_0, \theta_0)+R^{-1/2}(\rho_1, u_1, v_1, p_1, \theta_1)\\ &+R^{-1}(\rho_2, u_2, v_2, p_2, \theta_2)+\cdots].\end{aligned} \tag{6.4}$$

Substitution of the above expansion for $\tilde{p}$ into (6.1) leads to the equation for the leading-order pressure, $\mathscr{L}_w p_0 = 0$. The solution may be written in the form

$$p_0 = \bar{p}_0(\bar{x}, \bar{y})\exp(\mathrm{i}\alpha(x-ct-qy))+\text{c.c.}, \tag{6.5}$$

where $q = \sqrt{M^2(1-c)^2-1}$, and $\bar{p}_0$ is determined by considering the second-order term.

Proceeding to the next order, we obtain the equation for p_1

$$\mathscr{L}_w p_1 = 2\left[\frac{\partial^2 p_0}{\partial \bar{x}\partial x}+\frac{\partial^2 p_0}{\partial \bar{y}\partial y}-M^2\left(\frac{\partial}{\partial t}+\frac{\partial}{\partial x}\right)\frac{\partial p_0}{\partial \bar{x}}\right]. \tag{6.6}$$

It is worth pointing out that p_1 contains the incident wave, which satisfies the homogeneous equation and thus does not affect the radiation directly. In order to remove the secular terms in the expansion, the term proportional to p_0 on the right-hand side of the above equation is required to be zero, from which and (6.5), we obtain

$$[M^2(1-c)-1]\frac{\partial \bar{p}_0}{\partial \bar{x}}+q\frac{\partial \bar{p}_0}{\partial \bar{y}}=0, \tag{6.7}$$

which satisfies the boundary condition through matching with the main-layer solution

$$\bar{p}_0(\bar{x}, \bar{y}) = \mathscr{C}_\infty \bar{A}(\bar{x}) \quad \text{at } \bar{y}=0. \tag{6.8}$$

The solution to (6.7)–(6.8) is found by the method of characteristic lines as

$$\bar{p}_0(\bar{x}, \bar{y}) = \mathscr{C}_\infty \bar{A}(\bar{x}-q^{-1}[M^2(1-c)-1]\bar{y}), \tag{6.9}$$

which indicates that the amplitude modulation propagates along the characteristic lines

$$\bar{\xi} \equiv \bar{x}-q^{-1}[M^2(1-c)-1]\bar{y} = \text{constant}. \tag{6.10}$$

6.2. *Far field of the Mach wave beam*

As was pointed out by Wu (2005), the expansion (6.4) and the solution (6.9) are no longer valid in the far field corresponding to the region

$$\bar{y} = O(R^{1/2}), \quad \bar{\xi} = O(1). \tag{6.11a,b}$$

To construct the valid solution in this far field, we introduce the variable

$$\tilde{y} = R^{-1/2}\bar{y} = R^{-1}y, \tag{6.12}$$

and it follows that

$$\frac{\partial}{\partial y} \to \frac{\partial}{\partial y} - R^{-1/2}\frac{M^2(1-c)-1}{q}\frac{\partial}{\partial \bar{\xi}} + R^{-1}\frac{\partial}{\partial \tilde{y}}. \tag{6.13}$$

The expansion for the pressure takes the form

$$\begin{aligned}\tilde{p} = {} & \bar{\epsilon}_s R^{1/2}[\tilde{p}_0(\bar{\xi},\tilde{y}) + R^{-1}\tilde{p}_1(\bar{\xi},\tilde{y}) + \cdots]\exp(\mathrm{i}\alpha(x-ct-qy)) \\ & + \bar{\epsilon}_s \bar{p}_I \exp(\mathrm{i}\alpha(x-ct+qy)) + \text{c.c.}.\end{aligned} \tag{6.14}$$

Again the leading-order term satisfies the wave equation, but the secular condition for $\tilde{p}_1$ leads to (Wu 2005)

$$-2\mathrm{i}\alpha q\frac{\partial \tilde{p}_0}{\partial \tilde{y}} + q^{-2}M^2c^2\frac{\partial^2 \tilde{p}_0}{\partial \bar{\xi}^2} = 0, \tag{6.15}$$

which is different from (6.7). Matching with the near-field solution (6.9) gives the boundary condition

$$\tilde{p}_0(\bar{\xi},\tilde{y}) = \mathscr{C}_\infty \bar{A}(\bar{\xi}) \quad \text{at } \tilde{y}=0. \tag{6.16}$$

Equation (6.15) with (6.16) is solved by Fourier transform to give

$$\tilde{p}_0(\bar{\xi},\tilde{y}) = \frac{\exp(\pi\mathrm{i}/4)}{\sqrt{\tilde{y}}}\sqrt{\frac{\alpha q^3}{2\pi M^2c^2}}\mathscr{C}_\infty \int_{-\infty}^{\infty} \bar{A}(\zeta)\exp\left\{-\frac{\mathrm{i}\alpha q^3}{2M^2c^2\tilde{y}}(\bar{\xi}-\zeta)^2\right\}\mathrm{d}\zeta. \tag{6.17}$$

For a linear free mode, $\bar{A}(\bar{x}) = \bar{a}_0\exp(\sigma\bar{x}^2/2)$, and the solution has the explicit expression

$$|\tilde{p}_0(\bar{\xi},\tilde{y})| = \left|1+\frac{\mathrm{i}M^2c^2\sigma}{\alpha q^3}\tilde{y}\right|^{-1/2}\left|\mathscr{C}_\infty \bar{a}_0\exp\left\{\frac{1}{2}\sigma\bar{\xi}^2/\left(1+\frac{\mathrm{i}M^2c^2\sigma}{\alpha q^3}\tilde{y}\right)\right\}\right|. \tag{6.18}$$

6.3. *Numerical evaluation*

To compute the distribution of the sound field, we rewrite the far-field pressure (6.17) as

$$\begin{aligned}\tilde{p}_0(\check{x},\check{y}) = {} & \frac{R^{1/4}\exp(\pi\mathrm{i}/4)}{|\sigma_r|^{1/4}\sqrt{\check{y}}}\sqrt{\frac{\alpha q^3}{2\pi M^2c^2}}\mathscr{C}_\infty \int_{-\infty}^{\infty}\bar{A}(\zeta/\sqrt{|\sigma_r|})\exp\left\{-\frac{\mathrm{i}\alpha q^3R^{1/2}}{2M^2c^2\sqrt{|\sigma_r|}\check{y}}\right. \\ & \left.\times[\check{x}-q^{-1}(M^2(1-c)-1)\check{y}-\zeta]^2\right\}\mathrm{d}\zeta,\end{aligned} \tag{6.19}$$

where we have introduced

$$\check{x} = \sqrt{|\sigma_r|}\bar{x}, \quad \check{y} = \sqrt{|\sigma_r|}\bar{y}. \tag{6.20a,b}$$

As a highlight of the structure of the sound field, we first study the case of a linear free mode and consider the analytical formula (6.18) in terms of the variables $\check{x}$ and $\check{y}$. Let us

write $|\tilde{p}_0(\bar{\xi},\tilde{y})|$ as

$$|\tilde{p}_0(\bar{\xi},\tilde{y})| \equiv F(\check{x},\check{y}) = |\mathscr{C}_\infty \bar{a}_0| H^{-1/4}(\check{y}) \exp\left\{\tfrac{1}{2}\check{\sigma}_r(\check{x}-\check{q}\check{y})^2/H(\check{y})\right\}, \tag{6.21}$$

where we have put

$$\left.\begin{aligned} H(\check{y}) = (1-\sigma_i\check{Q}\check{y})^2 + (\sigma_r\check{Q}\check{y})^2, \quad \check{Q} = \frac{M^2c^2}{R^{1/2}\sqrt{|\sigma_r|}\alpha q^3}, \\ \check{q} = \frac{M^2(1-c)-1}{q}, \quad \check{\sigma}_r = \frac{\sigma_r}{|\sigma_r|}. \end{aligned}\right\} \tag{6.22a–d}$$

In order to locate a possible maximum/minimum (or saddle point) of $F(\check{x},\check{y})$, we seek stationary point(s) by setting $\partial F/\partial\check{x}=0$ and $\partial F/\partial\check{y}=0$. The first of the above equations implies that $\check{x}=\check{q}\check{y}$, use of which in the second gives $\partial H(\check{y})/\partial\check{y}=0$. The above equation yields a unique stationary point $(\check{x}_s,\check{y}_s)$,

$$\check{y}_s = \frac{\sigma_i}{(\sigma_r^2+\sigma_i^2)\check{Q}}, \quad \check{x}_s = \check{q}\check{y}_s, \tag{6.23a,b}$$

which indicates that a stationary point with $\check{y}_s>0$ exists only when $\sigma_i>0$. It is noted that the characteristic line emanating from the origin passes through the stationary point.

Next, we evaluate the second-order derivatives of $F(\check{x},\check{y})$ at $(\check{x}_s,\check{y}_s)$, and find that

$$\check{\Delta}(\check{x}_s,\check{y}_s) \equiv \frac{\partial^2F}{\partial\check{x}^2}\frac{\partial^2F}{\partial\check{y}^2} - \left(\frac{\partial^2F}{\partial\check{x}\partial\check{y}}\right)^2 = -\frac{1}{2}F^2\check{\sigma}_r\frac{(\sigma_r^2+\sigma_i^2)\check{Q}^2}{H^2} > 0. \tag{6.24}$$

Thus, we conclude that the stationary point $(\check{x}_s,\check{y}_s)$ is a local maximum.

For the present case, we have $\sigma_i>0$, so that there is a stationary point with $\check{y}_s>0$, which turns out to be the maximum. The fact that $\sigma_i>0$ in the present case is consistent with the result of Chuvakhov & Fedorov (2016). Figures 3 and 9 of their paper show that the phase speed decreases as the mode passes through the neutral point, indicating that the streamwise wavenumber increases and hence its derivative with respect to the streamwise coordinate at the neutral position is positive. Since in our theory σ_i is proportional to that derivative, it is positive. As a validation of our numerical code evaluating (6.19), we compare the result of the analytical formula (6.18) with the numerical evaluation of (6.19) in figure 19. The two are in complete agreement. Figure 19(*b*), which is a locally enlarged view of the 'focal region', shows that the stationary point is indeed a local maximum. For the case of $\sigma_i\le 0$, no physically meaningful stationary point exists; contours of the sound intensity are lobed, as is shown in Wu (2005).

We now turn to the acoustic field of a nonlinearly evolving mode with and without the incident sound. The pressure contours predicted using the solutions to the composite amplitude equation (5.10) with $R=10^4$ are displayed in figure 20. The pressure contours without an impinging sound are shown in figure 20(*a*) with the far field in figure 20(*b*). The emitted sound wave focuses first towards the point where the intensity attains its maximum, beyond which the contours feature a main lobe flanked by two secondary beams. The contours are rather smooth. Figure 20(*c*) depicts the pressure contours of a locally excited mode by the incident sound without any oncoming free mode. The distinct feature is that the contours exhibit multiple spikes. This is due to amplitude oscillations caused by the forcing. The structure in the far field is illustrated in figure 20(*d*). Figure 20(*e*) shows the acoustic field in the case where a free radiating mode is present in addition to the locally

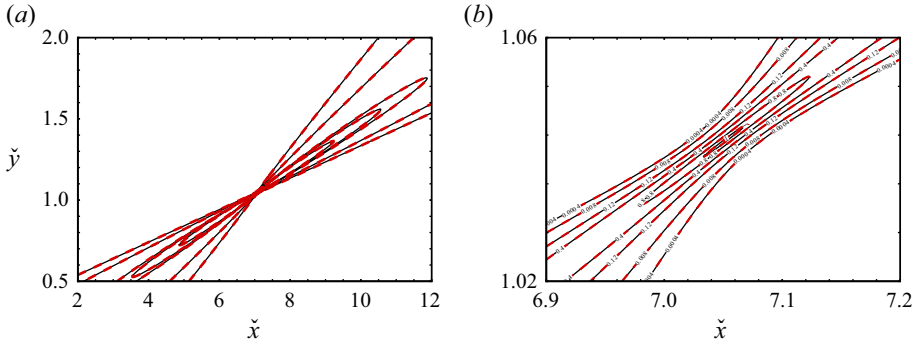

Figure 19. Contours of the far-field pressure $|\tilde{p}_0|$ of a linear free mode with $\bar{a}_0 = 3$ and $R = 10^4$. (b) Zooms into a region near the 'focal point' in (a). Solid lines: the analytical result (6.18); dashed lines: the numerical evaluation of (6.19).

excited mode. The far-field region in figure 20(f) shows that multiple spikes are again present as a result of the amplitude oscillations. In summary, the pattern of the Mach wave radiation is substantially changed in the presence of the impinging sound.

7. Summary and conclusions

The present paper has investigated the effects of impinging sound waves on linear and nonlinear instability of supersonic boundary layers at asymptotically large Reynolds numbers. The focus is on the flow conditions (Mach number and wall temperatures) under which there exists a radiating mode, which remains finite at the outer edge of the boundary layer and emits a Mach wave. We identified and described a particularly important mechanism, referred to as fundamental resonance, through which the radiating mode and the impinging sound with the same frequency and wavenumber interact effectively. As a result, the latter can, even with a rather low amplitude, alters substantially the linear and nonlinear evolution of the radiating mode.

In order to provide the context for this mechanism, we first considered reflection of an impinging slow sound wave by the boundary layer. The boundary-layer response, consisting of the absorbed and reflected waves, is predicted by a primarily inviscid analysis supplemented by a jump condition across the critical level, which is derived by analysing the viscous critical layer. We introduced the reflection coefficient $\mathscr{R}$, defined as the ratio of the magnitude of the outgoing wave to that of the incident wave. The scaled sound pressure $|\tilde{b}|$ at the critical level was used to measure the absorbed disturbance. We monitored the values of $|\mathscr{R}|$ and $|\tilde{b}|$ in a broad range of the incident angle and frequency, and found that both are extraordinarily large for a small subset of the sound incident angle and frequency. Furthermore, for a specific pairing of incidence angle and frequency, $\mathscr{R}$ becomes infinite, which is referred to as resonant over-reflection, and the reflected wave corresponds to the neutral radiating mode. The infinite reflection coefficient signals high sensitivity of the radiating mode to this particular incident sound wave.

The resonant over-reflection implies that, among broadband external acoustic disturbances, there exist ones whose wavenumber and frequency would coincide with those of the neutral radiating mode at each streamwise location. As a result, fundamental resonance takes place between the sound and the instability mode. The excitation of the radiating mode as well as its evolution were described by using the nonlinear critical-layer theory. Depending on the magnitude of the sound, the amplitude equations are derived

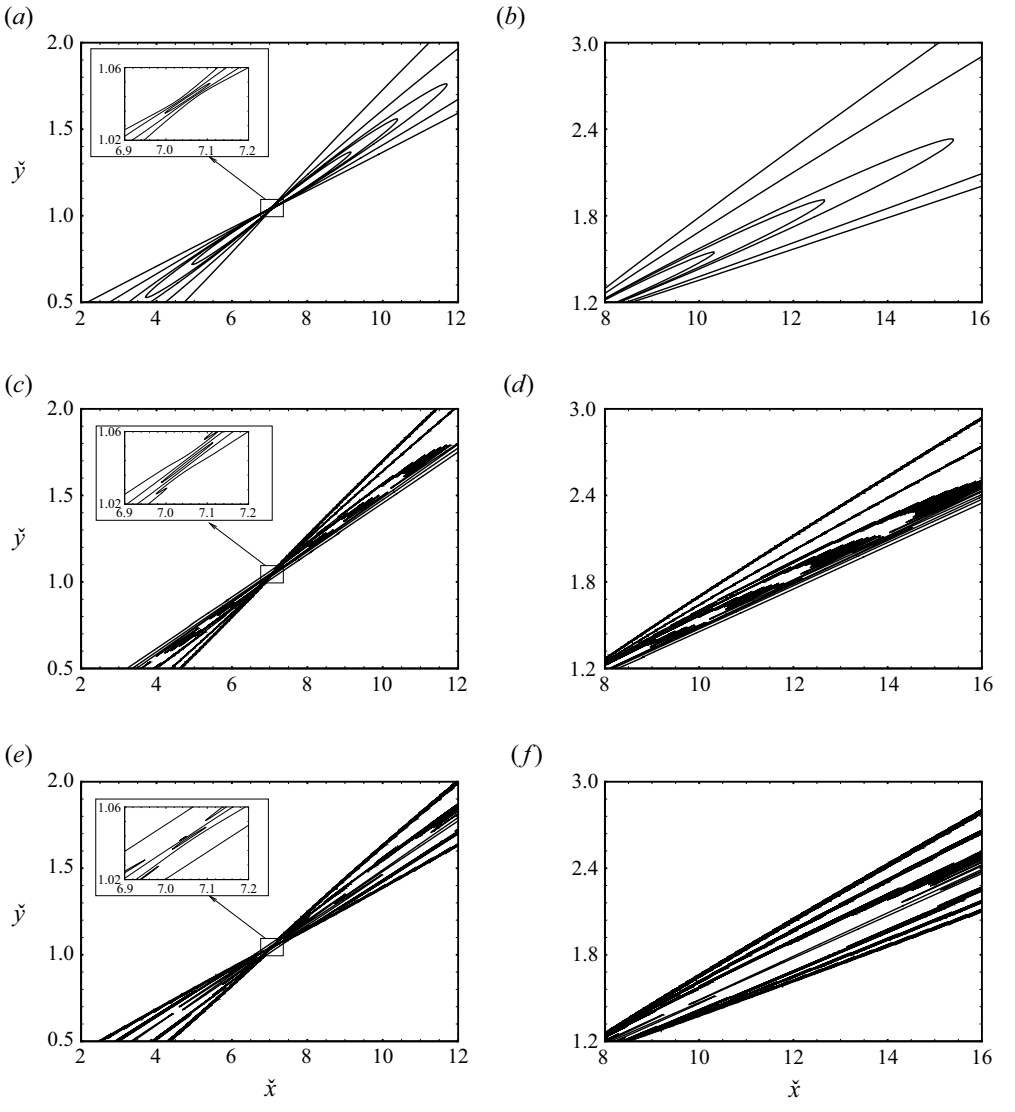

Figure 20. Contours of the far-field pressure $|\tilde{p}_0|$ using the solution to the composite amplitude equation (5.10) with $R = 10^4$. Panels show (*a*) $\bar{p}_I = 0$ and $\check{a}_0 = 3$, (*c*) $\bar{p}_I = 10$ and $\check{a}_0 = \bar{a}_{op}$, (*e*) $\bar{p}_I = 10$ and $\check{a}_0 = \bar{a}_{op} + 3$. (*b*,*d*,*f*) Show the far field of (*a*,*c*,*e*), respectively.

in the non-equilibrium parallel and equilibrium non-parallel regimes, respectively. In the non-equilibrium regime, which occurs when the incident sound is sufficiently strong, the amplitude equation admits an equilibrium solution representing the nonlinear response, which modifies the linear growth rate of the mode significantly. In the nonlinear evolution stage, the incident sound wave promotes nonlinear amplification and advances the eventual blow-up. In the equilibrium regime, in addition to the pre-existing free mode, the locally forced response evolves into a radiating mode. The evolution depends on both the intensity of the incident sound and the amplitude of the pre-existing free mode. With the amplitude equations derived for the two distinguished regimes, we then constructed a composite amplitude equation that takes into account non-parallel and non-equilibrium

effects simultaneously. This equation was solved numerically, and solutions showed that the incident sound influences the evolution significantly: with moderate intensity it inhibits the disturbance, but enhances amplification when the intensity is sufficiently large. The most obvious effect of the impinging sound wave is that the amplitude undergoes vigorous oscillations, whether attenuating or amplifying. The amplitude evolution predicted by the composite amplitude equation was then used to study the Mach wave radiation process. The Mach wave in the far field is drastically altered by the impinging sound wave: the characteristic simple lobed beam is replaced by a highly complex directivity.

The present theoretical investigation provides physical insights into how acoustic waves originated from the environment may influence the instability and acoustic radiation of supersonic boundary layers. The rather striking phenomena revealed and described are important when incident sound waves of an appreciable level are present, but may also be relevant if the experimental data are to be extrapolated to flight conditions. The results may be of relevance for flow control using acoustic actuation.

Finally, we comment on related issues that require further investigation. Free-stream acoustic waves in reality have a broadband spectrum whereas our theory considered a single discrete component. The simplification was based on the observation that, among all possible components, only those in a narrow band centred at the particular component with the same frequency and wavenumber of the radiating mode can take part in the fundamental resonance. Only one such component was considered in this paper for simplicity, but the analysis can be generalised to include a continuum of components in the narrow band, in which case the amplitude function A would be allowed to modulate simultaneously in time. Another issue concerns the fact that solutions to the amplitude equations blow up for a certain range of parameters. The present weakly nonlinear theory becomes invalid close to the blow-up location, where the disturbance would evolve on the short scale comparable to the boundary-layer thickness and be governed by the Euler equations (Leib 1991). It is also possible that the primary disturbance becomes susceptible to secondary instability. Either of the scenarios signals a cascade into small scales, the implication of which is unclear, but it might undermine the quantitative usefulness of asymptotic solutions as was argued by Cowley (2001). Predicting ensuing rapid evolution and/or onset of small-scale motions is a major challenge.

Acknowledgements. The referees are thanked for their comments and suggestions, which helped us improve the manuscript.

Funding. F.Q. acknowledges the support of an EPSRC-IDS scholarship from the Department of Mathematics of Imperial College London.

Declaration of interests. The authors report no conflict of interest.

Author ORCIDs.
Fufeng Qin https://orcid.org/0009-0006-3975-168X;
Xuesong Wu https://orcid.org/0000-0002-3406-8017.

Appendix A. Computation of neutral eigenmode and reflection coefficient

A.1. *Computation of the neutral eigenmode*

To solve Rayleigh equation (2.30) numerically, we recast it into a system of first-order differential equations. The integration starts at a position slightly beneath the critical level, $\eta_c - \tilde{d}$, with the initial values $\bar{\phi}_a(\eta_c - \tilde{d})$, $\bar{\phi}'_a(\eta_c - \tilde{d})$, $\bar{\phi}_b(\eta_c - \tilde{d})$ and $\bar{\phi}'_b(\eta_c - \tilde{d})$ calculated using (2.34) and (2.35). The governing equations are marched from $\eta = \eta_c - \tilde{d}$ to $\eta = 0$ by the fourth-order Runge–Kutta method, leading to $(\bar{p}_a(0), \bar{p}'_a(0))$ and

$(\bar{p}_b(0), \bar{p}_b'(0))$ at the wall. Imposing the first of the boundary condition (2.31), we obtain

$$\bar{a}^- = -\bar{p}_b'(0)/\bar{p}_a'(0). \tag{A1}$$

A second integration starts from the position $\eta = \eta_e = 20$, which represents the far field. According to (2.32), the initial condition can be taken as

$$\hat{p}_0 = \exp(-\mathrm{i}\alpha q \eta_e), \quad \hat{p}_0' = -\mathrm{i}\alpha q \exp(-\mathrm{i}\alpha q \eta_e). \tag{A2a,b}$$

The governing equations are marched from $\eta = \eta_e$ to $\eta = \eta_c + \tilde{d}$ again by the fourth-order Runge–Kutta method, yielding $(\hat{p}_0(\eta_c + \tilde{d}), \hat{p}_0'(\eta_c + \tilde{d}))$ just above the critical level. Equating $\mathscr{C}_\infty(\hat{p}_0(\eta_c + \tilde{d}), \hat{p}_0'(\eta_c + \tilde{d}))$ to the corresponding local analytical solution (2.33) at $\eta_c + \tilde{d}$, we obtain a pair of equations, eliminating from which the constant $\mathscr{C}_\infty$ yields the expression for $\bar{a}^+$

$$\bar{a}^+ = \frac{\hat{p}_0'(\eta_c + \tilde{d})\bar{\phi}_b(\eta_c + \tilde{d}) - \hat{p}_0(\eta_c + \tilde{d})\bar{\phi}_b'(\eta_c + \tilde{d})}{\hat{p}_0(\eta_c + \tilde{d})\bar{\phi}_a'(\eta_c + \tilde{d}) - \hat{p}_0'(\eta_c + \tilde{d})\bar{\phi}_a(\eta_c + \tilde{d})}. \tag{A3}$$

In addition, a linear critical-layer analysis (presented in § 4.1) determines the jump

$$\bar{a}^+ - \bar{a}^- = \frac{\alpha^2 \bar{T}_c^2}{3}\left(\frac{2\bar{T}_c'}{\bar{T}_c} - \frac{\bar{U}_c''}{\bar{U}_c'}\right)\pi\mathrm{i}, \tag{A4}$$

which corresponds to, as is well known, the phase of the logarithm in the Frobenius solution changing by $-\pi$ as η goes from η_c^+ to η_c^-. From (A1), (A3) and (A4) follows the dispersion relation

$$\begin{aligned}\Delta(\alpha, c) \equiv{}& \frac{\hat{p}_0'(\eta_c + \tilde{d})\bar{\phi}_b(\eta_c + \tilde{d}) - \hat{p}_0(\eta_c + \tilde{d})\bar{\phi}_b'(\eta_c + \tilde{d})}{\hat{p}_0(\eta_c + \tilde{d})\bar{\phi}_a'(\eta_c + \tilde{d}) - \hat{p}_0'(\eta_c + \tilde{d})\bar{\phi}_a(\eta_c + \tilde{d})} \\ &+ \bar{p}_b'(0)/\bar{p}_a'(0) - \frac{\alpha^2 \bar{T}_c^2}{3}\left(\frac{2\bar{T}_c'}{\bar{T}_c} - \frac{\bar{U}_c''}{\bar{U}_c'}\right)\pi\mathrm{i} = 0.\end{aligned} \tag{A5}$$

The Newton–Raphson method is employed to solve the dispersion relation for an initial guess of (α, c).

A.2. *Computation of the reflection coefficient and boundary-layer response*

For a given pairing (α_s, c_s), the reflection coefficient $\mathscr{R}$ and boundary-layer response are determined by using a combination of analytical results and numerical method. Using the similarity solution for $\bar{U}$ and $\bar{T}$, (3.3) for $\check{p}_s$ is recast in terms of η and then written as a system of first-order ordinary differential equations.

Near the critical level η_c (i.e. $\check{\eta} \equiv \eta - \eta_c \to 0$), the pressure takes the form

$$\check{p}_s = \tilde{a}^{\pm}\tilde{\phi}_a + b_s\tilde{\phi}_b, \tag{A6}$$

where $\tilde{\phi}_a$ and $\tilde{\phi}_b$ have the same expressions as (2.34) and (2.35), respectively, with α being replaced by α_s. Integrating from $\eta = \eta_c - \tilde{d}$ to $\eta = 0$ with the initial conditions

$(\tilde{\phi}_a(\eta_c-\tilde{d}), \tilde{\phi}'_a(\eta_c-\tilde{d}))$ and $(\tilde{\phi}_b(\eta_c-\tilde{d}), \tilde{\phi}'_b(\eta_c-\tilde{d}))$, we obtain $(p_a(0), p'_a(0))$ and $(p_b(0), p'_b(0))$, respectively. Then use of the impermeability condition gives

$$\tilde{a}^- p'_a(0) + b_s p'_b(0) = 0. \tag{A7}$$

In the far field, the pressure takes the form

$$\check{p}_s = p_I(\exp(\mathrm{i}\gamma_s\eta) + \mathscr{R}\exp(-\mathrm{i}\gamma_s\eta)). \tag{A8}$$

Given the initial values $(\exp(\mathrm{i}\gamma_s\eta_e), \mathrm{i}\gamma_s\exp(\mathrm{i}\gamma_s\eta_e))$ and $(\exp(-\mathrm{i}\gamma_s\eta_e), -\mathrm{i}\gamma_s\exp(-\mathrm{i}\gamma_s\eta_e))$, the governing equations are marched from $\eta=\eta_e$ to $\eta=\eta_c+\tilde{d}$ by the fourth-order Runge–Kutta method, leading to $(p_i(\eta_c+\tilde{d}), p'_i(\eta_c+\tilde{d}))$ and $(p_r(\eta_c+\tilde{d}), p'_r(\eta_c+\tilde{d}))$ above the critical level. Equating the numerical solution to the analytical formula (A6) yields

$$\tilde{a}^+\tilde{\phi}_a(\eta_c+\tilde{d}) + b_s\tilde{\phi}_b(\eta_c+\tilde{d}) = p_I[p_i(\eta_c+\tilde{d}) + \mathscr{R}p_r(\eta_c+\tilde{d})], \tag{A9}$$

$$\tilde{a}^+\tilde{\phi}'_a(\eta_c+\tilde{d}) + b_s\tilde{\phi}'_b(\eta_c+\tilde{d}) = p_I[p'_i(\eta_c+\tilde{d}) + \mathscr{R}p'_r(\eta_c+\tilde{d})]. \tag{A10}$$

In addition, the jump condition can be written as

$$\tilde{a}^+ - \tilde{a}^- = b_s J, \tag{A11}$$

where

$$J = \frac{\alpha_s^2\bar{T}_c^2}{3}\left(\frac{2\bar{T}'_c}{\bar{T}_c} - \frac{\bar{U}''_c}{\bar{U}'_c}\right)\pi\mathrm{i}. \tag{A12}$$

From (A7) and (A9)–(A11), we obtain the reflection coefficient

$$\mathscr{R}(\alpha_s, c_s) = \frac{\mathcal{B}p_i(\eta_c+\tilde{d}) - \mathcal{A}p'_i(\eta_c+\tilde{d})}{\mathcal{A}p'_r(\eta_c+\tilde{d}) - \mathcal{B}p_r(\eta_c+\tilde{d})}, \tag{A13}$$

where we have put

$$\mathcal{A} \equiv [J - p'_b(0)/p'_a(0)]\tilde{\phi}_a(\eta_c+\tilde{d}) + \tilde{\phi}_b(\eta_c+\tilde{d}), \tag{A14}$$

$$\mathcal{B} \equiv [J - p'_b(0)/p'_a(0)]\tilde{\phi}'_a(\eta_c+\tilde{d}) + \tilde{\phi}'_b(\eta_c+\tilde{d}). \tag{A15}$$

We introduce the scaled quantity $\tilde{b} \equiv b_s/p_I$, which measures the response in the critical layer. Substituting the expression of $\mathscr{R}$ into (A9), we find that

$$\tilde{b} = [p_i(\eta_c+\tilde{d}) + \mathscr{R}p_r(\eta_c+\tilde{d})]/\mathcal{A}. \tag{A16}$$

Appendix B. The mean-flow distortion and interaction at the cubic level

The mean-flow distortion driven by the nonlinear interaction of the fundamental wave is found to satisfy the equations

$$-\frac{c}{\bar{T}_c^2}\frac{\partial \Theta_M}{\partial \tilde{x}}+\frac{1}{\bar{T}_c}\frac{\partial V_M}{\partial Y}=\frac{V_0}{\bar{T}_c^2}\frac{\partial \Theta_1^*}{\partial Y}, \tag{B1a}$$

$$c\frac{\partial U_M}{\partial \tilde{x}}+\bar{U}_c' V_M-\lambda \bar{T}_c\bar{\mu}_c\frac{\partial^2 U_M}{\partial Y^2}=-V_0\frac{\partial U_1^*}{\partial Y}-\mathrm{i}\alpha P_0\Theta_1^*+\lambda\bar{T}_c\bar{\mu}_c'\bar{U}_c'\frac{\partial \Theta_M}{\partial Y}, \tag{B1b}$$

$$c\frac{\partial \Theta_M}{\partial \tilde{x}}-\lambda\bar{T}_c\bar{\mu}_c Pr^{-1}\frac{\partial^2\Theta_M}{\partial Y^2}=-V_0\frac{\partial \Theta_1^*}{\partial Y}, \tag{B1c}$$

where the asterisk indicates the complex conjugate. Equation (B1*c*) is solved to give

$$\begin{aligned}\Theta_M=\mathrm{i}\alpha^3\bar{T}_c'\bar{U}_c'\int_0^\infty\int_0^\infty \xi\exp(-s_p\xi^3-3s_p\xi^2\eta\\ +\mathrm{i}\alpha\bar{U}_c'\bar{Y}\xi)\tilde{A}(\tilde{x}-c\eta)\tilde{A}^*(\tilde{x}-c\eta-c\xi)\,\mathrm{d}\eta\mathrm{d}\xi.\end{aligned} \tag{B2}$$

Equations (B1*a*) and (B1*c*) imply that $V_M=\lambda\bar{\mu}_c Pr^{-1}\Theta_{M,Y}$, which is inserted into (B1*b*) to obtain

$$\left(c\frac{\partial}{\partial\tilde{x}}-\lambda\bar{T}_c\bar{\mu}_c\frac{\partial^2}{\partial Y^2}\right)U_M=-V_0\frac{\partial U_1^*}{\partial Y}-\mathrm{i}\alpha P_0\Theta_1^*+\lambda\bar{U}_c'(\bar{T}_c\bar{\mu}_c'-\bar{\mu}_c Pr^{-1})\frac{\partial\Theta_M}{\partial Y}. \tag{B3}$$

We find the solution to be

$$\begin{aligned}U_{M,YY}=\alpha^4(\bar{U}_c')^3\frac{\bar{T}_c'}{\bar{T}_c}\int_0^\infty\int_0^\infty\xi^2\exp(-s_p\xi^3-3s\xi^2\eta+\mathrm{i}\alpha\bar{U}_c'\bar{Y}\xi)\\ \times\left[1-\frac{\bar{T}_c\bar{\mu}_c'-\bar{\mu}_c Pr^{-1}}{\bar{\mu}_c(1-Pr^{-1})}\left(\exp((s_p-s)\xi^3)-\exp(3(s-s_p)\xi^2\eta)\right)\right.\\ \left.+\frac{\bar{T}_c}{\bar{T}_c'}\left(\frac{\bar{T}_c'}{\bar{T}_c}-\frac{\bar{U}_c''}{\bar{U}_c'}\right)\exp((s_p-s)\xi^3)\right]\\ \times\tilde{A}(\tilde{x}-c\eta)\tilde{A}^*(\tilde{x}-c\eta-c\xi)\,\mathrm{d}\eta\mathrm{d}\xi.\end{aligned} \tag{B4}$$

Now we proceed to consider the fundamental regenerated by the cubic interaction, whose governing equations are found to be

$$\left[c\frac{\partial}{\partial\tilde{x}}+\mathrm{i}\alpha(\bar{U}_c'Y+\bar{U}_{1c}\bar{x}_1)\right](-\Theta_2/\bar{T}_c^2)+\frac{1}{\bar{T}_c}(\mathrm{i}\alpha U_2+V_{2,Y})=\frac{V_0}{\bar{T}_c^2}\Theta_{M,Y}+\cdots, \tag{B5a}$$

$$\mathscr{L}_\mu U_2+\bar{U}_c'V_2=-\mathrm{i}\alpha\bar{T}_cP_2-V_0U_{M,Y}-\mathrm{i}\alpha P_0\Theta_M+\lambda\bar{T}_c\bar{\mu}_c'\bar{U}_c'\Theta_{2,Y}+\cdots, \tag{B5b}$$

$$\mathscr{L}_p\Theta_2=-V_0\Theta_{M,Y}+\cdots. \tag{B5c}$$

In order to find U_2 and hence the jump, we must calculate the temperature component Θ_2. Equation (B5*c*) is thus solved to give

$$\begin{aligned}\Theta_2=-\mathrm{i}\alpha^5(\bar{U}_c')^2\bar{T}_c'\int_0^\infty\int_0^\infty\int_{-\zeta}^\infty\zeta^2\exp[-s_p\xi^3-\mathrm{i}\alpha\bar{U}_c'\bar{Y}\xi-2s_p\zeta^3-3s_p\zeta^2\eta]\\ \times\tilde{A}(\tilde{x}-c\xi-c\zeta)\tilde{A}(\tilde{x}-c\xi-c\zeta-c\eta)\tilde{A}^*(\tilde{x}-c\xi-2c\zeta-c\eta)\,\mathrm{d}\xi\mathrm{d}\eta\mathrm{d}\zeta.\end{aligned} \tag{B6}$$

Equations (B5*a*) and (B5*b*) can be reduced to

$$\mathscr{L}_\mu U_{2,Y} = -V_0 U_{M,YY} - \mathrm{i}\alpha P_0 \Theta_{M,Y} + \lambda \bar{U}_c'(\bar{T}_c \bar{\mu}_c' - \bar{\mu}_c Pr^{-1})\Theta_{2,YY} + \cdots . \tag{B7}$$

The jump of U_2 can be obtained by performing Fourier transform of the above equation and setting the transform variable to zero. Matching U_2 with the outer solution (4.17) determines the jump

$$\begin{aligned} c^+ - c^- = {} & \frac{1}{3}\frac{\alpha^2}{\bar{T}_c}\left(\frac{\mathrm{i}c}{\alpha}\tilde{A}' - \bar{U}_{1c}\bar{x}_1\tilde{A}\right) j\pi\mathrm{i} + \left(\frac{\alpha^2 \bar{U}_c'}{3\bar{T}_c}\bar{x}_1\tilde{A}\right) j_1\pi\mathrm{i} + d\frac{\alpha^2}{3}\left(\frac{\bar{T}_c'}{\bar{T}_c} - \frac{\bar{U}_c''}{\bar{U}_c'}\right)\pi\mathrm{i} \\ & - \frac{2\pi\mathrm{i}\alpha^6(\bar{U}_c')^3\bar{T}_c'}{3\bar{T}_c^2}\int_0^\infty\int_0^\infty K(\xi,\eta)\tilde{A}(\tilde{x}-c\xi)\tilde{A}(\tilde{x}-c\xi-c\eta) \\ & \times \tilde{A}^*(\tilde{x}-2c\xi-c\eta)\,\mathrm{d}\eta\mathrm{d}\xi, \end{aligned} \tag{B8}$$

where the linear part of the jump corresponds to the $(-\pi)$ phase jump of the logarithmic singularity in (4.13), and the kernel function

$$\begin{aligned} K(\xi,\eta) = {} & \xi^2 \exp[-s(2\xi^3 + 3\xi^2\eta)]\left\{\exp[-(s_p - s)\xi^3]\right. \\ & + \exp[-(s_p - s)\xi^3 - 3(s_p - s)\xi^2\eta] \\ & \left. - \frac{\bar{T}_c\bar{\mu}_c' - \bar{\mu}_c Pr^{-1}}{\bar{\mu}_c(1 - Pr^{-1})}[1 - \exp(-(s_p - s)(2\xi^3 + 3\xi^2\eta))] + \frac{\bar{T}_c}{\bar{T}_c'}\left(\frac{\bar{T}_c'}{\bar{T}_c} - \frac{\bar{U}_c''}{\bar{U}_c'}\right)\right\}. \end{aligned} \tag{B9}$$

Appendix C. Recovery of the equilibrium and non-equilibrium regimes from the composite theory

In this appendix, we show that the amplitude equations in the equilibrium and non-equilibrium regimes can be recovered from the composite amplitude equation (5.10) as the appropriate limiting cases.

First, consider recovery of the equilibrium regime. Following Wu & Huerre (2009), we perform the substitution $\xi \to R^{-1/6}\xi$ and $\eta \to R^{-1/6}\eta$ and take the limit $R \gg 1$ in (5.10). The latter then reduces to (4.61).

Next, recall that in the non-equilibrium regime we have the nonlinear response $a_e \exp(\mathrm{i}\bar{\alpha}_d\tilde{x})$, where $a_e(\bar{x}_1)$ is governed by (4.38). Let $\bar{A}_e$ denote the corresponding nonlinear response written in terms of the scaled quantities and coordinate in the composite theory. Then we have

$$\bar{A}_e(\bar{x}) = R^{1/12}a_e(\bar{x}_1), \quad \bar{x} = R^{1/6}\bar{x}_1, \tag{C1}$$

where we have put $\tilde{x} = 0$ in (5.5). By using (C1) and noting

$$\bar{F} = R^{1/4}\tilde{F}, \quad \bar{\alpha}_d = R^{1/6}\tilde{\alpha}_d, \tag{C2a,b}$$

the response equation (4.38) is rewritten as

$$(\mathrm{i}\bar{\alpha}_d - \sigma\bar{x})\bar{A}_e = l\bar{A}_e|\bar{A}_e|^2 + \bar{F}. \tag{C3}$$

Figure 21 compares the nonlinear response with the solution to the composite amplitude equation in the absence of an oncoming free mode. The two solutions overlap in the

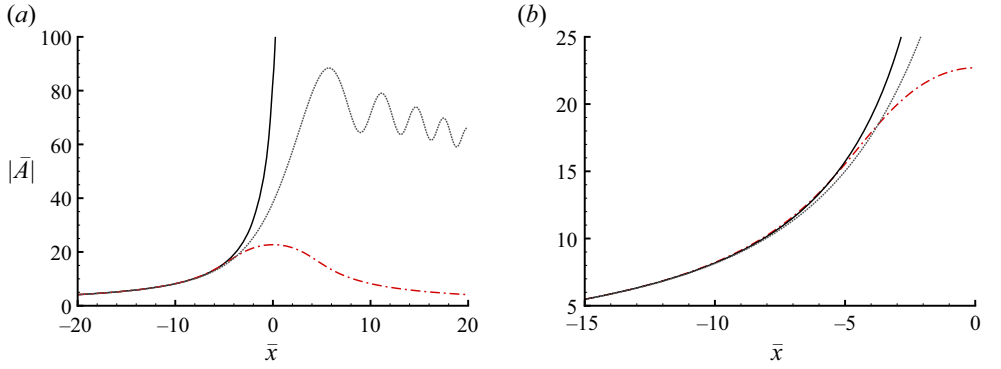

Figure 21. Comparison between the nonlinear response and the solution to the composite amplitude equation without an oncoming free mode for $\bar{p}_I = 160$ and $\bar{\alpha}_d = 0$. Solid lines: solution to (5.10) with $R = 10^4$; dotted lines: linear solution (5.12); dashed-dotted lines: nonlinear response governed by (C3). (*b*) Zooms into a range in (*a*).

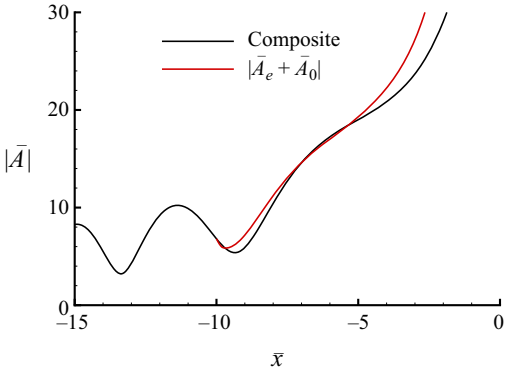

Figure 22. Comparison between the nonlinear response plus the nonlinear perturbation and the solution to the composite amplitude equation (5.10) in the presence of an oncoming free mode with $\hat{a}_0 = 3$ for $\bar{p}_I = 160$, $\bar{\alpha}_d = 0$ and $R = 10^4$.

upstream region, suggesting that the former can be recovered from the latter in the upstream limit. An enlarged view, figure 21(*b*), shows that the solution to the composite amplitude equation evolves through a stage which is nonlinear and captured by the nonlinear response.

We consider next the evolution of the perturbation with the growth rate modified by the nonlinear response. The perturbation in the non-equilibrium regime satisfies the initial condition (4.55) with the modified growth rate κ being given by (4.53), and the eigenvector (a_r, a_i) given in (4.54*a*,*b*). Let $\bar{A}_0$ denote the corresponding perturbation under the scaling of the composite theory, that is, $\bar{A}_0(\bar{x}) = R^{1/12}A_0(\tilde{x})$. On noting (5.5), the perturbation can be written as

$$\bar{A}_0 = 2|\bar{a}_0| \exp(\bar{\kappa}_r\bar{x})[|\bar{a}_{0r}| \cos(\bar{\kappa}_i\bar{x} + \bar{\theta}_1 + \bar{\phi}_0) + \mathrm{i}|\bar{a}_{0i}| \cos(\bar{\kappa}_i\bar{x} + \bar{\theta}_2 + \bar{\phi}_0)], \tag{C4}$$

where the modified growth rate $\bar{\kappa} \equiv R^{1/6}\kappa$ and the eigenvector $(\bar{a}_r, \bar{a}_i)$ satisfy the same equations as (4.53) and (4.54*a*,*b*) in the non-equilibrium regime, respectively, provided that the parameter $\bar{x}_1$ is replaced by the variable $\bar{x}$ and the parameters Υ and s are replaced

by $\bar{\Upsilon}$ and $\bar{s}$ with

$$\bar{\Upsilon} = \Upsilon R^{2/3}, \quad \bar{s} = sR^{1/2}. \tag{C5a,b}$$

Similarly, the rescaled nonlinear evolution equation for the perturbation in the composite theory has the same form as (4.45) in the non-equilibrium regime, provided that $\bar{x}_1$ is replaced by $\bar{x}$ and the rescaled quantities in (C5*a*,*b*) are used.

In order to compare the solution to the composite amplitude equation (5.10) in the presence of an oncoming free mode with the nonlinear response plus the nonlinear perturbation, the constants $|\bar{a}_0|$ and $\bar{\phi}_0$ are first determined by fitting $\bar{A}_e + \bar{A}_0$ with the composite solution at a particular location $\bar{x} = -10$. The resulting initial condition (C4) is used to solve the rescaled version of the nonlinear evolution equation (4.45). Figure 22 shows the comparison between the two solutions. The sum of $\bar{A}_e$ and $\bar{A}_0$ represents the nonlinear response and the nonlinear perturbation under the scaling of the composite theory. There is good agreement between the two solutions. This indicates that the composite theory captures the characteristics of the non-equilibrium effects.

References

Balakumar, P. 2005 Transition in a supersonic boundary layer due to acoustic disturbances. *AIAA Paper* 2005-0096.

Balakumar, P. 2009 Receptivity of a supersonic boundary layer to acoustic disturbances. *AIAA J.* **47**, 1069–1078.

Beckwith, I.E. & Miller, C.G., III. 1990 Aerothermodynamics and transition in high-speed wind tunnels at NASA Langley. *Annu. Rev. Fluid Mech.* **22**, 419–439.

Bitter, N.P. & Shepherd, J.E. 2015 Stability of highly cooled hypervelocity boundary layers. *J. Fluid Mech.* **778**, 586–620.

Cerminara, A., Durant, A., André, T., Sandham, N.D. & Taylor, N.J. 2019 Receptivity to freestream acoustic noise in hypersonic flow over a generic forebody. *J. Spacecr. Rockets* **56**, 447–457.

Chang, C.-L., Malik, M.R. & Hussaini, M.Y. 1990 Effects of shock on the stability of hypersonic boundary layers. *AIAA Paper* 90-1448.

Chang, C.-L., Vinh, H. & Malik, M.R. 1997 Hypersonic boundary-layer stability with chemical reactions using PSE. *AIAA Paper* 97-2012.

Choudhari, M., Li, F., Chang, C.-L., Edwards, J., Kegerise, M. & King, R. 2010 Laminar-turbulent transition behind discrete roughness elements in a high-speed boundary layer. *AIAA Paper* 2010-1575.

Chuvakhov, P.V. & Fedorov, A.V. 2016 Spontaneous radiation of sound by instability of a highly cooled hypersonic boundary layer. *J. Fluid Mech.* **805**, 188–206.

Corke, T.C., Barsever, A. & Morkovin, M.V. 1986 Experiments on transition enhancement by distributed roughness. *Phys. Fluids* **29**, 3199–3213.

Cowley, S.J. 2001 Laminar boundary-layer theory: a 20th century paradox? In *Mechanics for a New Millennium* (ed. H. Aref & J.W. Phillips), pp. 389–411. Springer.

Cowley, S.J. & Hall, P. 1990 On the instability of hypersonic flow past a wedge. *J. Fluid Mech.* **214**, 17–42.

De Tullio, N., Paredes, P., Sandham, N.D. & Theofilis, V. 2013 Laminar-turbulent transition induced by a discrete roughness element in a supersonic boundary layer. *J. Fluid Mech.* **735**, 613–646.

Dong, M., Liu, Y. & Wu, X. 2020 Receptivity of inviscid modes in supersonic boundary layers due to scattering of free-stream sound by localised wall roughness. *J. Fluid Mech.* **896**, A23.

Duan, L., Choudhari, M.M. & Wu, M. 2014 Numerical study of acoustic radiation due to a supersonic turbulent boundary layer. *J. Fluid Mech.* **746**, 165–192.

Duck, P.W., Ruban, A.I. & Zhikharev, C.N. 1996 Generation of Tollmien–Schlichting waves by free-stream turbulence. *J. Fluid Mech.* **312**, 341–371.

Edelmann, C. & Rist, U. 2013 Impact of forward-facing steps on laminar-turbulent transition in transonic flows without pressure gradient. *AIAA Paper* 2013-0080.

Fedorov, A.V. 2003*a* Receptivity of a high-speed boundary layer to acoustic disturbances. *J. Fluid Mech.* **491**, 101–129.

Fedorov, A.V. 2003*b* Receptivity of hypersonic boundary layer to acoustic disturbances scattered by surface roughness. *AIAA Paper* 2003-3731.

FEDOROV, A.V. 2011 Transition and stability of high-speed boundary layers. *Annu. Rev. Fluid Mech.* **43**, 79–95.

FEDOROV, A.V. & KHOKHLOV, A.P. 1991 Excitation of unstable modes in a supersonic boundary layer by acoustic waves. *Izv. Akad. Nauk SSSR Mekh. Zhidk. Gaza* **4**, 67–74.

FEDOROV, A.V. & KHOKHLOV, A.P. 2001 Prehistory of instability in a hypersonic boundary layer. *Theor. Comput. Fluid Dyn.* **14**, 359–375.

GAJJAR, J.S.B. 1995 On the nonlinear evolution of a stationary cross-flow vortex in a fully three-dimensional boundary layer flow. *NASA Tech. Rep.* 198405. NASA Lewis Research Center.

GAJJAR, J.S.B. 1996 Nonlinear stability of nonstationary cross-flow vortices in compressible boundary layers. *Stud. Appl. Maths* **96**, 53–84.

GOLDSTEIN, M.E. 1983 The evolution of Tollmien–Schlichting waves near a leading edge. *J. Fluid Mech.* **127**, 59–81.

GOLDSTEIN, M.E. 1985 Scattering of acoustic waves into Tollmien–Schlichting waves by small streamwise variations in surface geometry. *J. Fluid Mech.* **154**, 509–529.

GOLDSTEIN, M.E. 1995 The role of nonlinear critical layers in boundary layer transition. *Phil. Trans. R. Soc. Lond.* **352**, 425–442.

GOLDSTEIN, M.E. & CHOI, S.W. 1989 Nonlinear evolution of interacting oblique waves on two-dimensional shear layers. *J. Fluid Mech.* **207**, 97–120.

GOLDSTEIN, M.E. & HULTGREN, L.S. 1988 Nonlinear spatial evolution of an externally excited instability wave in a free shear layer. *J. Fluid Mech.* **197**, 295–330.

GOLDSTEIN, M.E. & HULTGREN, L.S. 1989 Boundary layer receptivity to long-wave free-stream turbulence. *Annu. Rev. Fluid Mech.* **21**, 137–166.

GOLDSTEIN, M.E. & LEIB, S.J. 1988 Nonlinear roll-up of externally excited free shear layers. *J. Fluid Mech.* **191**, 481–515.

GOLDSTEIN, M.E. & LEIB, S.J. 1989 Nonlinear evolution of oblique waves on compressible shear layers. *J. Fluid Mech.* **207**, 73–96.

GOLDSTEIN, M.E. & RICCO, P. 2018 Non-localized boundary layer instabilities resulting from leading edge receptivity at moderate supersonic Mach numbers. *J. Fluid Mech.* **838**, 435–477.

GOLDSTEIN, M.E. & WUNDROW, D.W. 1995 Interaction of oblique instability waves with weak streamwise vortices. *J. Fluid Mech.* **284**, 377–407.

GROSKOPF, G. & KLOKER, M.J. 2016 Instability and transition mechanisms induced by skewed roughness elements in a high-speed laminar boundary layer. *J. Fluid Mech.* **805**, 262–302.

HALL, P. & SMITH, F.T. 1982 A suggested mechanism for nonlinear wall roughness effects on high Reynolds number flow stability. *Stud. Appl. Maths* **66**, 241–265.

HE, J., BUTLER, A. & WU, X. 2019 Effects of distributed roughness on crossflow instability through generalized resonance mechanisms. *J. Fluid Mech.* **858**, 787–831.

HERNÁNDEZ, C.G. & WU, X. 2019 Receptivity of supersonic boundary layers over smooth and wavy surfaces to impinging slow acoustic waves. *J. Fluid Mech.* **872**, 849–888.

HICKERNELL, F.J. 1984 Time-dependent critical layers in shear flows on the beta-plane. *J. Fluid Mech.* **142**, 431–449.

KACHANOV, Y.S. 1994 Physical mechanisms of laminar-boundary-layer transition. *Annu. Rev. Fluid Mech.* **26**, 411–482.

KENDALL, J.M. 1971 JPL experimental investigations. In *Proceedings of the Boundary Layer Transition Workshop*, vol. 4, pp. 82816–16. Aerospace Corp.

KIMMEL, R.L. 2003 Aspects of hypersonic boundary-layer transition control. *AIAA Paper* 2003-772.

KING, R.A. 1992 Three-dimensional boundary-layer transition on a cone at Mach 3.5. *Exp. Fluids* **13**, 305–314.

KLEBANOFF, P.S. & TIDSTROM, K.D. 1972 Mechanism by which a two-dimensional roughness element induces boundary-layer transition. *Phys. Fluids* **15**, 1173–1188.

KNISELY, C.P. & ZHONG, X. 2017 An investigation of sound radiation by supersonic unstable modes in hypersonic boundary layers. *AIAA Paper* 2017-4516.

KNISELY, C.P. & ZHONG, X. 2019*a* Sound radiation by supersonic unstable modes in hypersonic blunt cone boundary layers. I. Linear stability theory. *Phys. Fluids* **31**, 024103.

KNISELY, C.P. & ZHONG, X. 2019*b* Sound radiation by supersonic unstable modes in hypersonic blunt cone boundary layers. II. Direct numerical simulation. *Phys. Fluids* **31**, 024104.

LAUFER, J. 1961 Aerodynamic noise in supersonic wind tunnels. *J. Aero. Sci.* **28**, 685–692.

LAUFER, J. 1964 Some statistical properties of the pressure field radiated by a turbulent boundary layer. *Phys. Fluids* **7**, 1191–1197.

LEES, L. & LIN, C.C. 1946 Investigation of the stability of the laminar boundary layer in a compressible fluid. *Tech. Rep.* 1115. NACA Tech. Note.

LEIB, S.J. 1991 Nonlinear evolution of subsonic and supersonic disturbances on a compressible free shear layer. *J. Fluid Mech.* **224**, 551–578.
LEIB, S.J. & LEE, S.S. 1995 Nonlinear evolution of a pair of oblique instability waves in a supersonic boundary layer. *J. Fluid Mech.* **282**, 339–371.
LIU, Y., DONG, M. & WU, X. 2020 Generation of first Mack modes in supersonic boundary layers by slow acoustic waves interacting with streamwise isolated wall roughness. *J. Fluid Mech.* **888**, A10.
MA, Y. & ZHONG, X. 2003 Receptivity of a supersonic boundary layer over a flat plate. Part 2. Receptivity to free-stream sound. *J. Fluid Mech.* **488**, 79–121.
MA, Y. & ZHONG, X. 2005 Receptivity of a supersonic boundary layer over a flat plate. Part 3. Effects of different types of free-stream disturbances. *J. Fluid Mech.* **532**, 63–109.
MACK, L.M. 1975 Linear stability theory and the problem of supersonic boundary-layer transition. *AIAA J.* **13**, 278–289.
MACK, L.M. 1984 Boundary-layer linear stability theory. *AGARD Rep.* 709, 3, 1–81.
MACK, L.M. 1987 Review of linear compressible stability theory. In *Stability of Time Dependent and Spatially Varying Flows* (ed. D.L. Dwoyer & M.Y. Hussaini), pp. 164–187. Springer.
MACK, L.M. 1993 Effect of cooling on boundary-layer stability at Mach number 3. In *Instabilities and Turbulence in Engineering Flows* (ed. D.E. Ashpis, T.B. Gatski & R. Hirsh), pp. 175–188. Springer.
MARXEN, O., IACCARINO, G. & SHAQFEH, E.S.G. 2010 Disturbance evolution in a Mach 4.8 boundary layer with two-dimensional roughness-induced separation and shock. *J. Fluid Mech.* **648**, 435–469.
MASAD, J.A. & IYER, V. 1994 Transition prediction and control in subsonic flow over a hump. *Phys. Fluids* **6**, 313–327.
MASUTTI, D., SPINOSA, E., CHAZOT, O. & CARBONARO, M. 2012 Disturbance level characterization of a hypersonic blowdown facility. *AIAA J.* **50**, 2720–2730.
MORKOVIN, M.V. 1969 Critical evaluation of transition from laminar to turbulent shear layers with emphasis on hypersonically travelling bodies. *Tech. Rep.* AFFDL-TR-68-149. US Air Force Flight Dynamics Laboratory, Wright Patterson Air Force Base.
MORTENSEN, C.H. 2018 Toward an understanding of supersonic modes in boundary-layer transition for hypersonic flow over blunt cones. *J. Fluid Mech.* **846**, 789–814.
NAYFEH, A.H., RAGAB, S.A. & AL-MAAITAH, A.A. 1988 Effect of bulges on the stability of boundary layers. *Phys. Fluids* **31**, 796–806.
PATE, S.R. & SCHUELER, C.J. 1969 Radiated aerodynamic noise effects on boundary-layer transition in supersonic and hypersonic wind tunnels. *AIAA J.* **7**, 450–457.
PIOT, E., CASALIS, G. & RIST, U. 2008 Stability of the laminar boundary layer flow encountering a row of roughness elements: biglobal stability approach and DNS. *Eur. J. Mech.* B/*Fluids* **27**, 684–706.
QIN, F. 2024 Roles of sound waves and acoustic feedback in instability and aeroacoustics of supersonic boundary layers. PhD thesis, Imperial College London.
QIN, F. & WU, X. 2016 Response and receptivity of the hypersonic boundary layer past a wedge to free-stream acoustic, vortical and entropy disturbances. *J. Fluid Mech.* **797**, 874–915.
RICCO, P. & WU, X. 2007 Response of a compressible laminar boundary layer to free-stream vortical disturbances. *J. Fluid Mech.* **587**, 97–138.
RUBAN, A.I. 1984 On the generation of Tollmien–Schlichting waves by sound. *Izv. Akad. Nauk SSSR Mekh. Zhidk. Gaza* **5**, 44–52.
SALEMI, L.C. & FASEL, H.F. 2018 Synchronization of second-mode instability waves for high-enthalpy hypersonic boundary layers. *J. Fluid Mech.* **838**, R2.
SCHNEIDER, S.P. 2001 Effect of high-speed tunnel noise on laminar-turbulent transition. *J. Spacecr. Rockets* **38**, 323–333.
SCHNEIDER, S.P. 2008 Development of hypersonic quiet tunnels. *J. Spacecr. Rockets* **45**, 641–664.
SCHNEIDER, S.P. 2015 Developing mechanism-based methods for estimating hypersonic boundary-layer transition in flight: the role of quiet tunnels. *Prog. Aerosp. Sci.* **72**, 17–29.
SMITH, F.T. 1989 On the first-mode instability in subsonic, supersonic or hypersonic boundary layers. *J. Fluid Mech.* **198**, 127–153.
SPANGLER, J.G. & WELLS, C.S. 1968 Effects of freestream disturbances on boundary-layer transition. *AIAA J.* **6**, 543–545.
STEWARTSON, K. 1964 *The Theory of Laminar Boundary Layers in Compressible Fluids*. Clarendon.
TAM, C.K.W. 1995 Supersonic jet noise. *Annu. Rev. Fluid Mech.* **27**, 17–43.
TAM, C.K.W. & BURTON, D.E. 1984*a* Sound generated by instability waves of supersonic flow. Part 1. Two-dimensional mixing layers. *J. Fluid Mech.* **138**, 249–271.
TAM, C.K.W. & BURTON, D.E. 1984*b* Sound generated by instability waves of supersonic flow. Part 2. Axisymmetric jets. *J. Fluid Mech.* **138**, 273–295.

WU, X. 1992 The nonlinear evolution of high-frequency resonant-triad waves in an oscillatory Stokes-layer at high Reynolds number. *J. Fluid Mech.* **245**, 553–597.

WU, X. 1995 Viscous effects on fully coupled resonant-triad interactions: an analytical approach. *J. Fluid Mech.* **292**, 377–407.

WU, X. 1999 Generation of Tollmien–Schlichting waves by convecting gusts interacting with sound. *J. Fluid Mech.* **397**, 285–316.

WU, X. 2001*a* On local boundary-layer receptivity to vortical disturbances in the free stream. *J. Fluid Mech.* **449**, 373–393.

WU, X. 2001*b* Receptivity of boundary layers with distributed roughness to vortical and acoustic disturbances: a second-order asymptotic theory and comparison with experiments. *J. Fluid Mech.* **431**, 91–133.

WU, X. 2005 Mach wave radiation of nonlinearly evolving supersonic instability modes in shear layers. *J. Fluid Mech.* **523**, 121–159.

WU, X. 2019 Nonlinear theories for shear flow instabilities: physical insights and practical implications. *Annu. Rev. Fluid Mech.* **51**, 451–485.

WU, X. & COWLEY, S.J. 1995 On the nonlinear evolution of instability modes in unsteady shear layers: the Stokes layer as a paradigm. *Q. J. Mech. Appl. Maths* **48**, 159–188.

WU, X. & DONG, M. 2016 A local scattering theory for the effects of isolated roughness on boundary-layer instability and transition: transmission coefficient as an eigenvalue. *J. Fluid Mech.* **794**, 68–108.

WU, X. & HUERRE, P. 2009 Low-frequency sound radiated by a nonlinearly modulated wavepacket of helical modes on a subsonic circular jet. *J. Fluid Mech.* **637**, 173–211.

WU, X., LEE, S.S. & COWLEY, S.J. 1993 On the weakly nonlinear three-dimensional instability of shear layers to pairs of oblique waves: the Stokes layer as a paradigm. *J. Fluid Mech.* **253**, 681–721.

WU, X. & STEWART, P.A. 1996 Interaction of phase-locked modes: a new mechanism for the rapid growth of three-dimensional disturbances. *J. Fluid Mech.* **316**, 335–372.

WU, X., STEWART, P.A. & COWLEY, S.J. 2007 On the catalytic role of the phase-locked interaction of Tollmien–Schlichting waves in boundary-layer transition. *J. Fluid Mech.* **590**, 265–294.

XU, H., SHERWIN, S.J., HALL, P. & WU, X. 2016 The behaviour of Tollmien–Schlichting waves undergoing small-scale localised distortions. *J. Fluid Mech.* **792**, 499–525.

XU, J. & WU, X. 2022 Surface-roughness effects on crossflow instability of swept-wing boundary layers through generalized resonances. *AIAA J.* **60**, 2887–2904.

ZHONG, X. & WANG, X. 2012 Direct numerical simulation on the receptivity, instability and transition of hypersonic boundary layers. *Annu. Rev. Fluid Mech.* **44**, 527–561.